POLITECNICO DI TORINO

Master's Degree in Automotive Engineering

Master's Degree Thesis

Analysis and Simulation of a Radial Piston Hydraulic Motor

Academic Supervisor:

Prof. Massimo Rundo

Candidate:

Francesco Giavarini

Academic Year 2021/2022

Abstract

This thesis is focused on the study and the simulation of a radial piston hydraulic motor, used for applications where low rotational speed and high torque are needed. This typology can be part of a hydrostatic transmission mounted on vehicles; coupled to the wheels, it can provide traction. Starting from a model kindly donated to the FPRL by Poclain Hydraulics® (identified by catalogue research as a MSE02 Classic), a three-dimensional representation has been done with the aim of obtaining an animation capable to faithfully reproduce the actual kinematics; the software used for this purpose has been SolidWorks®. Then, after the evaluation of some fundamental parameters such as flow areas development, piston chamber volume and its derivative with respect to the angle of rotation, a simulation has been conducted in Amesim® environment. Two approaches have been used: the first one, which has been taken by an already existing formulation, reproduces the motor by means of parallel hydraulic lines that simulate every single piston chamber. The second one has been developed by means of the more recent vectorial blocks with the aim to obtain the same results in a more compact and simple way. After the main simulation (in which the motor behaviour has been quantified by means of shaft speed, pressure, flow rate and other significative parameters), some further analyses have been done about the impact of the number of pistons and on the results obtained implementing a variable displacement layout.

TABLE of CONTENTS

LIST of FIGURES

1) Introduction

In this chapter it is reported a brief presentation on the hydraulic machines, the hydrostatic transmissions and the vehicle simplified dynamics. Then, the radial piston hydraulic motor that has been the subject of this work will be presented with some of its possible applications.

1.1) Hydraulic Machines

Rotative hydraulic machines are devices that make possible the transfer of work through an uncompressible fluid, by means of conversions between mechanical and hydraulic power. The fluid, which has standardized properties and is commonly referred to as *oil*, flows through chambers with variable volume ranging between a maximum and a minimum value. These chambers are alternatively put in communication with two hydraulic lines at different pressure levels. According to the different method by which the chamber volume is varying, hydraulic machines are divided in various categories; here are listed the main ones:

- piston hydraulic machines (axial or radial);
- gear hydraulic machines (external or internal);
- vane hydraulic machines (balanced rotor or unbalanced rotor).

Another characterization is the one by which the power conversion direction takes place; the hydraulic machines can be in fact subdivided in:

- hydraulic pumps, if the mechanical power is converted into hydraulic power;
- hydraulic motors, if the hydraulic power is converted into mechanical power.

The mechanical power is coming from (or going to) a rotating shaft.
One of the most important parameters of the hydraulic machines is the displacement. Here it is shown how to calculate it:

$$V_{hm} = N * V_0 * n_{cycles} \text{ (eq. 1.1.1),}$$

Where N is the number of chambers present in the machine, V_0 is the unit displacement (which is equal to the difference between maximum and minimum chamber volume), and n_{cycles} is the number of work cycles that the chamber does for each shaft revolution.
The working cycle of a hydraulic machine is composed of four phases:

- inlet phase (*AB*), where the volume increases from the minimum to the maximum value;
- compression (*BC*), in which the pressure inside the chamber increases from p_{min} to p_{max};
- outlet phase (*CD*), where the volume decreases from the maximum to the minimum value;
- expansion (*DA*), in which the pressure decreases from p_{max} to p_{min}.
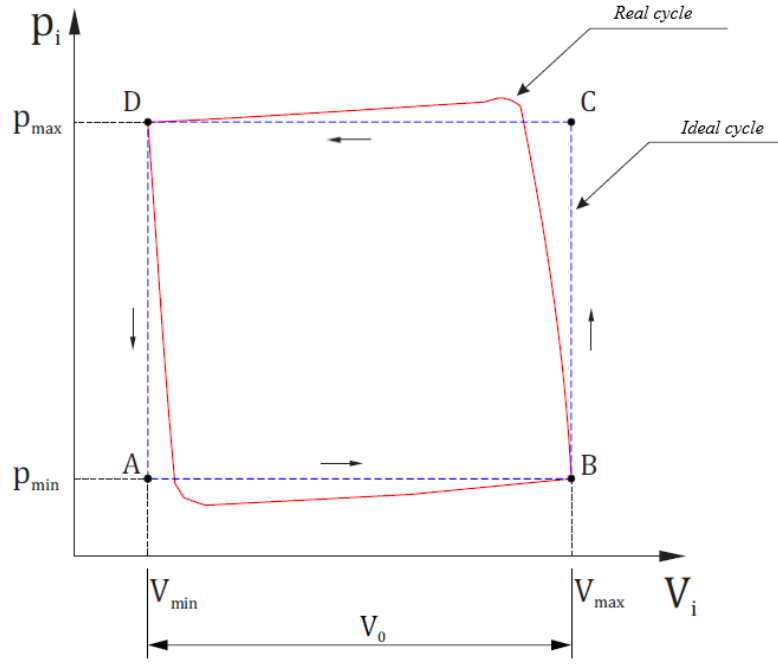
Figure 1.1 - Ideal and real working cycle of a hydraulic machine

If the machine is a pump, the cycle is followed in the presented order, while if it is a motor the sequence is the exact opposite. The ideal cycle considers both ideal machine and fluid: in this case flow leakages, friction, compressibility and incomplete filling are not taken into account.

1.1.1 Pump

As indicated before, a pump is a machine that converts mechanical power into hydraulic power. A rotational speed is imposed on its shaft by a motor (commonly referred to as *prime mover*). As a result, it generates a certain amount of flow rate.

The instantaneous flow rate $Q(\vartheta)$ produced by one chamber is:

$$Q_i(\vartheta) = \frac{\partial Vol_i}{\partial t} = \frac{\partial Vol_i}{\partial \vartheta} * \frac{\partial \vartheta}{\partial t} = \frac{\partial Vol_i}{\partial \vartheta} * \omega \ \textit{(eq. 1.1.2)},$$

where Vol_i is the i-th chamber volume and ω the shaft speed of rotation. Anyway, the flow rate is just produced when the volume is reduced. For this reason, a parameter called $F(\vartheta)$ can be considered with the following formulation:

$$F_i(\vartheta) = \begin{cases} -\frac{\partial Vol_i}{\partial \vartheta}, if \ \frac{\partial Vol_i}{\partial \vartheta} \leq 0 \\ 0, if \ \frac{\partial Vol_i}{\partial \vartheta} > 0 \end{cases} \textit{(eq. 1.1.3).}$$

In conclusion, the instantaneous flow rate generated by the pump is equal to:

$$Q(\vartheta) = \omega * \sum_{i=1}^{N} F_i(\vartheta) \ \textit{(eq. 1.1.4).}$$
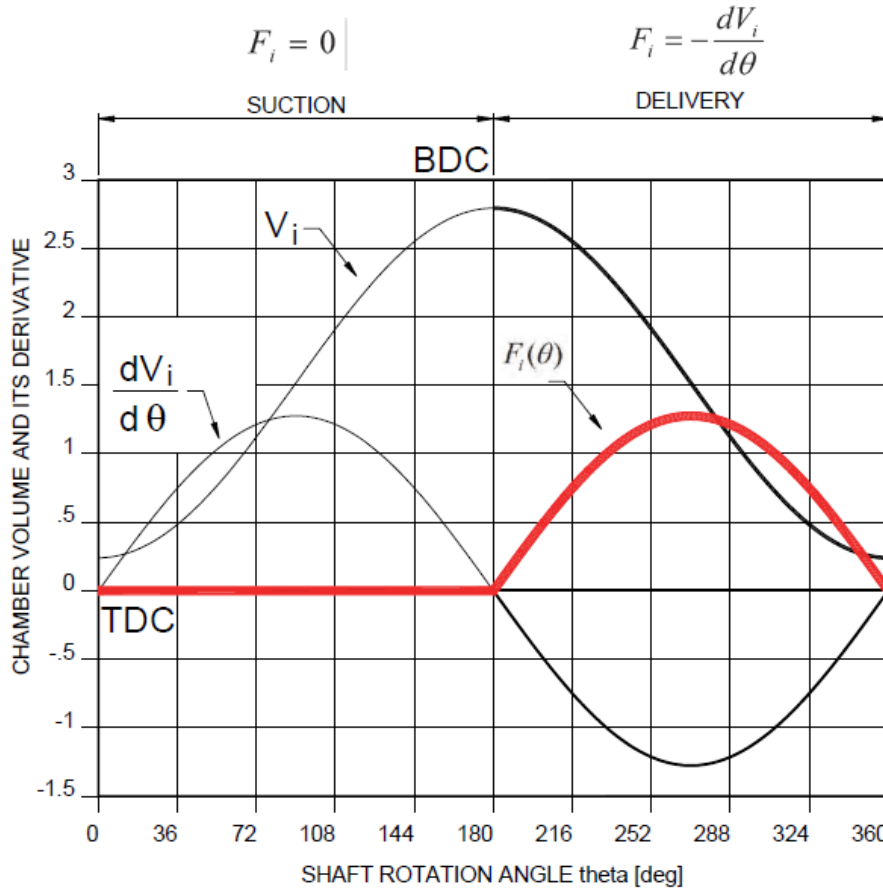
Figure 1.2 - Volume, volume derivative and F function with respect to shaft angle

The theoretical mean flow rate can be found once the $F(\vartheta)$ parameter has been defined. It can be demonstrated that:

$$\bar{Q} = \frac{1}{\Theta} * \int_0^\Theta \omega * \sum_{i=1}^N F_i(\vartheta) \, d\vartheta = \frac{N*\omega}{\Theta} * \int_0^\Theta F_1(\vartheta) d\vartheta = \frac{N*\omega*V_0}{\Theta} = \omega * V \ (eq.1.1.5).$$

For what concerns the instantaneous and average torque T absorbed by the pump, it can be said that:

$$\begin{cases} T(\vartheta) = \Delta p * \sum_{i=1}^N F_i(\vartheta) = \Delta p * F(\vartheta) \\ \bar{T} = \Delta p * V \end{cases} \ (eq. \ 1.1.6),$$

where Δp is the delta pressure across the pump. Real machines have always lower performances with respect to their ideal counterparts: for what concerns a real pump, its real delivered flow rate is lower with respect to the ideal one, while the torque absorbed is higher. In order to calculate these real pump performances, the efficiency of the machine has to be considered. It can be subdivided into two main contributions:

1. Volumetric efficiency, that takes into account the flow rate leakages. For a pump, its formulation is the following:

$$\eta_{vol} = \frac{Q_r}{Q_{th}} = \frac{Q_{th} - Q_{leak}}{Q_{th}} = 1 - \frac{Q_{leak}}{\omega * V} = \eta_{vol}(\Delta p, \omega, T) \ (eq.1.1.7).$$

2. Mechanical-hydraulic efficiency, which takes into account with the parameter T_f both viscous and Coulomb frictions. For a pump, its formulation is:

$$\eta_{mech} = \frac{T_{th}}{T_r} = \frac{T_{th}}{T_{th}+T_f} = \frac{1}{1+\frac{T_f}{V*\omega}} = \eta_{mech}(\Delta p, \omega, T) \ (eq. \ 1.1.8).$$

The total pump efficiency is equal to the product of these two contributions.

$$\eta_{pump} = \eta_{vol} * \eta_{mech} = \frac{Useful \ Power}{Expended \ Power} = \frac{Q_r * \Delta p}{T_r * \omega} \ (eq. \ 1.1.9)$$
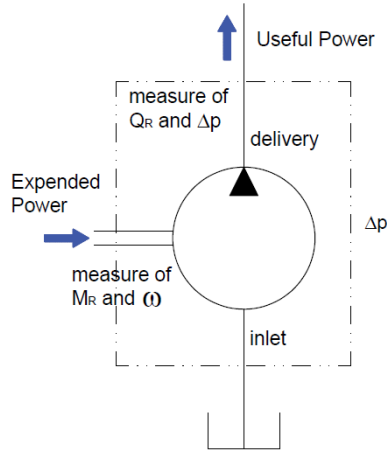
Figure 1.3 - ISO-1219 pump representation

1.1.2 Motor

A hydraulic motor is a machine that converts hydraulic power into mechanical power. It receives a certain amount of flow rate of pressurized oil, thanks to which the load on the shaft is contrasted and a rotation is obtained. All the formulations seen in the pump paragraph can be also done in this case. The main difference is on the parameters on which the focus is concentrated.
The instantaneous and mean shaft speed can be calculated in this way:

$$\begin{cases} \omega(\vartheta) = \frac{Q}{F(\vartheta)} \\ \bar{\omega} = \frac{Q}{V} \end{cases} (eq.1.1.10).$$

The instantaneous and mean pressure can be instead calculated with the following formulation:

$$\begin{cases} p(\vartheta) = \frac{T}{F(\vartheta)} \\ \bar{p} = \frac{T}{V} \end{cases} (eq. \ 1.1.11).$$

In the case of the real motor, the real flow rate needed to have a certain rotational speed is higher with respect to the theoretical one, while the real shaft torque is lower. This time the two efficiency contributions can be written as:

$$\begin{cases} \eta_{vol} = \dfrac{Q_{th}}{Q_r} = \dfrac{Q_{th}}{Q_{th}+Q_{leak}} = \dfrac{1}{1+\frac{Q_{leak}}{V*\omega}} = \eta_{vol}(\Delta p, \omega, T) \\[2ex] \eta_{mech} = \dfrac{M_r}{M_{th}} = \dfrac{M_{th}-M_f}{M_{th}} = 1 - \dfrac{M_f}{V*\Delta p} = \eta_{mech}(\Delta p, \omega, T) \end{cases} \quad (eq.\ 1.1.12).$$

Since the volumetric efficiency of the motor studied in this thesis is going to be quantified in chapter 5, here it is reported the generic theoretical trend with respect to pressure and speed.

$$\eta_v = \frac{1}{1+c_1 \cdot \Delta p}$$

$$\eta_v = \frac{1}{1+\frac{c_2}{\omega}}$$

$$\omega = 0 \qquad \eta_v = \frac{1}{\infty} = 0$$
$$\omega \to \infty \qquad \eta_v \to 1$$
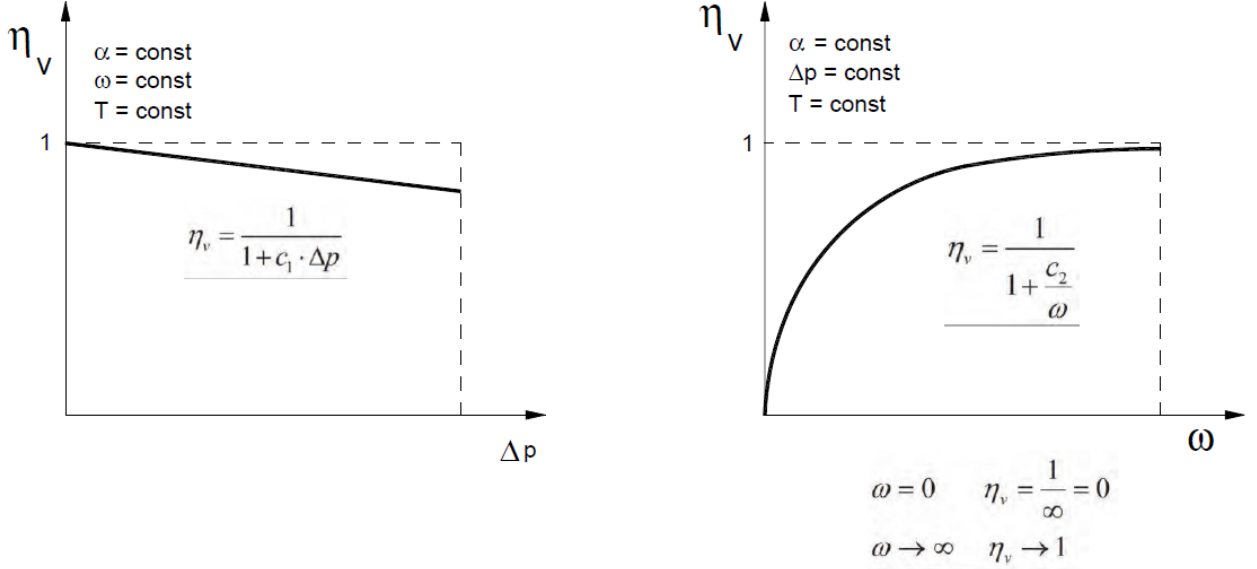
Figure 1.4 – Motor volumetric efficiency with respect to delta pressure and shaft speed of rotation

Obviously, also in this case the total motor efficiency is equal to the product of the two contributions:

$$\eta_{motor} = \eta_{vol} * \eta_{mech} = \frac{Useful\ Power}{Expended\ Power} = \frac{T_r*\omega}{Q_r*\Delta p} \ (eq.\ 1.1.13).$$
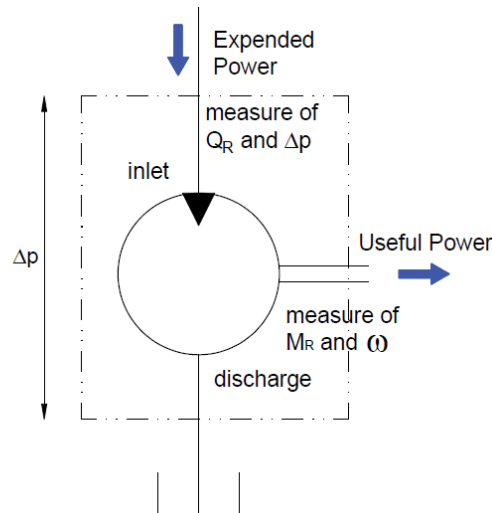
Figure 1.5 - ISO-1219 motor representation

1.2) Hydrostatic Transmissions

A hydrostatic transmission is a system composed of two rotative units capable to convert mechanical energy into hydraulic and again into mechanical one. It is constituted by the following components:

- pump driven by a prime mover (also called *primary unit*);
- hydraulic circuit constituted by safety and control valves;
- hydraulic motor connected to the load (also called *secondary unit*).

With this system it is possible to:

- continuously vary the torque T and the speed of rotation ω accordingly to the needs of the load;
- transmit power among two shafts notably far away from each other.

A hydrostatic transmission is considered with an open circuit if the pump takes the oil from the tank and the motor discharges it there; it is instead considered with a closed circuit if the discharged flow rate from the motor is directly sent to the pump.
Here are presented some of the main parameters of the hydraulic transmissions:

1. The *transmission ratio τ* is the ratio between the shaft speed of the secondary unit and the shaft speed of the primary unit.

$$\tau = \frac{\omega_{mot}}{\omega_{pump}} = \frac{\alpha_{pump}*V_{pump}}{\alpha_{mot}*V_{mot}} * \eta_{vol,mot} * \eta_{vol,pump} \text{ (eq. 1.2.1)},$$

   where α is the displacement modulation factor (which is constant and equal to 1 if the machine is at fixed displacement). This evaluation has been done considering a flow equilibrium condition, in which all the flow delivered by the pump reaches the hydraulic motor.

2. The *dynamic ratio k* is the ratio between the shaft torque at the secondary unit and the one at the primary unit.

$$k = \frac{T_{mot}}{T_{pump}} = \frac{\alpha_{mot}*V_{mot}}{\alpha_{pump}*V_{pump}} * \eta_{mech,mot} * \eta_{mech,pump} \text{ (eq. 1.2.2).}$$

   This evaluation has been done considering the same delta pressure across the two hydraulic machines.

3. The *overall transmission efficiency η_{HT}* is the ratio between the power generated by the secondary unit and the power required by the primary unit.

$$\eta_{HT} = \frac{P_{mot}}{P_{pump}} = \tau * k = \eta_{vol,mot} * \eta_{vol,pump} * \eta_{mech,mot} * \eta_{mech,pump} = \eta_{mot} * \eta_{pump} \text{ (eq. 1.2.3)}$$

In figure 1.6 it is reported a scheme of a closed hydrostatic transmission with variable displacement primary unit and fixed displacement secondary unit.
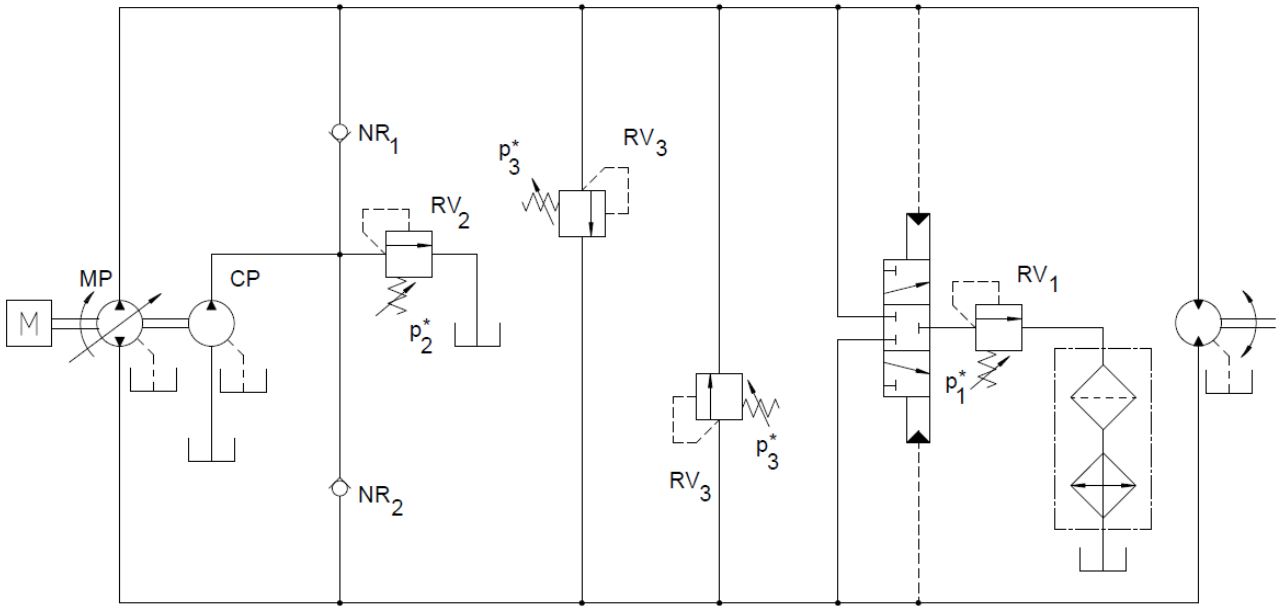
Figure 1.6 – Closed circuit hydrostatic transmission with variable primary unit and fixed secondary unit

There are four possible combinations between primary and secondary units.

1. The most common configuration is the one presented in figure 1.6, with variable primary and fixed secondary (*PVSF*). The transmission is controlled by adjusting the displacement modulation factor of the pump. In this configuration, considering both flow rate and pressure coupling:

$$\begin{cases} \tau = \alpha_{pump} * \dfrac{V_{pump}}{V_{mot}} = \tau(\alpha_{pump}) \\ k = \dfrac{V_{mot}}{V_{pump} * \alpha_{pump}} = \dfrac{1}{\tau} = k(\alpha_{pump}) \end{cases}$$

$$T_{mot} = V_{mot} * \Delta p$$
$$P_{mot} = T_{mot} * \omega_{mot} = T_{mot} * \omega_{pump} * \tau(\alpha_{pump})$$

With this configuration it can be seen that at fixed delta pressure the torque is constant, while the motor power linearly depends on the *transmission ratio* (and consequently on the pump displacement modulation factor).
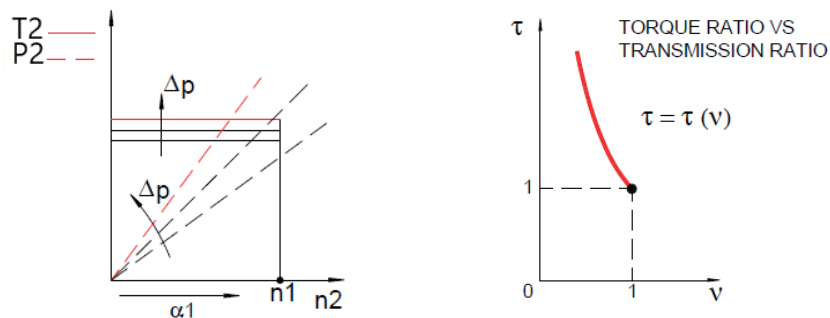
Figure 1.7 – Characteristics of the variable primary unit, fixed secondary unit hydrostatic transmission

2. If both primary and secondary are with constant displacement, the simplest layout is obtained but there is just one possible point of operation since no regulation is allowed.

$$\begin{cases} \tau = \dfrac{V_{pump}}{V_{mot}} = constant \\ k = \dfrac{V_{mot}}{V_{pump}} = \dfrac{1}{\tau} = constant \end{cases}$$

The torque and the power of the motor are functions only of the load.

3. The configuration with fixed primary and variable secondary (*PFSV*) is seldom encountered in practical applications, since the motor in this case can't be controlled at low speeds.

$$\begin{cases} \tau = \dfrac{V_{pump}}{\alpha_{mot} * V_{mot}} = \tau(\alpha_{mot}) \\ k = \dfrac{\alpha_{mot} * V_{mot}}{V_{pump}} = \dfrac{1}{\tau} = k(\alpha_{mot}) \end{cases}$$

$$T_{mot} = \alpha_{mot} * V_{mot} * \Delta p = \frac{V_{pump} * \Delta p}{\tau(\alpha_{mot})}$$

$$P_{mot} = T_{mot} * \omega_{mot} = \frac{V_{pump} * \Delta p}{\tau(\alpha_{mot})} * \omega_{pump} * \tau(\alpha_{mot}) = V_{pump} * \Delta p * \omega_{pump}$$

With this configuration it can be seen that at fixed load the power is constant, while the torque depends on the *transmission ratio* (and consequently on the motor displacement modulation factor). Looking at figure 1.8 it can be understood why the variable secondary leads to uncontrollable low speeds.
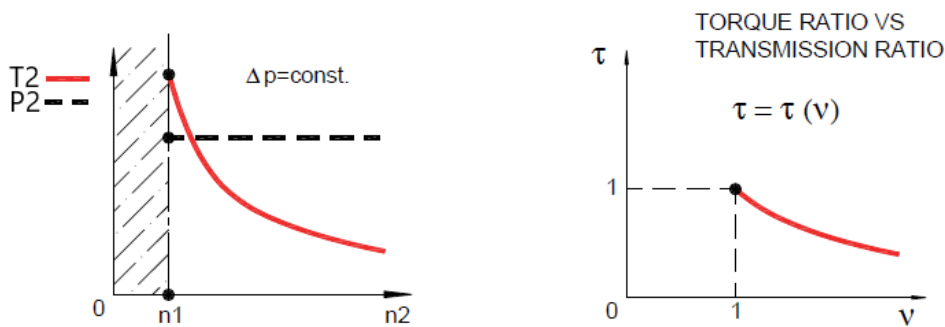
Figure 1.8 – Characteristics of the fixed primary unit, variable secondary unit hydrostatic transmission

4. The last possible layout, in which both primary and secondary unit are variable, is the most complex since both motor and pump can be simultaneously regulated: transmission ratio and dynamic ratio depend on both motor and pump displacement modulation factors. For this reason, a precise control strategy has to be followed: the characteristics of the *PFSV* and *PVSF* are combined together.
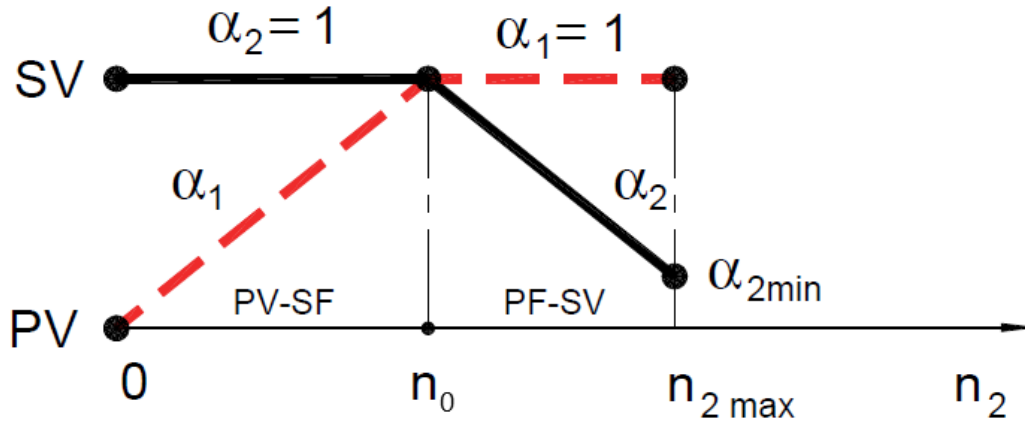
Figure 1.9 - Control strategy of PVSV configuration (1=pump, 2=motor)

It can be seen how the pump displacement is gradually increased at low motor speeds up to n_0, at which it reaches its maximum value ($\alpha_{pump} = 1$). The motor displacement is kept constant and equal to its maximum all along this range. In this working region, the hydrostatic transmission works in *PVSF* mode. Then, further increasing the motor speed, the pump displacement is kept constant while the motor one is gradually decreased (*PFSV* working mode). In this way the motor shaft speed can be controlled in a very much wide range.
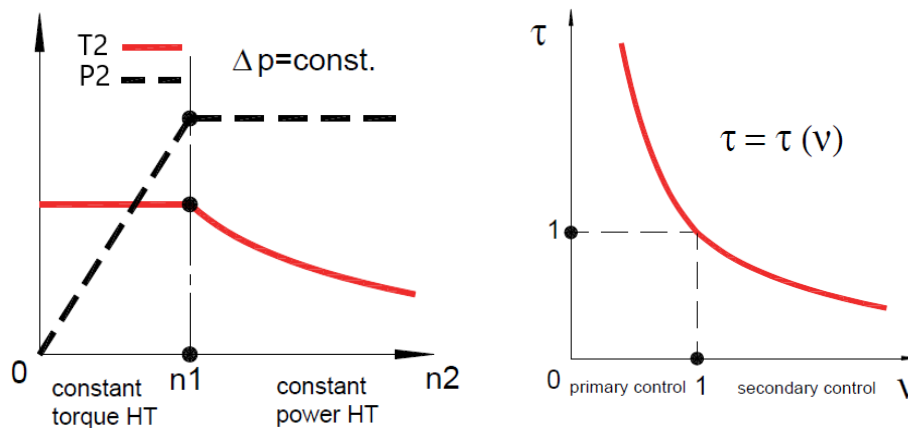
Figure 1.10 – Characteristics of the variable primary unit, variable secondary unit hydrostatic transmission

1.3) Vehicle Dynamics Simplified Theory

Being the studied motor mounted on vehicles for propulsion, it is reasonable to make a brief recall on the vehicle dynamics for identifying the road request in terms of torque and power. In order to do so, it is mandatory to analyse the different typologies of vehicle frictions.

1.3.1   Rolling Resistance

The rolling resistance depends with decreasing importance on the tyre material hysteresis, on the tyre-road creeping and on the wheel-transmission friction. Its evaluation is quite difficult, because it depends on a lot of different factors. The rolling resistance coefficient in fact is calculated taking into account the vehicle speed, the tyre pressure, the load, the contact area between tyre tread and road,

the tyre material, the road conditions and many others. The modelling of the tyre rolling behaviour is really complex: polynomial functions with experimentally evaluated parameters are used. This is the formulation used for evaluating the rolling resistance at a generic road slope.

$$\begin{cases} F_{roll} = M * g * k_{roll} * \cos(\alpha) \\ T_{roll} = M * g * r_w * k_{roll} * \cos(\alpha) \ (eq.\ 1.3.1), \\ P_{roll} = M * g * k_{roll} * V * \cos(\alpha) \end{cases}$$

where M is the vehicle mass, g is the gravity constant, k_{roll} is the rolling coefficient, r_w is the wheel radius, V is the vehicle velocity and α the angle of the road inclination.

1.3.2   Aerodynamic Resistance

The aerodynamic resistance depends on the air density ρ_{air}, the vehicle frontal area A_f, the aerodynamic drag coefficient C_x and the vehicle relative speed V_r. Its classic formulation is the following one:

$$\begin{cases} F_{aero} = \frac{1}{2} * \rho_{air} * A_f * C_x * V_r^2 \\ T_{aero} = \frac{1}{2} * \rho_{air} * A_f * C_x * V_r^2 * r_w \ (eq.\ 1.3.2). \\ P_{aero} = \frac{1}{2} * \rho_{air} * A_f * C_x * V_r^3 \end{cases}$$

As it can be seen, these values are independent from the road inclination. At level road ($\alpha = 0°$), the characteristic speed V_{char} is the one at which the rolling and aerodynamic resistances reach the same value. Due to the speed dependency, for $V < V_{char}$ the rolling resistance prevails on the aerodynamic one and vice versa.
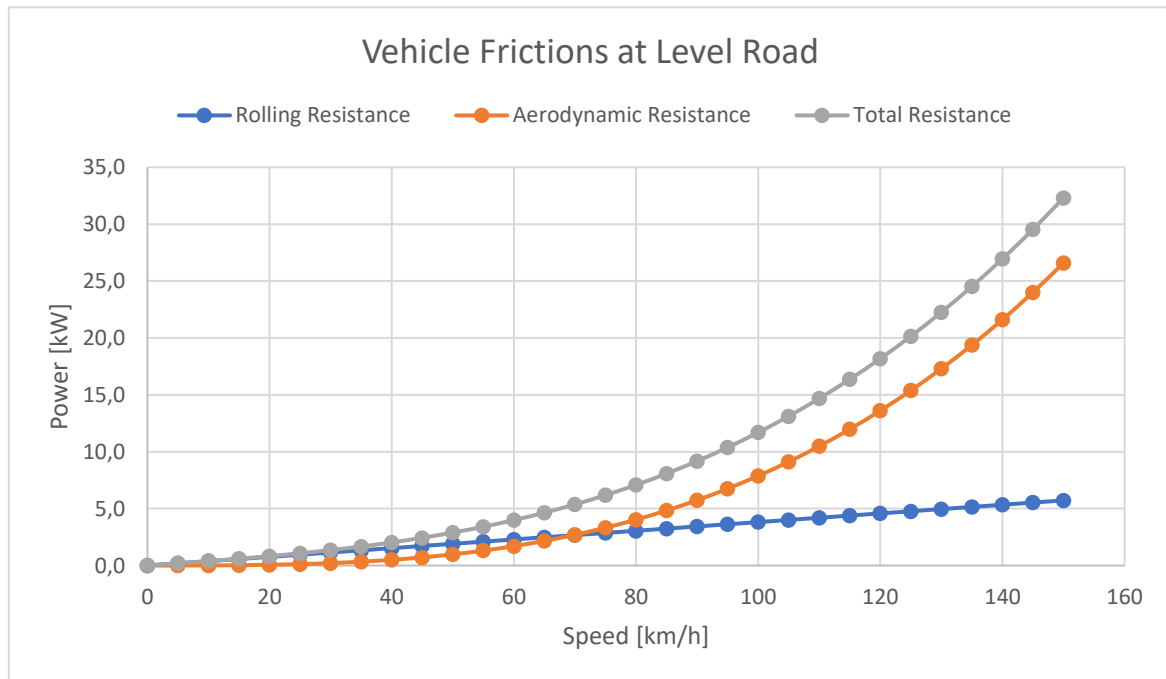
Figure 1.11 - Road frictions with respect to speed at zero slope for a generic vehicle

1.3.3   Resistance due to the Slope of the Road

The slope contribution to the total friction can be identified in the following way:

$$\begin{cases} F_{slope} = M * g * sin\,(\alpha) \\ T_{slope} = M * g * r_w * sin\,(\alpha) \textit{ (eq. 1.3.3)}. \\ P_{slope} = M * g * V * sin\,(\alpha) \end{cases}$$

1.3.4   Vehicle Dynamics

If an acceleration is made, the inertia has to be correctly considered by means of the vehicle apparent mass.

$$M_{app} = M + J_{mot} * \frac{\tau_I^2}{r_w^2} + J_{trans} * \frac{\tau_{II}^2}{r_w^2} + \frac{J_{wheels}}{r_w^2} \textit{ (eq. 1.3.4)},$$

where J_x is the x-element moment of inertia, τ_I is the transmission ratio between motor and wheels and τ_{II} is the transmission ratio between transmission and wheels. The vehicle acceleration a contribution can be written in this form:

$$\begin{cases} F_{acc} = M_{app} * a \\ T_{acc} = M_{app} * a * r_w \textit{ (eq. 1.3.3)}. \\ P_{acc} = M_{app} * a * V \end{cases}$$

If the motor is linked to the wheels by some gear coupling, it is still fundamental to convert the speed and the torque by means of the transmission ratio. Knowing all these formulations, it is possible to quantify the motor requested torque and power for precise operating conditions of the vehicle, such as for example a certain constant speed or an acceleration on a road with a certain slope.

1.4) MSE02 Classic

As anticipated in the abstract, the analysed motor is a model produced by *Poclain Hydraulics®*. More specifically, it belongs to the MS family of motors and is identified among it with the *MSE02 Classic* nomenclature. These types of motors are designed to be installed on the wheels through a *direct drive*, so that thanks to the hydrostatic transmission architecture they can provide traction to the vehicle. Two possible configurations are possible: with single (*1C*) or double (*2C*) displacement. The exemplar studied in this work has a single displacement, but in chapter 7 also the other solution has been partially analysed. Some solutions also make possible the adoption of drum, disc or multidisc braking systems.

The *MSE02 Classic* is a radial piston hydraulic motor, constituted by eight equally spaced pistons that travel on a path defined by a cam-profile stator with six lobes. For each lobe, every piston undergoes a full working cycle: it receives oil while the volume is increasing and it discharges it while the volume is decreasing. These pistons are entrained in devoted chambers *radially hollowed out* into a metal *"disc"* that acts as the rotor of the system. The rotor is coupled with a spline to a shaft, that ends at its opposite side with a flange whose task is the coupling with the vehicle wheel. If

the brake is present, the rotor spline has to cover both brake shaft and propulsion shaft realising both the couplings. The motor communication with the two pressure lines of the hydrostatic transmission is made possible by the distribution and the distribution seat: once correctly positioned, these two components form two independent constant volumes of oil.

Figure 1.12 – Poclain Hydraulics MS Classic and MS HighFlow™ motors. The second one is distinguished by performance advantages in terms of speed and power

This type of motor has the main characteristic of working at low speed of rotation and high torque (they can in fact be called *Slow Motors*). For this reason, off-roads applications are normally preferred. Here some examples are reported.

1. Mini loader:

Figure 1.13 – Mini loader and its hydraulic components

For this application MS motors are suggested as long as MG ones. The latter have the main advantage of being steerable. For both the solutions anyway, a direct drive transmission system is ensured.

2. Aircraft tractor:
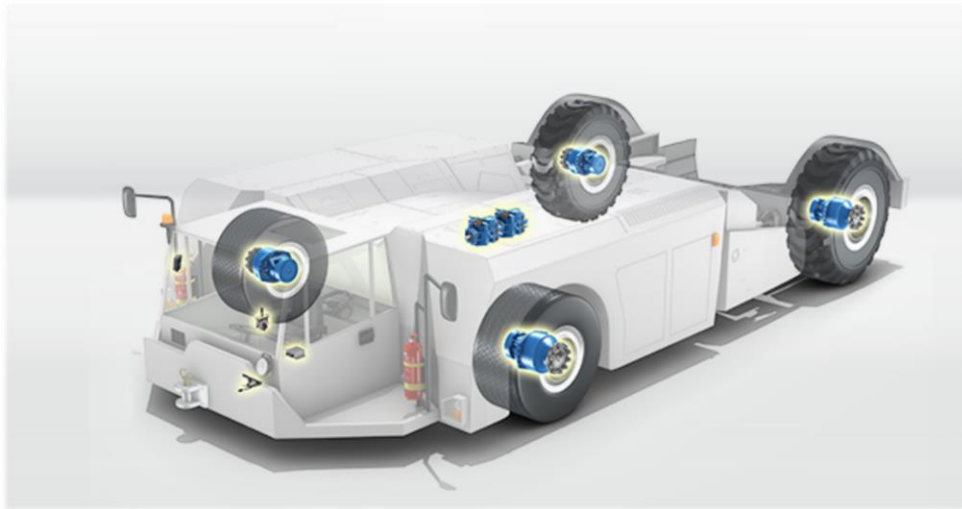
Figure 1.14 - Aircraft tractor and its hydraulic components

3. Snow removal machine:
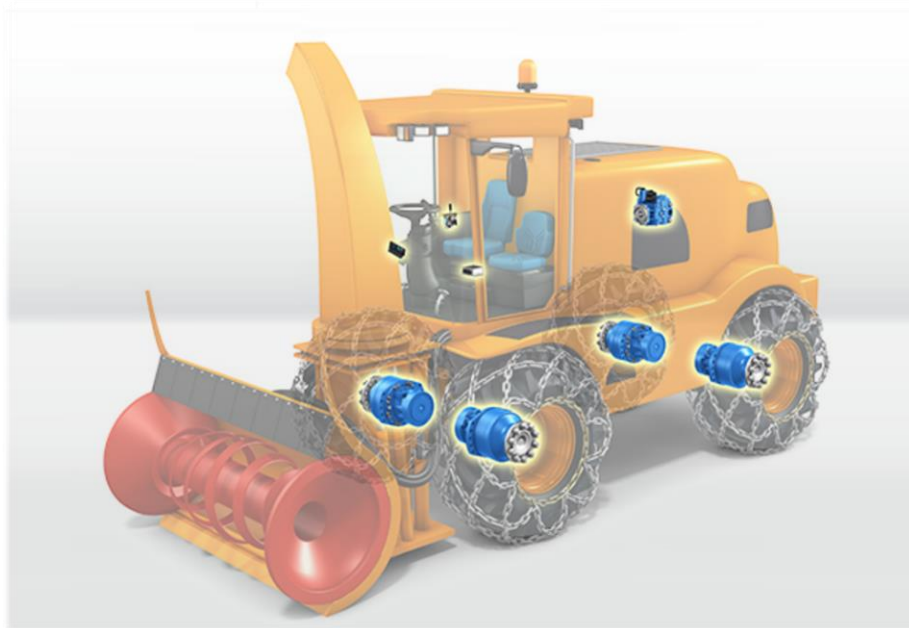
Figure 1.15 – Snow removal machine and its hydraulic components

It is important to point out that for some of these applications the *MSE02* could not be the proper solution, being this model the less performant among the whole MS family product. Besides, apart from the internal characteristics such as number of pistons and chamber volumes (that affect the value of the motor displacement), all of them have very similar configurations and the same working principles.

4. Sweeper:

Figure 1.16 - Sweeper and its hydraulic components

5. Grape harvester:

Figure 1.17 - Grape harvester and its hydraulic components

For some applications with particularly demanding operating conditions, a further system has been developed in the motors: the *TwinLock™* hydraulic anti-skid. In the case of the grape harvester, in presence of very strong slopes (up to 50% and more) this system adapts the traction on the front wheels transferring the excess torque to the rear axle. In this way skidding is prevented and a certain

vehicle constant speed is ensured. More in general, the TwinLock™ solution transfers the torque from the wheels that are slipping to the wheels with greatest grip, increasing consistently the off-road driving capability.

Talking about the hydrostatic transmission, if the studied *MSE02 Classic* is installed it is of the *PVSF* typology (the pump and motor respectively have variable and fixed displacement). If motors with variable displacement are chosen, in this case this fact should not lead to think about a *PVSV* configuration: the displacement is just discretely variable, and once one of the available values is set it remains constant up to the next shift. So, also in this case the hydrostatic transmission still works as a *PVSF* one, just at different steps.
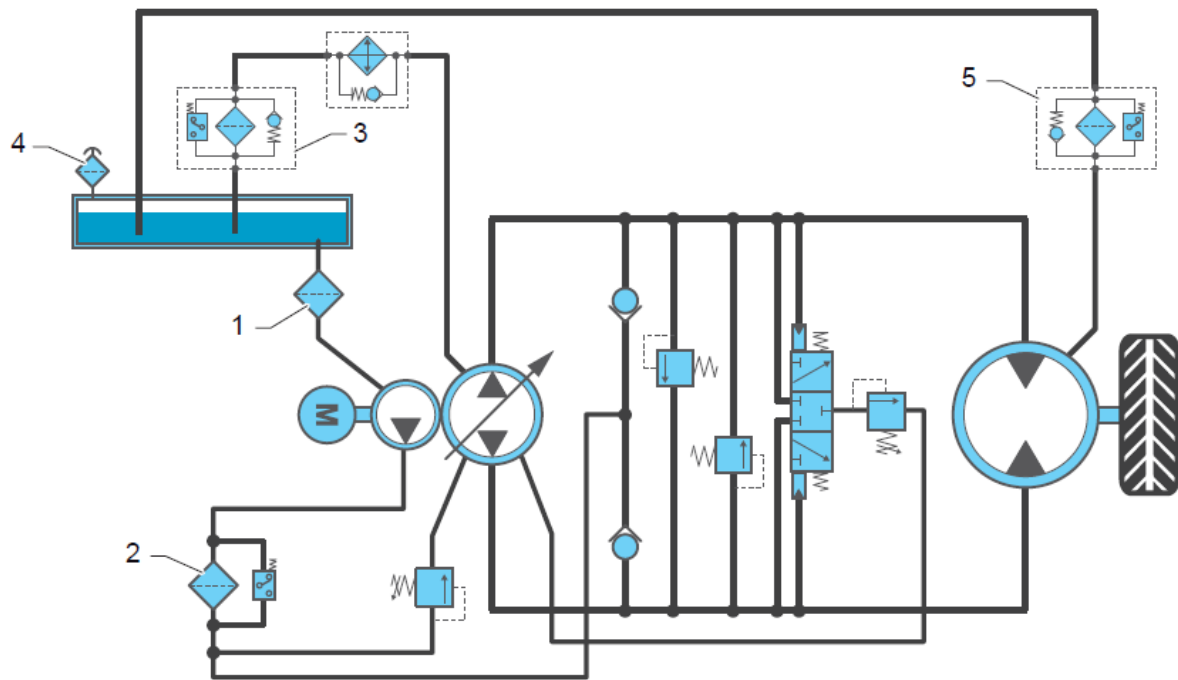
Figure 1.18 - Example of a closed loop hydrostatic transmission with decontamination and filtration loops. 1) intake line strainer; 2) and 3) low pressure filters with clogging indicator; 4) breather; 5) magnetic or low-pressure filter (optional)

2) 3D CAD Reproduction

2.1) Components and Assembly Reconstruction

The first step of this work has been the reproduction of the hydraulic motor in a CAD environment. Measurements of the various components have been conducted by means of a *Vernier caliper*, and for this reason it has to be taken into account the 0.05 mm resolution that can lead to little discrepancies with the actual dimensional values. The software used for this task has been *Solidworks®*.

In this chapter the main steps made to obtain the final assembly will be explained.

2.1.1 Stator

The stator can be seen as a disc element with a complex cam-shaped internal profile, which is of paramount importance since it defines the motion of the pistons. The external diameter and the thickness respectively measure 183.00 mm and 31.20 mm. The internal profile consists in six equal lobes, built in such a way that the piston top dead centre (*TDC*) lays on a circumference of diameter equal to 67.30 mm and is far 76.80 mm from the stator axis, while the bottom dead centre (*BDC*) is located on a circumference of diameter 43.00 mm and whose centre is at a distance of 66.51 mm from the stator one. Due to the fact that the piston motion is fundamental for the evaluation of the motor behaviour and performances, particular attention has been paid to represent the cam. Hence, highlights for its precise reproduction are right away reported.

At first a simple circle with the external diameter value has been drawn and then extruded by the previous defined thickness. The particular internal profile has been reproduced starting from the drawing of a simple hexagon, whose corners were taken as a reference for the piston top dead centre location. Then, after the circumferences to define the lobes were sketched, the shape has been polished through the "*Trim Entities*" command. Once the profile has been obtained, an "*Extruded Cut*" was performed to form the cavity. Here is reported a picture with the main geometrical references of the sketch.
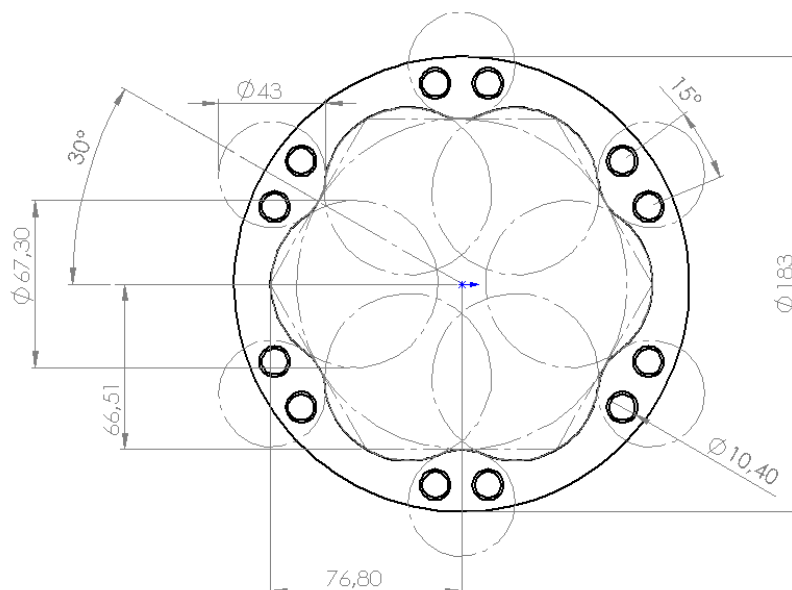
Figure 2.1 - Stator 2D representation and its main geometrical properties

It can also be seen the presence of the twelve holes through which the screws pass across. It is important to note that they are not threaded: the tightening is ensured in the shaft cover, which is axially next to the cam itself. Here it can be seen the final three-dimensional sketch compared to the real component.
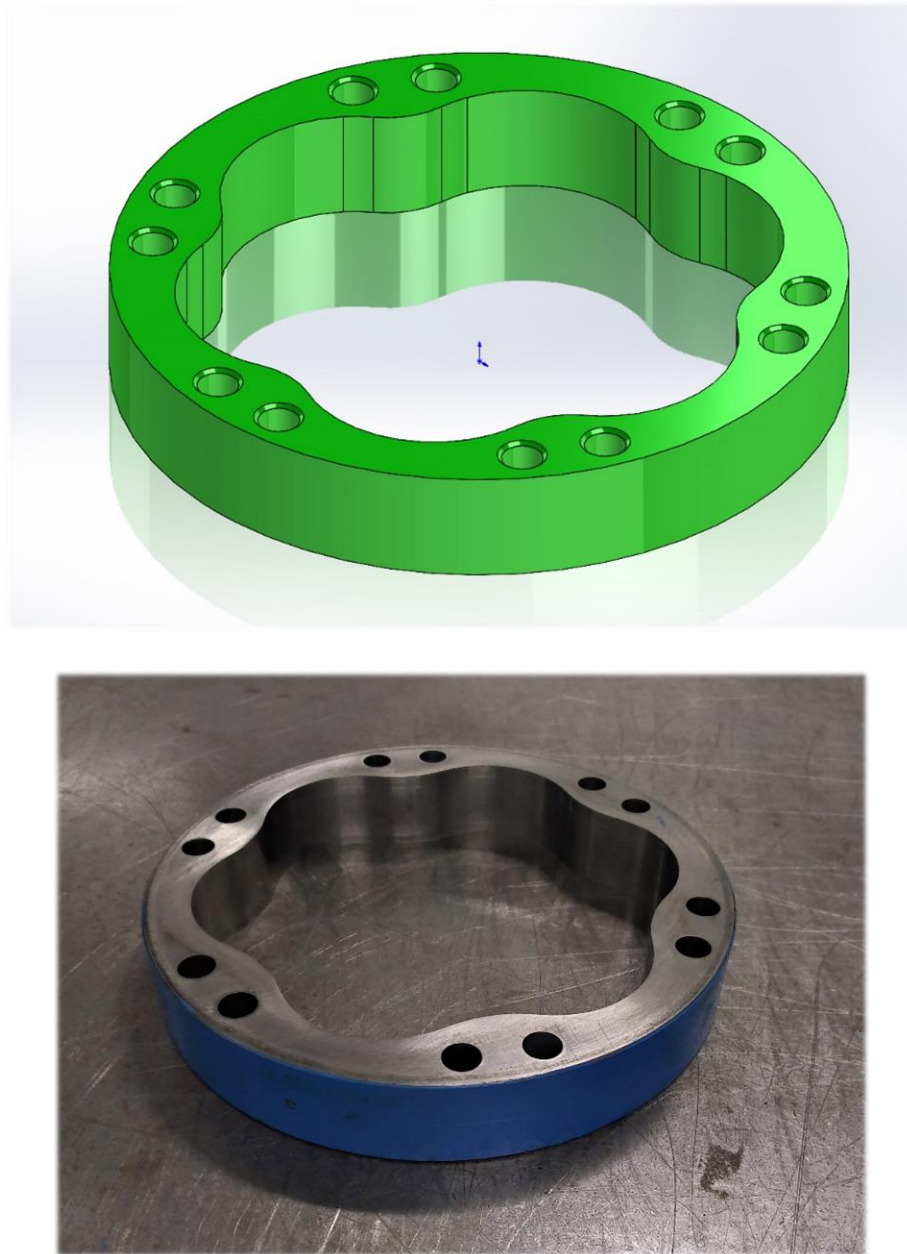
Figure 2.2 - Stator 3D representation in comparison with the actual one

2.1.2   Rotor

The rotor is the component through which the piston motion derived from the cam is *"converted"* into rotational speed. It can be seen again as a disc element with an external diameter of 132.00 mm and a thickness of 42.00 mm. The internal diameter has a value of 40.00 mm and hosts a spline dedicated to the coupling with the shaft (and eventually even to a mechanical brake). The front surface is dedicated to the interfacing with the distribution: eight cylindrical ducts of diameter equal to 7.00

mm link the piston chambers to the distribution ones. They are built on a circumference of radius equal to 29.80 mm centred in the rotor axis. Particular attention has to be dedicated to the drawing of the piston chambers, since these volumes define the displacement of the hydraulic machine.

Due to the particular shape of the pistons, two different cavities have to be formed. The *Solidworks®* function *"Hole Wizard"* has been used to create the radial holes of larger diameter, which constitute the lower part of the piston chamber. Then, a simple circular extruded cut was performed starting from the newly generated hole bottom surface. The diameters measure respectively 31.00 mm and 17.50 mm. In picture 2.3 some other important dimensions are indicated too, such as the references for the axial dimensions of the chamber. In particular:

- $a = \frac{132}{2} - 39.55 = 26.45 \ mm$, length of the larger diameter cavity;
- $b = 39.55 - 23.95 = 15.60 \ mm$, length of the smaller diameter cavity.
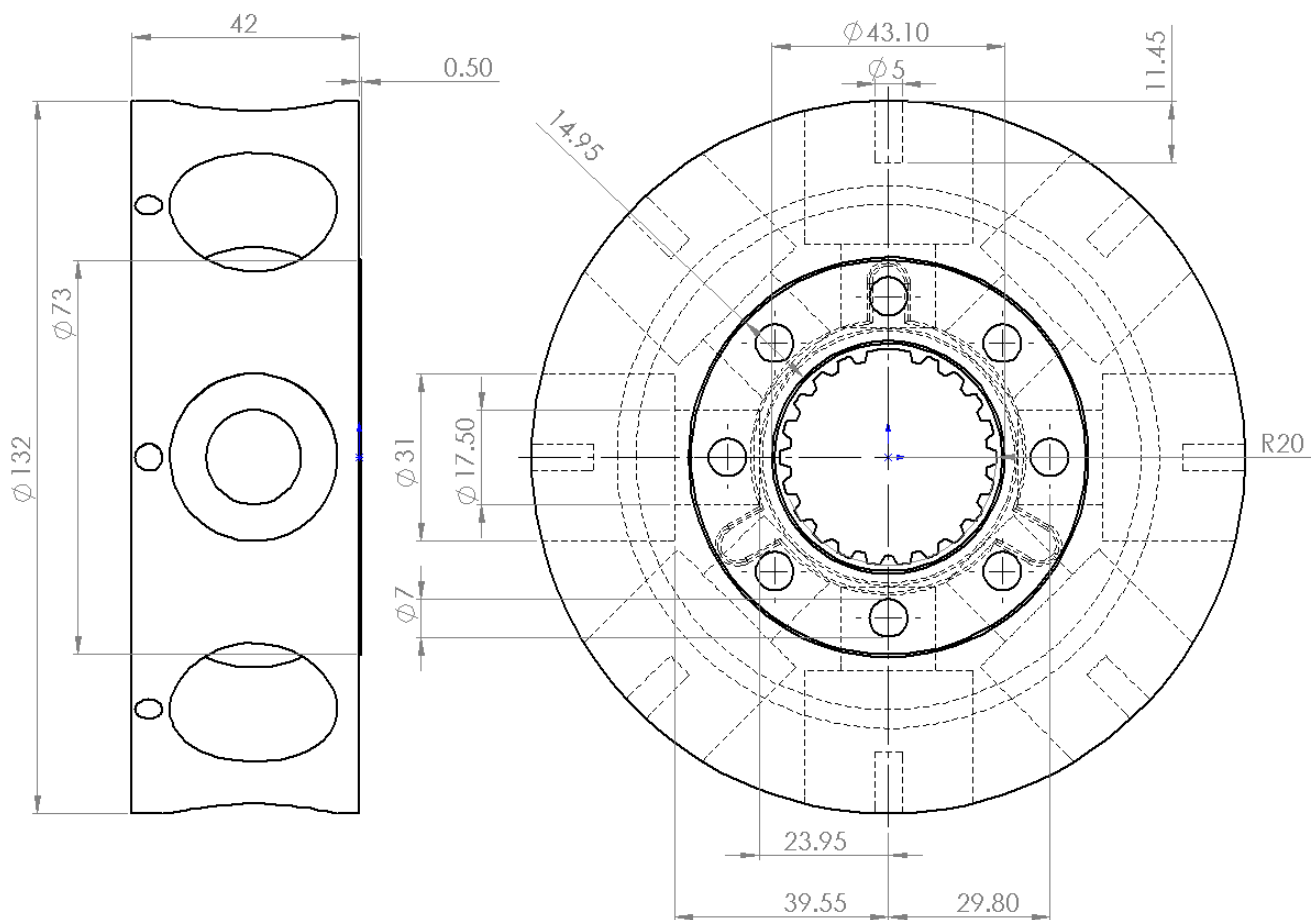
Figure 2.3 - Rotor 2D representation and its main geometrical properties

The smaller radial holes that can be seen next to the piston chamber cavities are devoted to the housing of clips whose task is the fixing and centring of the piston. In figure 2.4 there is the final representation of the rotor compared with the actual piece.
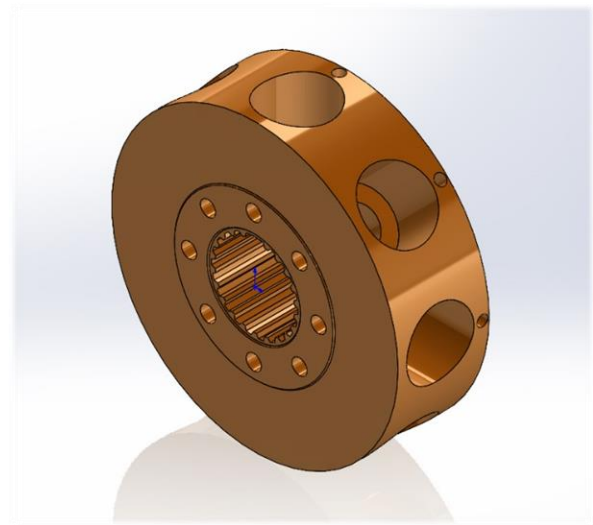
Figure 2.4 - Rotor 3D representation in comparison with the actual one

2.1.3 Piston

The pistons are assemblies composed of different elements. First of all, the rollers enable a correct contact with the cam profile. Both their diameter and axial length are 20.00 mm. The piston main structure consists into two cylindrical parts whose diameters coincide with the ones of the two chamber cavities. The part which contains the roller has a diameter of 31.00 mm and has two lateral spacers with the aim to maintain a proper position balancing of the roller itself. A bushing with a thickness of 1.00 mm is present between the roller and the piston body. The upper part has a diameter of 17.50 mm, but on two sides the material is cut so that the oil can flow into (or out from) the chamber. In this way a surface perpendicular to the oil feeding lines is created. The elastic ring is needed in order to limit as maximum as possible the leakages between piston and chamber walls. In the following picture the sketch with the main dimensional parameters is reported.
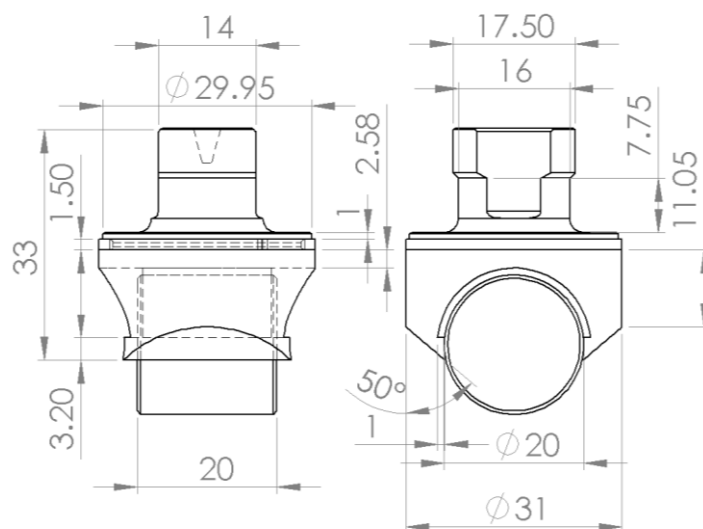
Figure 2.5 - Piston assembly 2D representation and its main geometrical properties
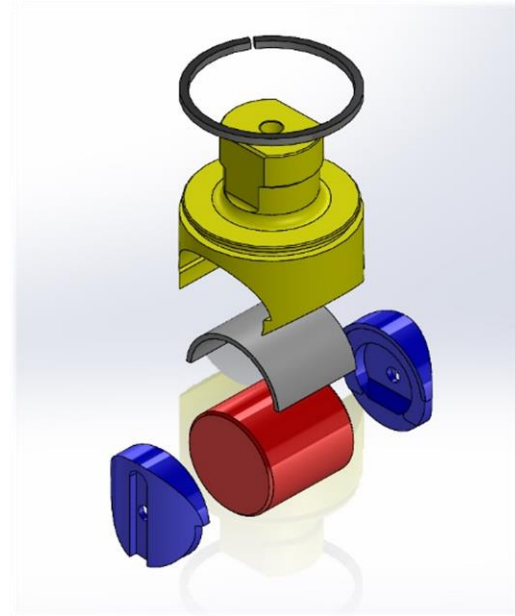
Figure 2.6 - Piston exploded assembly 3D representation in comparison with the actual one

2.1.4   Distribution

The distribution is the component which transmits the oil to the piston chamber during the inlet phase and that receives the oil from the chamber during the discharge phase. It is constituted by two circumferential layers which, thanks to the dedicated housing, generate two distinct oil volumes. One volume has oil under pressure (which is directed to the rotor), while the other one has discharged oil coming from the rotor and directed to the tank. These two layers communicate with the piston chambers through axial holes, whose diameter is 8.20 mm. There are in total twelve holes (six for each volume) and they are disposed in an alternated sequence along a circumference of radius 29.80 mm centred on the axis. The main structure has been obtained by drawing the profile and performing a revolved extrusion around the central axis with the *"Revolved Boss/Base"* command. The holes have been obtained by circular *"Extruded Cuts"* starting from the frontal face up to the desired surface. Their axial dimensions are 39.40 mm and 22.90 mm. The circular radial holes on the layer with the larger diameter have been obtained through the function *"Hole Wizard"* and have a radius of 4.30 mm. In the bottom surface there are also four spring housings for ensuring a correct contact between rotor and distribution and a pin housing to avoid any relative rotation between the distribution and its seat.
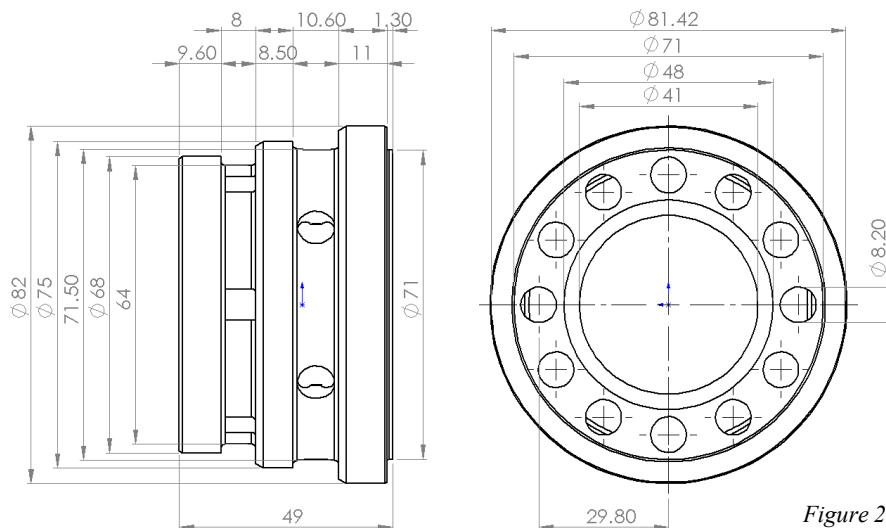
Figure 2.7 - Distribution 2D representation and its main geometrical properties
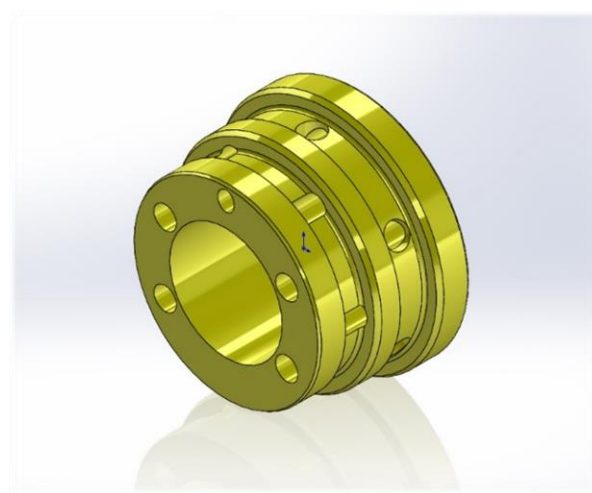
Figure 2.8 - Distribution 3D representation and comparison with the actual one

2.1.5 Distribution Flange

The distribution flange is the component dedicated to the mounting of the motor on the chassis of the desired vehicle and to the linking of the distribution with the rest of the hydraulic circuit, both the high-pressure and low-pressure lines. Its geometry, in combination with the distribution one, forms two independent oil volumes whose values are 22.00 and 14.00 cubic centimetres. Both these volumes communicate with the hydraulic circuit through two holes (P-T) in the distribution seat structure. They are generated from an inclined plane with an angle of 15.00° with respect to the main rotation axis and have a diameter equal to 18.50 mm, which gets further restricted to 11.50 mm. A third hole (Y) of diameter equal to 15.35 mm is present: it constitutes the drain line and communicates through a small axial duct of Ø7 with the internal volume of the motor (space between cam, rotor, distribution and distribution seat), so that the oil here accumulated due to leakages can flow back to the reservoir. In the front face the cam profile is present: it has been generated with the same procedure indicated in the dedicated section. On this surface it is mounted the cam itself, and the twelve Ø10.40 holes through which the screws pass enable a correct fixing avoiding any relative rotation between the two components. On the two external ears there are in total ten holes of diameter equal to 14.00 mm, needed for the motor mounting on the chassis.
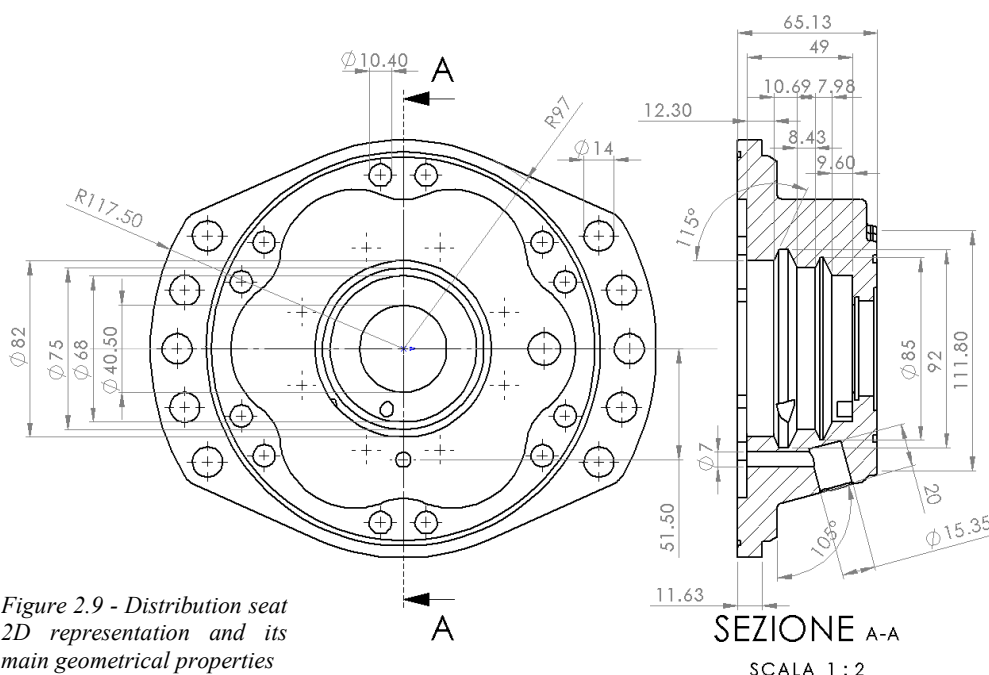
Figure 2.9 - Distribution seat 2D representation and its main geometrical properties
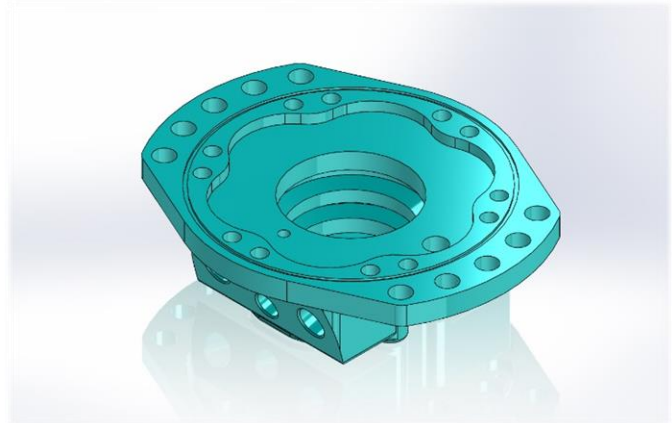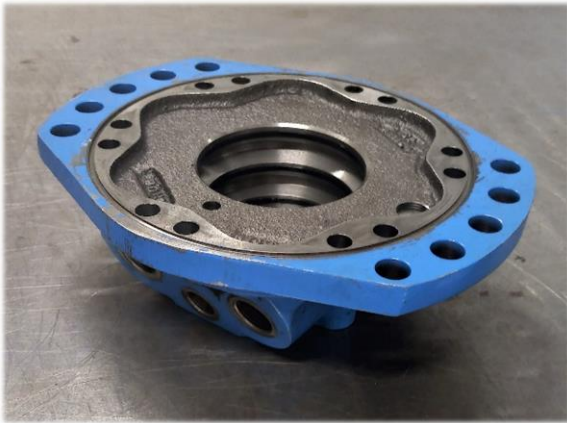
Figure 2.10 - Distribution seat 3D representation and comparison with the actual one. P, T and Y holes can be seen on the inclined surface

2.1.6 Shaft

The shaft is the element that enables the wheel rotation and so the vehicle motion. It is coupled to the rotor by means of a spline, so that the transmission of the torque produced by the pistons is possible. The shaft structure evolves axially with three different steps. From the base to the top, the diameters measure respectively 40.00, 45.00 and 50.00 mm and the axial lengths are 29.00, 19.00 and 57.00 mm. There are three retaining grooves for elastic rings, two of which fix the position of the shaft bearings. The remaining one, which is located in correspondence of the spline, fixes the relative axial position between shaft and rotor. The base is constituted by a flange with five equally spaced holes of diameter equal to 18.00 mm, constructed on a circumference of radius 69.00 mm. These holes aim to fix the flange to the vehicle's wheel. The flange's diameter is equal to 169.00 mm.
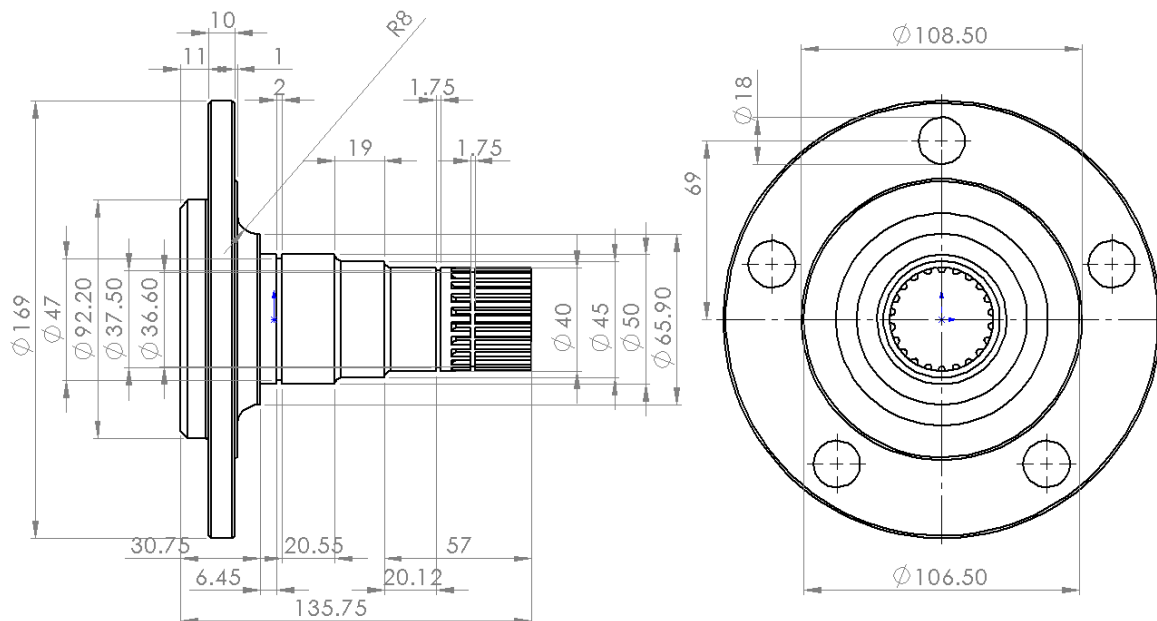
Figure 2.11 - Shaft 2D representation and its main geometrical properties

In figure 2.12 it is reported the 3D CAD modelling result confronted with the actual piece.
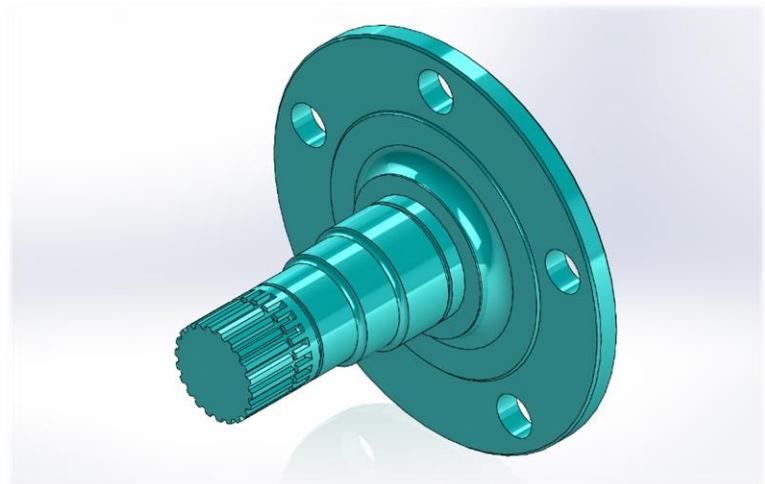
Figure 2.12 - Shaft 3D representation and comparison with the actual one

After all the components were reproduced (including bearings, screws, distribution seat lid, gasket and shaft cover) the total assembly has been constructed. While in general just standard mates have been used (such as concentricity or parallelism), for the piston-stator coupling it has been used the *"Cam"* mechanical mate, since in this way it has been also possible to create an animation of the working condition of the motor. Here it is reported a final confrontation, this time between the 3D assembly and the actual one.
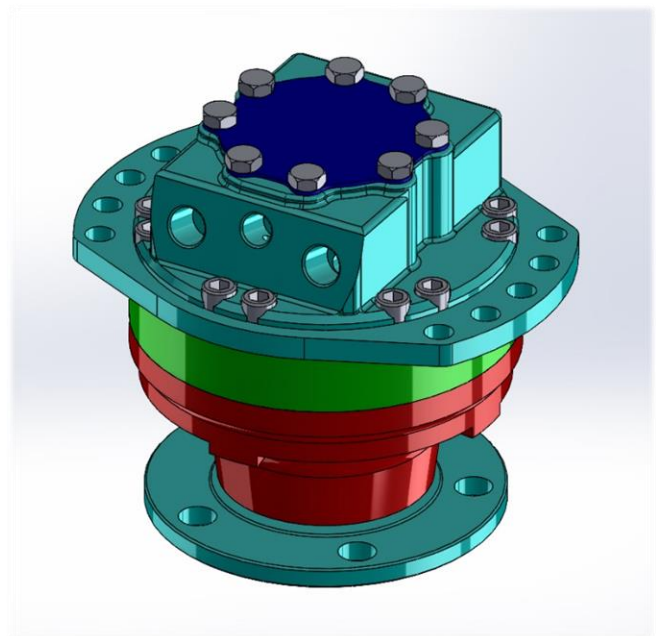
Figure 2.13 - Final 3D assembly and comparison with the actual motor

In figures 2.14, 2.15 and 2.16 there are reported some views of the assembly, so that all the components can be seen.
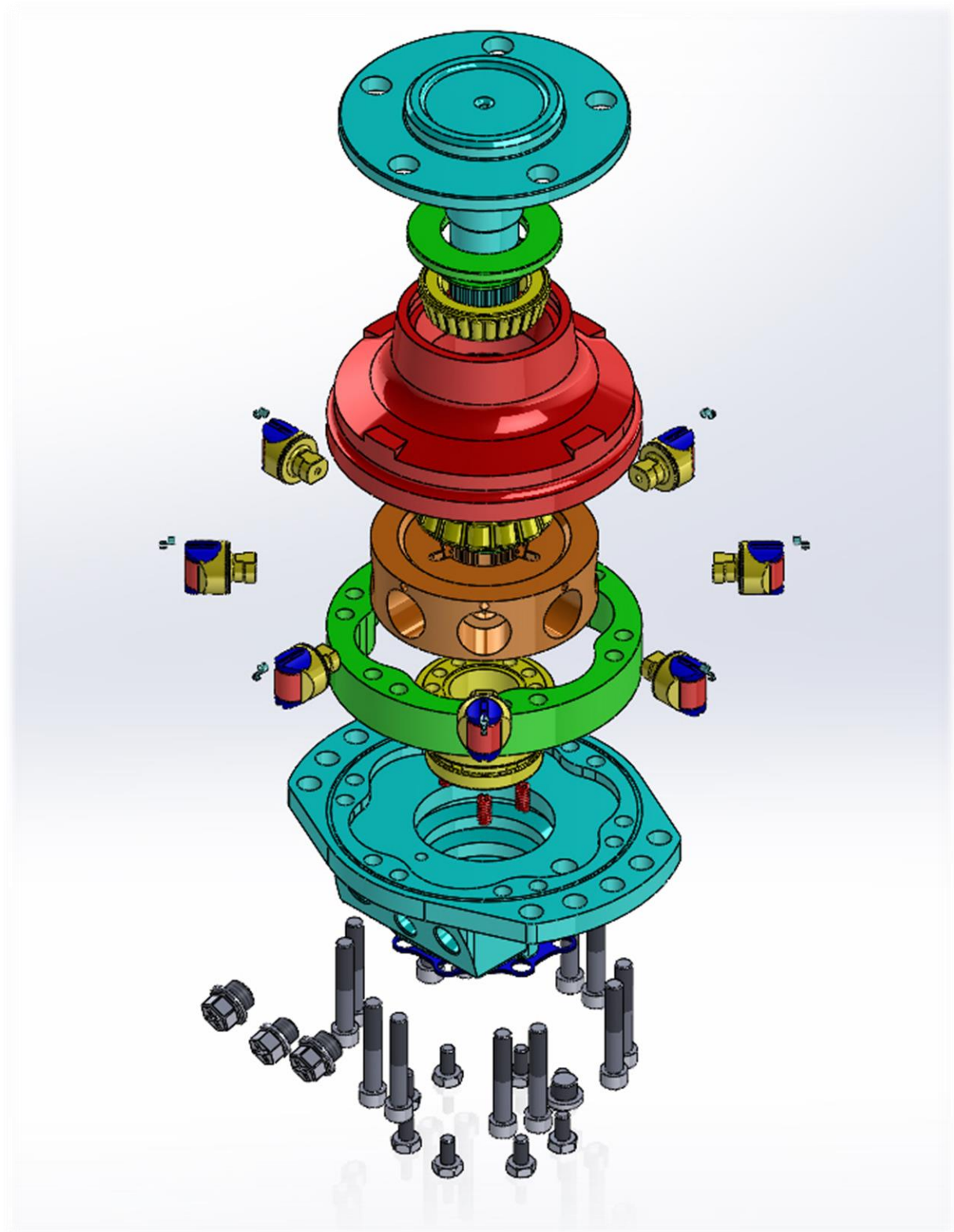
Figure 2.14 - Exploded isometric view of the radial piston hydraulic motor
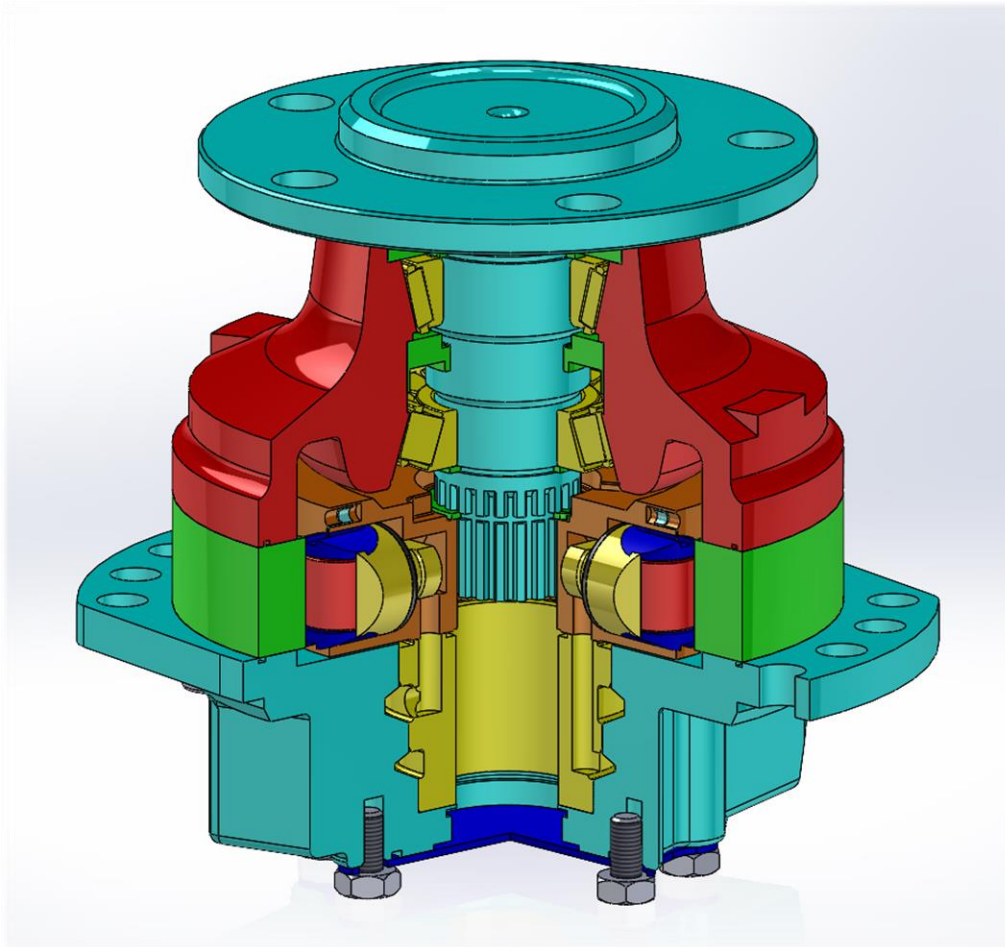
Figure 2.15 - Section view of the motor assembly
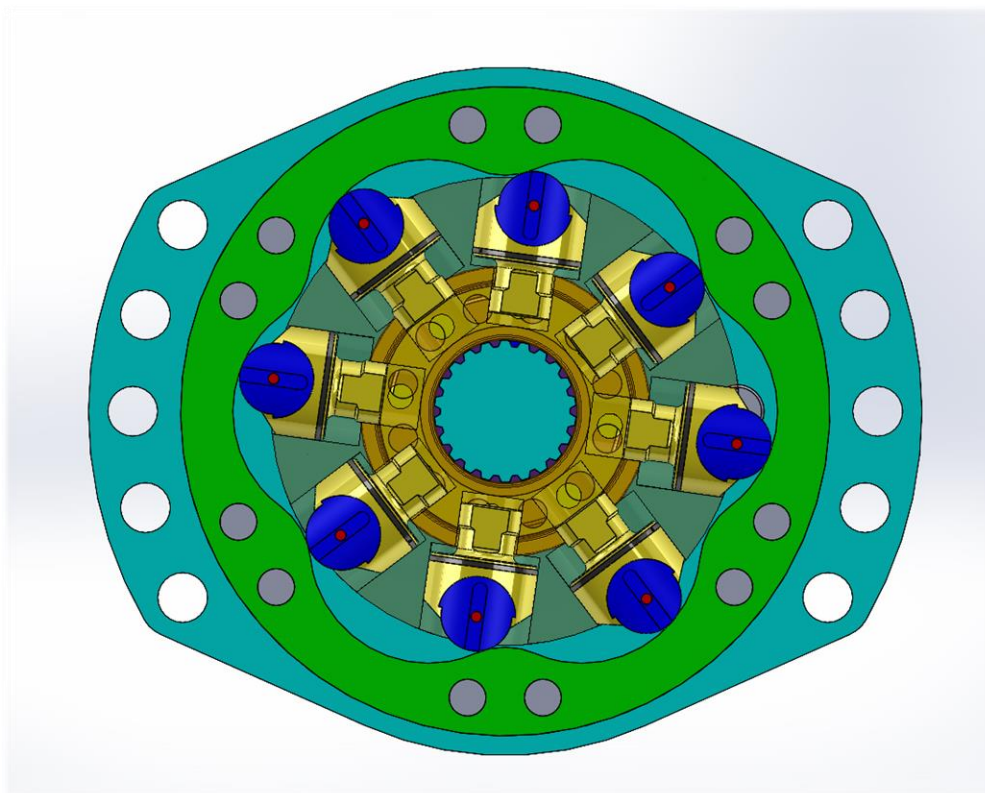
Figure 2.16 - Pistons view at a generic shaft angle position

2.2) Motion Analysis

After the total assembly reproduction, the next step has been the development of its proper animation. For this purpose, it has been used the *"Motion Analysis"* Add-In of *Solidworks®*. It has been sufficient to impose a rotary motion to the rotor to make the animation work successfully. This thanks to the various mates defined, and in particular:

- *"cam"* between pistons and stator;
- *"concentricity"* between pistons and pistons chambers;
- *"coincidence"* between rotor and shaft at spline level;
- stator taken as the fixed element of the assembly.

The animation can be found at this link: *"fprl.polito.it/teaching/animations/radial_piston_motor"*.
In *Motion Analysis* it is also possible to calculate some parameters as function of time. In this case the piston lift and the piston linear velocity has been calculated. Since a constant referential direction is needed for these evaluations, a reverse approach has been used: the rotational speed has been imposed on the stator instead of the rotor. In this way, the piston simply travels "up and down", maintaining constant the vertical reference axis. The piston lift has been calculated taking as a reference the lowest surface of the piston chamber.
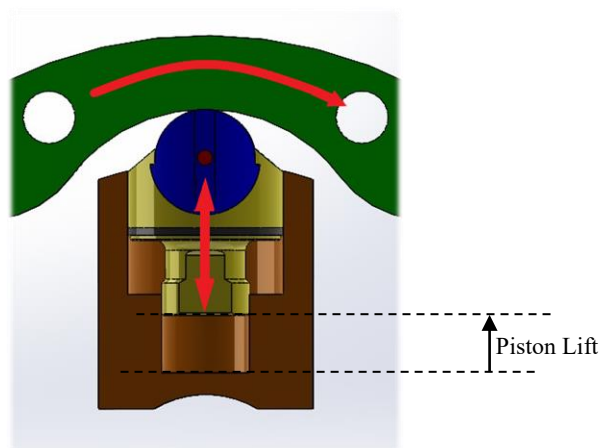
Figure 2.17 – Reverse approach: stator rotation, piston vertical translation and rotor standing still

Since time, rotational velocity and angle are strictly related, it is possible and preferable to evaluate lift and speed not as a function of time but as a function of rotation angle.
For a proper calculation it is necessary to impose a high enough resolution: for what concerns the piston lift a rotational speed of 4 rpm and 30 frames per second have been imposed. For what concerns the piston linear speed instead, a rotational speed of 60 rpm and 500 frames per second have been used.
The obtained results, in particular those ones about the piston lift, are of paramount importance for the simulation of the motor, since as it will be shown further they are the key to evaluate the volume of the piston chamber and the motor displacement.
In the figures 2.18 and 2.19 present in the next page the plots of the two investigated parameters are reported, as previously suggested, as a function of the rotation angle. The piston starts moving in both cases from the Bottom Dead Centre configuration.
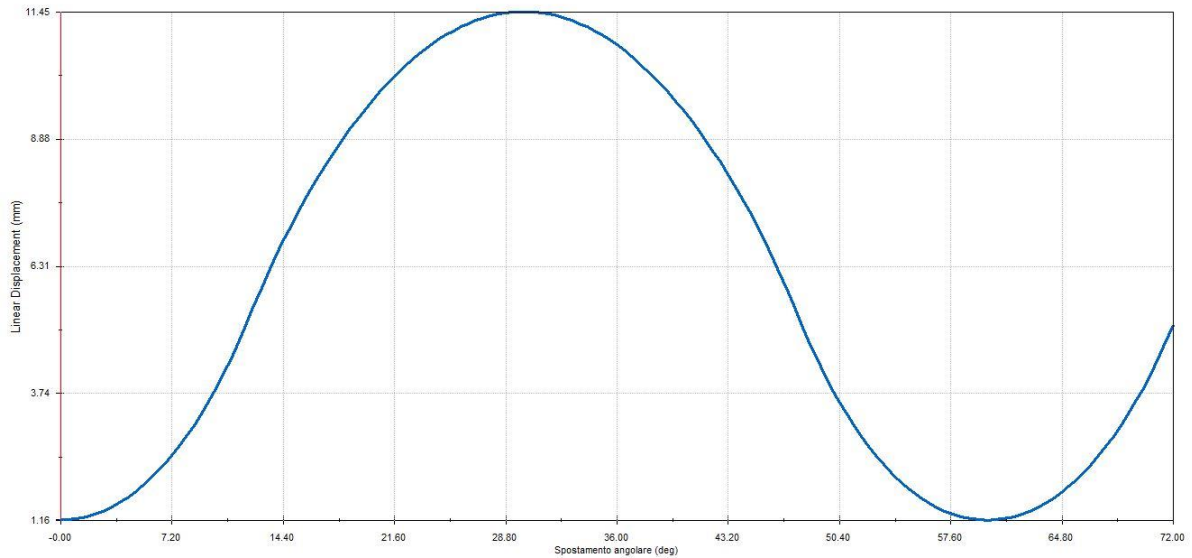
Figure 2.18 - Piston lift vs shaft angle

From the plot of the piston lift it can be seen the minimum and maximum position of the piston with respect to the bottom surface of the chamber.

- $Lift_{min} = 1.165\ mm$. This condition corresponds to the Bottom Dead Centre;
- $Lift_{max} = 11.455\ mm$. This condition corresponds to the Top Dead Centre.

Another important consideration that can be made regards the periodicity of the system. Being the cam profile composed of six equal lobes, the lift behaviour will be periodic with a periodicity of:

$$\frac{full\ rotation}{n_{lobes}} = \frac{360°}{6} = 60°.$$

The number of the lobes simply indicates how many work cycles are made in one full shaft revolution. As it will further be shown, also the volume vs angle trend will have a similar "sinusoidal-like" behaviour, with the same periodicity of the piston lift.
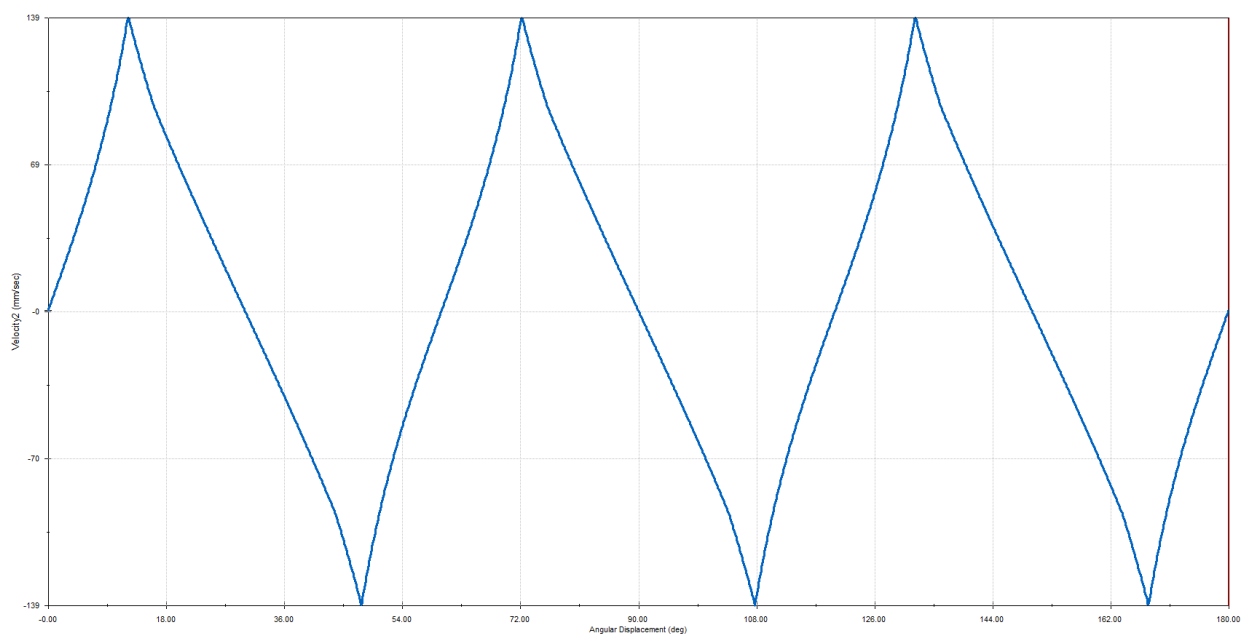
Figure 2.19 - Piston linear velocity vs shaft angle (@ ω=60 rpm)

In the plot of the figure 2.19, it can be seen the maximum and minimum linear speed of the piston. They are equal in modulus since the lobes are perfectly symmetric, and their value is 139 mm/s circa. The velocity gets to zero at $n * 30°$ and at $m * 60°$ (with $\{n, m\} = 1,2,3 ...$), since in these angle values the piston is respectively in the TDC and BDC position. The sign simply indicates the direction of the motion, due to the convention of the reference axis: if it is greater than zero then the piston is moving from BDC to TDC, and vice versa. The maximum speed in modulus is reached 12.33° after BDC and 17.67° after TDC (that is the same as 12.33 before BDC). This non-symmetrical speed trend between BDC and TDC (which is half the period) is due to the different radii of the circumferences on which the cam profile is built. Looking back at it in fact it can be seen that the circumference of diameter equal to 43.00 mm on which the BDC lays leads to a way steeper path with respect to the other one of Ø67.30.

3) Volume Evaluation

After the first evaluations about the piston lift have been performed by means of the *"Motion Analysis"* tool, the natural next step has been the piston chamber volume calculation. In fact, it is a fundamental parameter for the simulation, needed as an input by the *Amesim®* environment. The lift results obtained have been used in combination with the *"Flow Simulation"* function present in *Solidworks®*.

3.1) Data Extraction from the CAD

First of all, the points that constitutes the plot of the piston vertical displacement versus shaft rotation angle have been extracted and saved into the *.csv* format. It has been possible so to read these data in an *Excel®* file. In total, 150 points have been extrapolated in a range between 0° and 72°. Being the range of interest just the period, the values corresponding to an angle over $\vartheta_{BDC} = 60°$ have been discarded. Considering also that the cam path is symmetrical, it is sufficient to take into account the data between BDC and TDC and just to mirror them in the following cycle window. In conclusion, just the points between 0° and 30° have been considered, for a total amount of 64.

Once a dedicated assembly has been constructed again on *Solidworks®*, constituted just by the piston and by a limited portion of the rotor making sure to have the internal volume of the chamber completely isolated, a distance mate has been established between the lowest surface of the chamber and the piston one which faces it. This imposed distance corresponds to the piston lift, which this time has been used as an input data.
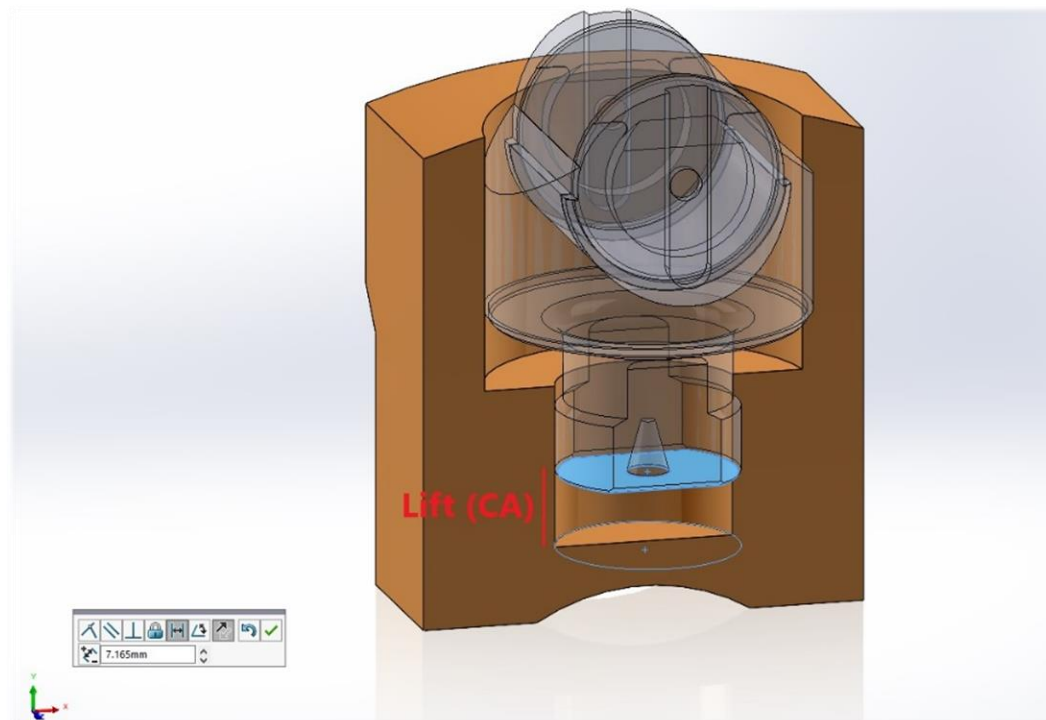
Figure 3.1 - Dedicated piston-rotor assembly and setting of the distance mate

Using the *Flow Simulation* environment, it is possible to obtain the 3D CAD model of the isolated volume of the chamber. The voice *"Check Geometry"* is first chosen, and after the selection of the *"internal"* analysis type it is sufficient to click on the *"create fluid body assembly"* option. After this quick procedure, clicking on *"check"*, some information about the volume is shown and, more importantly, the solid itself is automatically created. Here is reported an example for an intermediate working cycle condition.
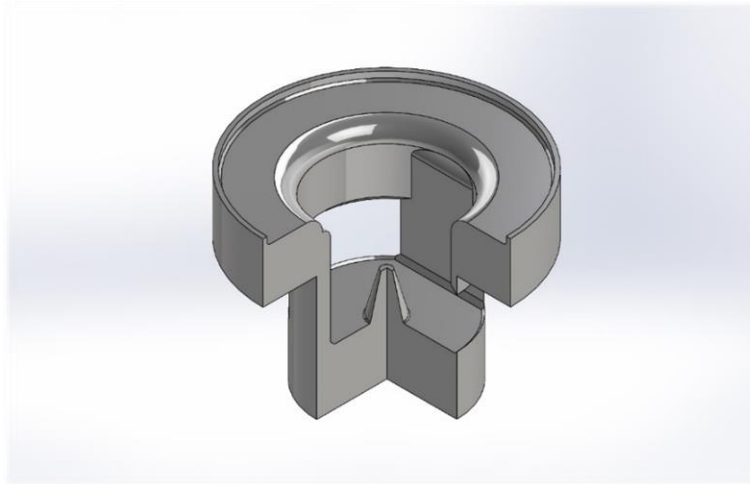
Figure 3.2 - Oil volume at piston lift = 7.1mm and angle = 14.88° aBDC

Once that the CAD of the oil inside the chamber is obtained, it is possible to know its volume just looking in the *"Evaluate"* section under the *"Mass Properties"* voice.

This simple procedure has been repeated as many times as many are the available data of the piston lift versus shaft angle, and for every iteration the volume value has been saved. In this way the trend of the piston chamber volume versus the shaft angle has been obtained for half the working cycle. As suggested before, in order to analyse the rest of the cycle (from $\vartheta_{TDC} = 30°$ to $\vartheta_{BDC} = 60°$), a simple mirroring of the results has been done. The maximum volume is found at TDC condition and is equal to 8904.99 mm^3, while the minimum one is located at BDC and is equal to 1139.19 mm^3. Here it is reported the plot of the volume vs angle constituted by the points obtained in this way.
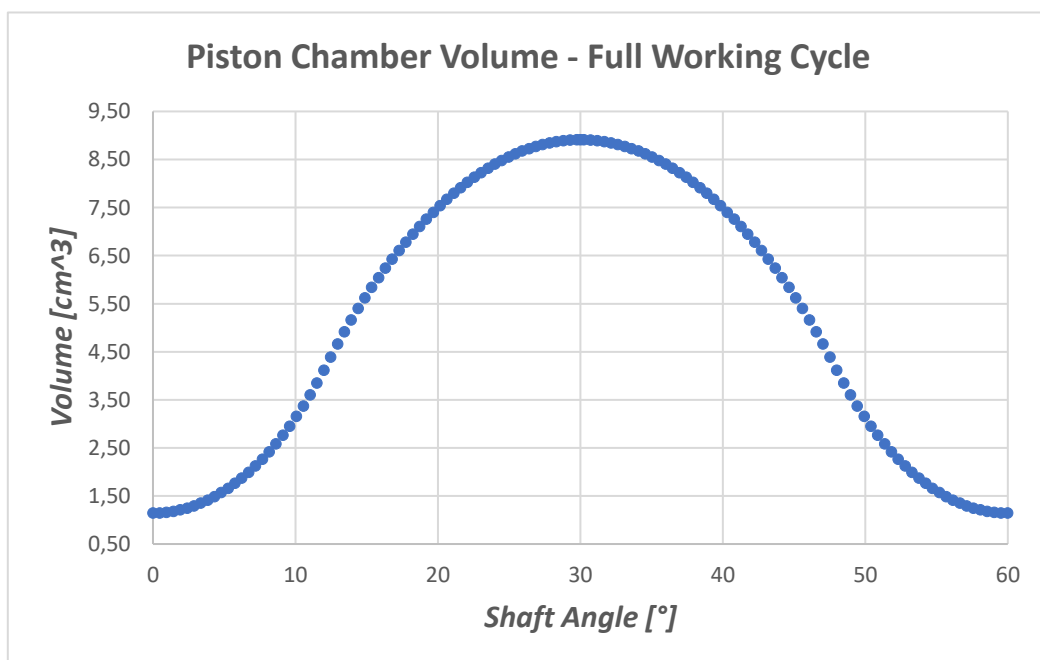
Figure 3.3 - Volume vs shaft angle trend obtained by means of Flow Simulation with an iterative procedure

3.2) Volume Interpolation

After the first volume examination has been done, in order to have a good simulation it has been necessary to increase the number of the data. For this reason, they have been exported from *Excel®* to *Matlab®*, where numerical approaches can be used. A code has been developed, in which the best way to represent this trend has been investigated comparing different types of interpolation and trying to recreate it with a sinusoidal function. The three interpolation methods experimented are:

- spline (piecewise cubic interpolation);
- pchip (shape-preserving piecewise cubic interpolation);
- polynomial (use of the command polyfit imposing the grade equal to 6).

The sinusoidal function has been imposed with the following parameters:

- period = T = 60°;
- amplitude equal to $A = \frac{V_{max} - V_{min}}{2}$;
- symmetry horizontal axis equal to $d = A + V_{min}$;

Hence, the sinusoidal function results equal to:

$$V(\vartheta) = -A * \cos\left(\frac{pi * \vartheta[deg]}{30}\right) + d \ (eq. \ 3.2.1)$$

Among these four possibilities the spline is the best one for a proper interpolation of the interested points, as it can be seen in the next picture.
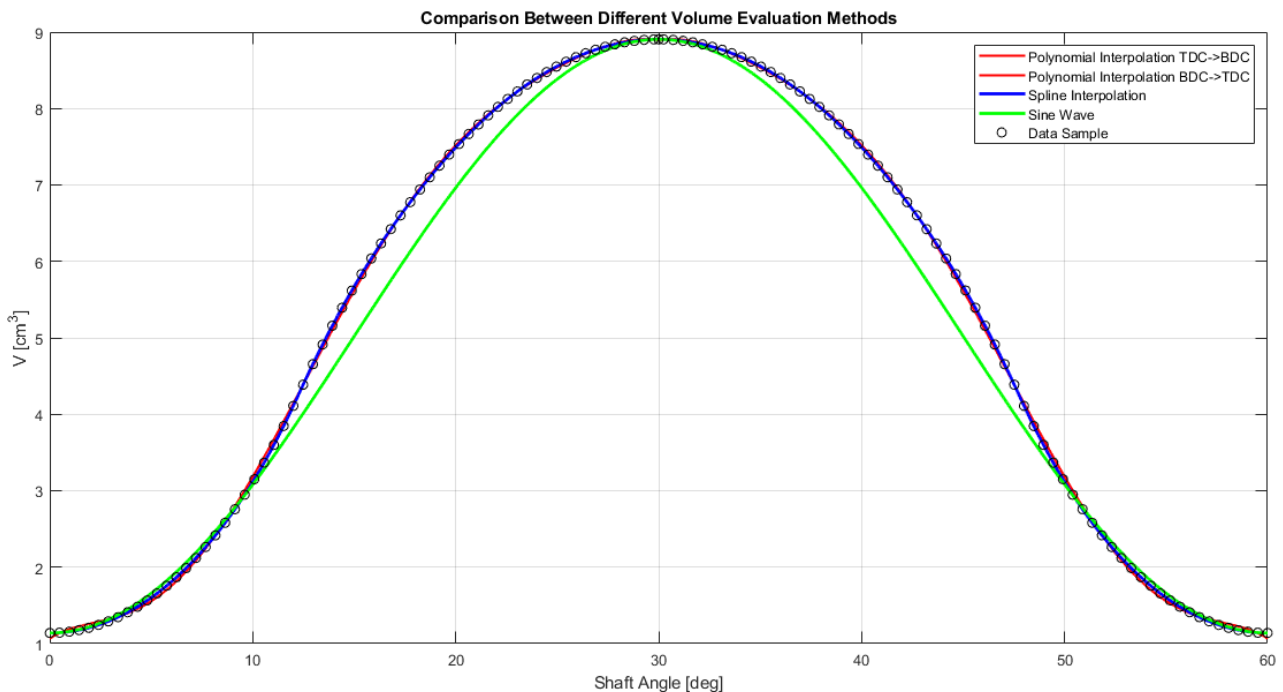
Figure 3.4 - Comparison between different interpolation methods of the data sample

A further consideration has to be made. If a single cycle is used for the interpolation, its extreme values, which in theory should be the minimum, are not identified in the same way by the algorithm: the interpolated minimum is located just after and before the extreme abscissa values. For this reason,

in order to obtain better results, a single *spline* interpolation has been done over a dataset of three full working cycles. In this way just the values at the beginning of the first cycle and at the end of the last one have been corrugated, leaving the middle one under the best possible shape. So, the final interpolation on three cycles have been performed creating a total number of 180,000 points (60,000 for each cycle), and just the ones of the second cycle have been considered for the simulation. Here is reported part of the simple *Matlab®* code used for the procedure.

```matlab
clear all
clc

%% 1) Volume Interpolation

SA=xlsread('VariazioneVolume.xlsx', 'C4:C382');        %Shaft angular position
Volume=xlsread('VariazioneVolume.xlsx', 'H4:H382');    %Chamber Volume in cm^3
X=0:0.001:180;                                         %Angle in deg
int=interp1(SA,Volume,X,'spline');                     %Volume Interpolation

X_2c=X(1:60001);                                       %shaft angle rescaling
int_2c=int(60001:120001);                              %just 2nd cycle
```

Here is shown the final volume versus shaft angle representation, obtained with the procedure previously explained.
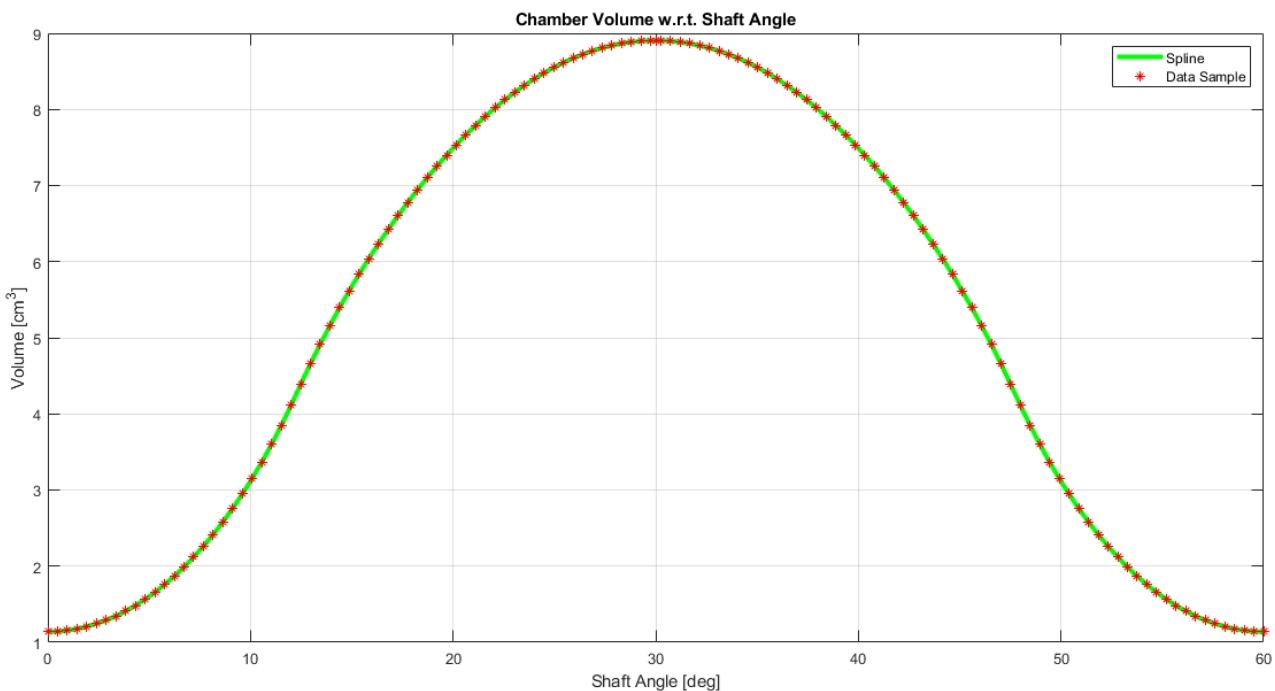
Figure 3.5 - Piston chamber volume variation with respect to shaft angle

This procedure has also been done for what concerns the piston lift vs shaft angle curve. Obviously even in this case the best interpolation method remains the *"spline"* one. Also this time the total number of points is equal to 180,000 and just the second cycle is taken into account for what concerns the accuracy of the results. In the next page it is reported the final plot of the piston lift versus shaft angle.
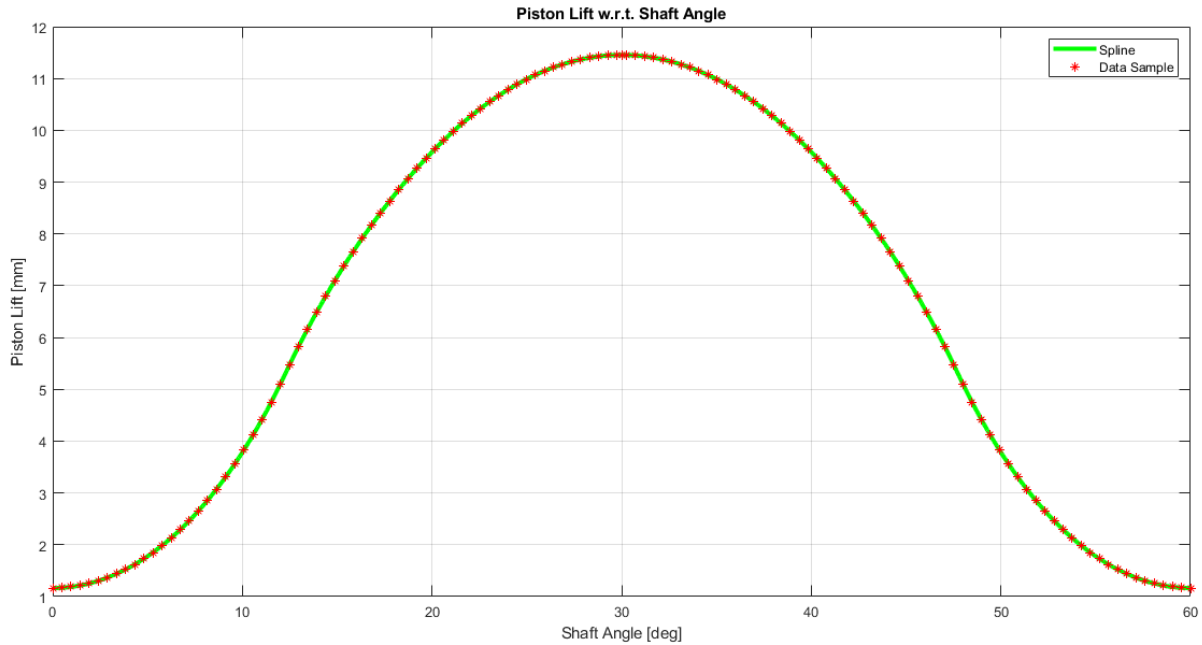
Figure 3.6 - Piston lift vs shaft angle plot

3.3) *Volume Derivative Calculation*

Another fundamental parameter needed for the simulation is the volume derivative with respect to the shaft angle. Its calculation has been done on *Matlab®*, obviously taking as a starting point the evolution of the volume over the shaft angle. Two possible methods have been tested, and both of them has correctly led to the same result.

- A) Use of the command *"gradient"*.
- B) Implementation inside a *for loop* of simple calculations based on the derivative definition as "incremental ratio".

Here is the simple script portion dedicated to the derivative calculation.

```
%% 2.1) Spline Derivative with gradient command

dVoldCA=gradient(int,0.001);          %derivative of the interpolated points
dVoldCA_2c=dVoldCA(60001:120001);     %just 2nd cycle

%% 2.2) Spline Derivative calculated with incremental ratio

k=length(X);
for i=1:(k)
    if i==k
        delta=int(1)-int(i);
    else
        delta=int(i+1)-int(i);
    end
    derivata(i)=delta/0.001;
    i=i+1;
end
```

Here is reported the plot derived from the previous calculations.
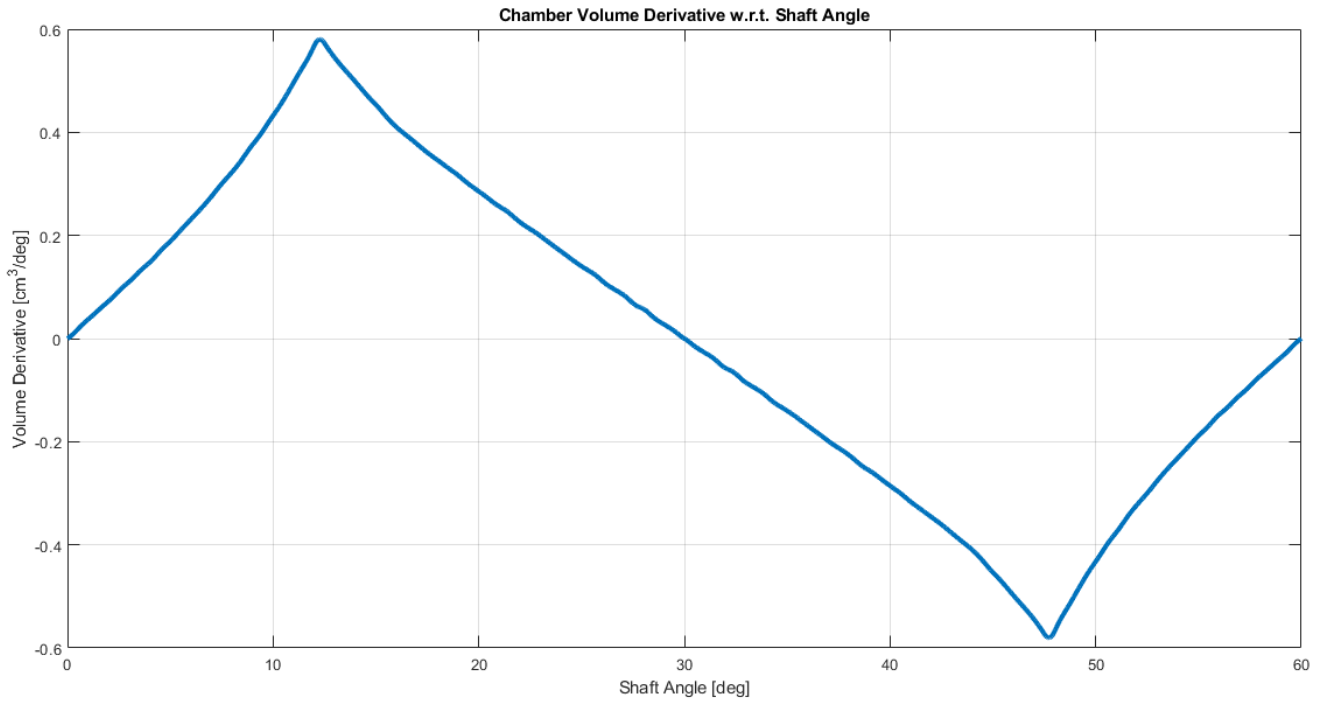
Figure 3.7 - Volume derivative with respect to shaft angle

It can be seen that the volume derivative trend recalls a lot the one of the piston linear speed, seen in figure 2.19. The plot gets to zero when the piston is at Top and Bottom Dead Centre, while it reaches its maximum at ~12.3° aBDC and minimum at ~17.7° aTDC. Their value in modulus is equal to $0.5804 \frac{cm^3}{deg}$.

A better visualization can be made putting both the trends of the volume and volume derivative onto the same plot.
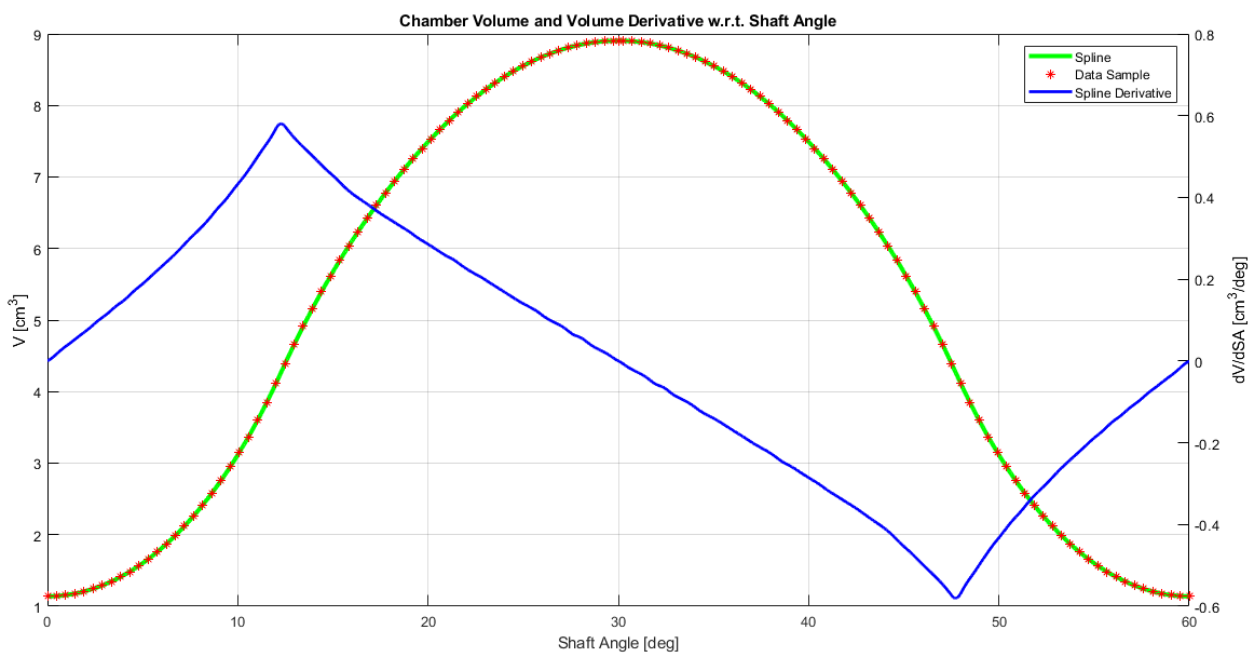
Figure 3.8 - Volume and volume derivative with respect to shaft angle

3.4) Comparison with Theoretical Calculations

In order to check the reliability of the results, the ones obtained in the previous two paragraphs have been confronted with calculations directly derived from the theoretical formulations. Due to the possible reversibility of the hydraulic machines, the comparison has been made hypotizing both pump and motor working conditions. All the procedure has been done on *Matlab®*.
First of all, the displacement of the hydraulic machine has been calculated:

$$V = N * V_0 * n_c = 8 * (8.90499 - 1.13919) * 6 = 372.7584 \frac{cm^3}{rev} \text{ (eq. 3.4.1),}$$

Where N is the pistons number, V_0 is the unit displacement and n_c is the number of cycles per shaft revolution. The result obtained is in line with the values declared by the constructor, differing for some units due to some little measurement uncertainties.
Starting from the volume derivative it has been possible to calculate for each piston the parameter *F(θ)*, already presented in chapter 1, paying attention to the angular phasing between them of 360°/8 = 45°. Just for a brief recall,

$$F_i(\vartheta) = \begin{cases} -\frac{dV_i}{d\vartheta} & if \ \frac{dV_i}{d\vartheta} < 0 \\ 0 \ if \ \frac{dV_i}{d\vartheta} \geq 0 \end{cases} \text{ (pump working condition)}$$

$$F(\vartheta) = \sum_{i=1}^{8} F_i(\vartheta).$$

Thanks to the particular symmetry of the system, the parameter *F(θ)* is equal in both motor and pump working conditions. Here is shown the plot in which also the mean of the parameter F has been identified.
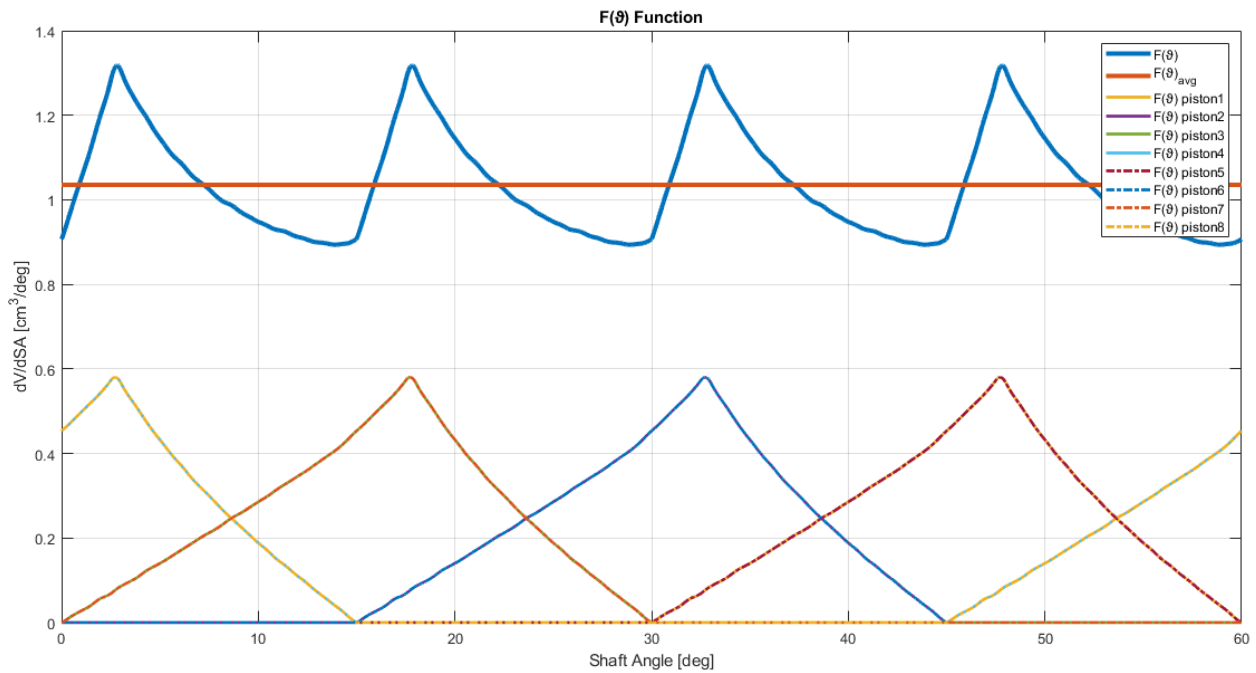
Figure 3.9 - F(ϑ) parameter calculation

3.4.1 Pump Working Condition Calculations

In pump working condition the hydraulic machine rotates thanks to the action of a prime mover (for example an electric motor), and as a result it generates a certain amount of flow rate. The calculation has been made considering the displacement previously shown and a constant input velocity equal to $\omega = 150 \ rpm$.
The theoretical procedure establishes that the ideal generated flow rate is equal to:

$$Q_{th} = V * \omega = 55.9138 \frac{L}{min} \ (eq. \ 3.4.2)$$

If the F function is taken into account instead, the instantaneous and average flow rate can be calculated in this way:

$$\begin{cases} Q_{inst} = F(\vartheta) * \omega \\ Q_{avg} = \overline{Q_{inst}} = \overline{F(\vartheta) * \omega} = F_{avg} * \omega \end{cases} \ (eq. \ 3.4.3)$$

The average flow rate obtained from the instantaneous values of the parameter $F(\vartheta)$, which is in turn derived from the volume derivative with respect to the shaft angle, is equal to 55.9136 L/min. So, the two methods have led to very similar result, which can be reasonably approximated as equivalent. Here is reported the script used in *Matlab®*. All the i-th piston values of $F(\vartheta)$ have been written on a dedicated *Excel®* file used as an input.

```
clear all
clc

x=xlsread('SfasamentoPistoni2.xlsx', 'B3:B60003');  %Shaft Angle
p1=xlsread('SfasamentoPistoni2.xlsx', 'D3:D60003'); %F(ϑ) piston 1
p2=xlsread('SfasamentoPistoni2.xlsx', 'G3:G60003'); %F(ϑ) piston 2
p3=xlsread('SfasamentoPistoni2.xlsx', 'F3:F60003'); %F(ϑ) piston 3
p4=xlsread('SfasamentoPistoni2.xlsx', 'E3:E60003'); %F(ϑ) piston 4
p5=xlsread('SfasamentoPistoni2.xlsx', 'H3:H60003'); %F(ϑ) piston 5
p6=xlsread('SfasamentoPistoni2.xlsx', 'K3:K60003'); %F(ϑ) piston 6
p7=xlsread('SfasamentoPistoni2.xlsx', 'J3:J60003'); %F(ϑ) piston 7
p8=xlsread('SfasamentoPistoni2.xlsx', 'I3:I60003'); %F(ϑ) piston 8
F=p1+p2+p3+p4+p5+p6+p7+p8;

k=length(x);
V_max=8.90499;                      %[cm^3]
V_min=1.13919;                      %[cm^3]
cycles=6;
V_cil=n*(V_max-V_min)*cycles;  %[cm^3/rev]

%% Pump Working Condition
rpm=150;                        %[rpm]
Q_inst=rpm*360*F/1000;          %Instantaneous Flow Rate [l/min]
Q_1=V_cil/1000*rpm;             %Flow Rate from Displacement [l/min]

for i=1:k
    Q_der(i)=mean(Q_inst);      %Average Flow Rate from Instantaneous One [l/min]
    Q_displ(i)=Q_1;
end
```

Here is finally reported the plot generated from these calculations.
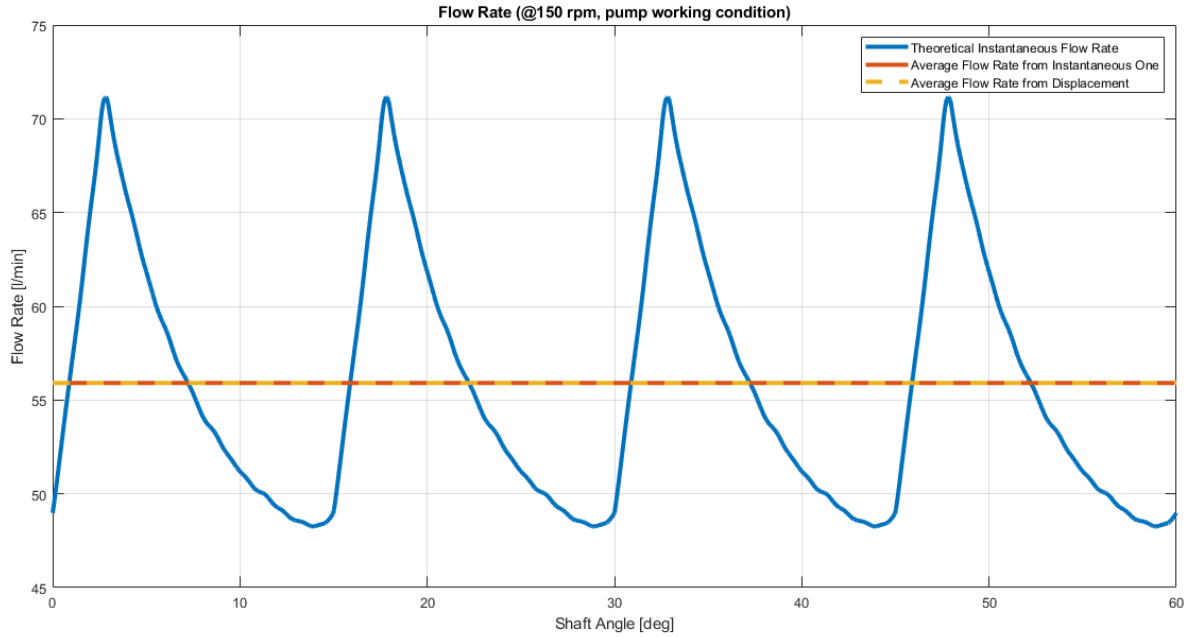
Figure 3.10 - Flow rate with pump working conditions @150rpm

From the plot it can be seen that there is a quite high flow rate ripple: the instantaneous value oscillates between 48.26 and 71.17 litres per minute. This is due to the piston and stator coupling (for example depending on the number of pistons and on the number of cycles per shaft revolution). It is interesting to note that the oscillation period of the total emitted flow rate is one fourth of the one of the piston chamber volume (15° for the first one and 60° for the latter). This is due to the fact that there are 8 pistons, which form four couples working at the same time in four different working conditions. Anyway this aspect is going to be furtherly investigated in chapter 6.

3.4.2 Motor Working Condition Calculations

In motor working condition the hydraulic machine is fed by a pressurized circuit (pump and valves) with a certain amount of flow rate which applies a rotation to the shaft. The calculation has been made considering the displacement previously shown and a constant input flow rate equal to $Q_{input} = 50 \frac{L}{min}$.

Similarly to what has been done in the previous section, the theoretical procedure establishes that the generated shaft rotational speed is equal to:

$$\omega_{th} = \frac{Q_{input}}{V} = 134.14 \ rpm \ (eq. \ 3.4.4)$$

If the F function is taken into account instead, the instantaneous and average rotational speed can be calculated in this way:

$$\begin{cases} \omega_{inst} = \frac{Q_{input}}{F(\vartheta)} \\ \omega_{avg} = \overline{\omega_{inst}} = \overline{(\frac{Q_{input}}{F(\vartheta)})} = Q_{input} * \overline{\left(\frac{1}{F(\vartheta)}\right)} = Q_{inupt} * \left(\frac{1}{F}\right)_{avg} \end{cases} (eq. \ 3.4.5)$$

The average rotational speed obtained from the instantaneous values of the parameter $1/F(\vartheta)$, is equal to 136.02 rpm. This time the two methods have led to two results with a weaker similarity with respect to the ones of the pump working condition. It seems that the theoretical procedure which uses the displacement slightly underestimates the result obtained by the instantaneous velocity. In the appendix A a possible reason for this little discrepancy is explained. Here is reported the script used in *Matlab®*.

```matlab
clear all
clc

x=xlsread('SfasamentoPistoni2.xlsx', 'B3:B60003');  %Shaft Angle
p1=xlsread('SfasamentoPistoni2.xlsx', 'D3:D60003'); %F(ϑ) piston 1
p2=xlsread('SfasamentoPistoni2.xlsx', 'G3:G60003'); %F(ϑ) piston 2
p3=xlsread('SfasamentoPistoni2.xlsx', 'F3:F60003'); %F(ϑ) piston 3
p4=xlsread('SfasamentoPistoni2.xlsx', 'E3:E60003'); %F(ϑ) piston 4
p5=xlsread('SfasamentoPistoni2.xlsx', 'H3:H60003'); %F(ϑ) piston 5
p6=xlsread('SfasamentoPistoni2.xlsx', 'K3:K60003'); %F(ϑ) piston 6
p7=xlsread('SfasamentoPistoni2.xlsx', 'J3:J60003'); %F(ϑ) piston 7
p8=xlsread('SfasamentoPistoni2.xlsx', 'I3:I60003'); %F(ϑ) piston 8
F=p1+p2+p3+p4+p5+p6+p7+p8;

k=length(x);
V_max=8.90499;                      %[cm^3]
V_min=1.13919;                      %[cm^3]
cycles=6;
V_cil=n*(V_max-V_min)*cycles;       %[cm^3/rev]


%% Motor working condition
Q_input=50;                         %[l/min]
omega_inst=1000/360*Q_input./F;     %theoretical instantaneous velocity [rpm]
w_0=Q_input*1000/V_cil;             %velocity calculated from displacement [rpm]

for i=1:k
    avg_omega(i)=mean(omega_inst);  %Average velocity from inst. one [rpm]
    w(i)=w_0;
end
```
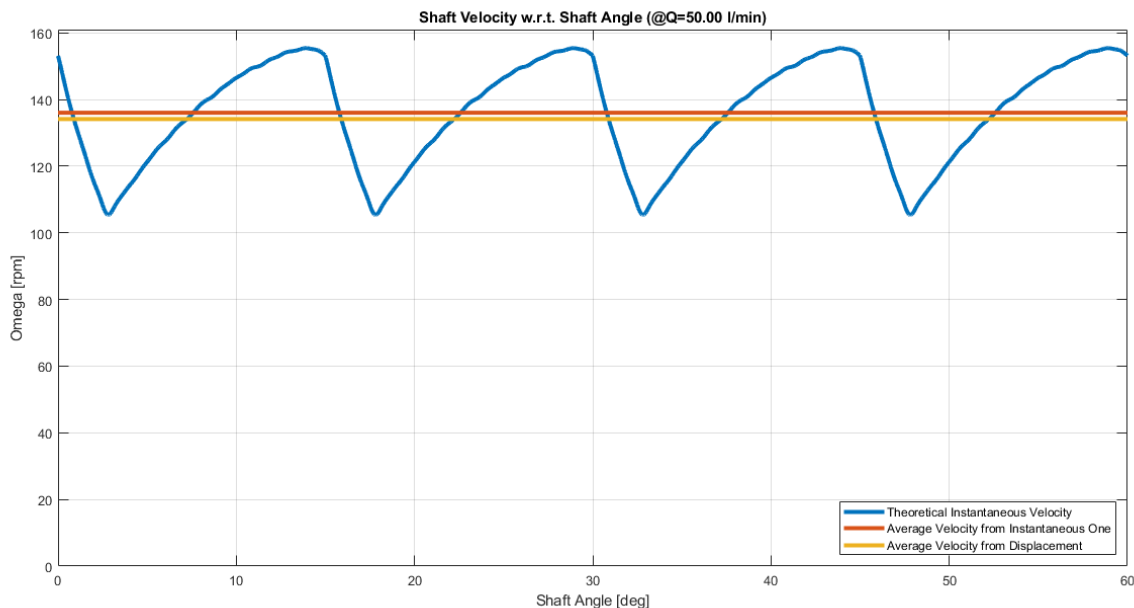

Figure 3.11 - Shaft rotational speed in motor working condition (@50 L/min)

From this plot it can be seen again that there is a quite high ripple. The maximum and minimum velocities are respectively equal to 155.41 rpm and 105.39 rpm. The oscillation period is equal to one fourth of the one of the cycle, as it was for the flow rate in pump working condition: the same considerations can be made.

4) Flow Areas Evaluation

Before proceeding with the simulation, another important parameter is still needed to be analysed: the evolution of the flow areas with respect to the shaft angle. In order to comprehend it, it is first necessary to point out the relative position of the distribution with respect to the cam. As said in chapter 2.1, the piston chambers communicate with the high-pressure and low-pressure lines through an alternated sequence of twelve axial holes present in the distribution. These axial ducts are positioned in such a way that the Bottom Dead Centre and Top Dead Centre positions are under isolated volumes conditions. In other words, when the piston is in these states the piston chamber does not communicate neither with the high nor with the low-pressure lines.
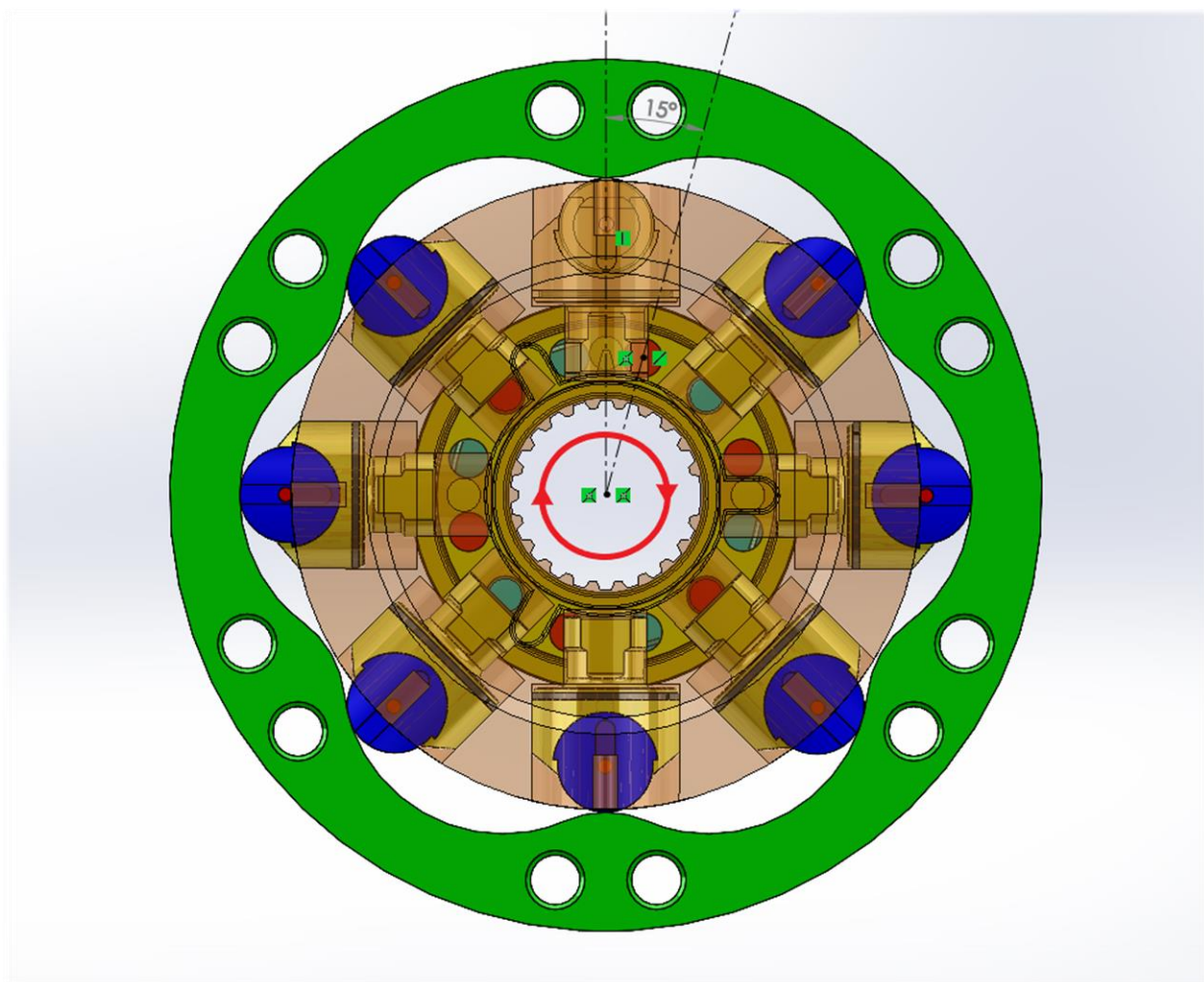
Figure 4.1 - Cam and distribution relative position

In figure 4.1 it is represented a view composed of cam, rotor (seen in transparency), pistons and distribution. The axial ducts communicating with the high-pressure chamber are in red, while in light blue there are the ones that communicate with the low-pressure chamber. It can be seen that when the piston is at TDC or BDC the piston chamber is isolated. The circular red line indicates the verse of rotation. From BDC to TDC the piston is moved by the oil that enters into its chamber and follows the descending cam path. Between TDC and BDC instead, the piston is forced to follow the ascending section of the stator profile and, by doing so, it discharges the oil from its chamber. The direction of

rotation can be changed by means of a directional control valve, capable to invert the oil feeding of the two constant distribution volumes. The two construction lines present in the picture represent the main symmetry axes of the distribution and of the stator; they have a relative angular position of 15°.

4.1) Data Extraction from the CAD

In order to obtain the trend of the flow areas with respect to the shaft angle, a dedicated assembly constituted just by the rotor and the distribution has been made in *Solidworks®*. Looking at it from the frontal view and entering into the *"sketch"* mode, it has been possible to draw circumferences taking as a reference the ones of the piston chamber and distribution ducts already present. After their drawing then, by means of the command *"Trim Entities"*, just the surface of their intersection (which is the actual flow area) has been maintained. Ultimately, thanks to the function *"Evaluate"*, the value of this area has been visualized and saved into an *Excel®* file. This procedure has been conducted with regular intervals of angular relative position between the two motor components. 78 points have been collected between the Bottom Dead Centre and Top Dead Centre; for the successive half cycle it has been simply sufficient to copy the results. Here is visually reported the procedure just explained.
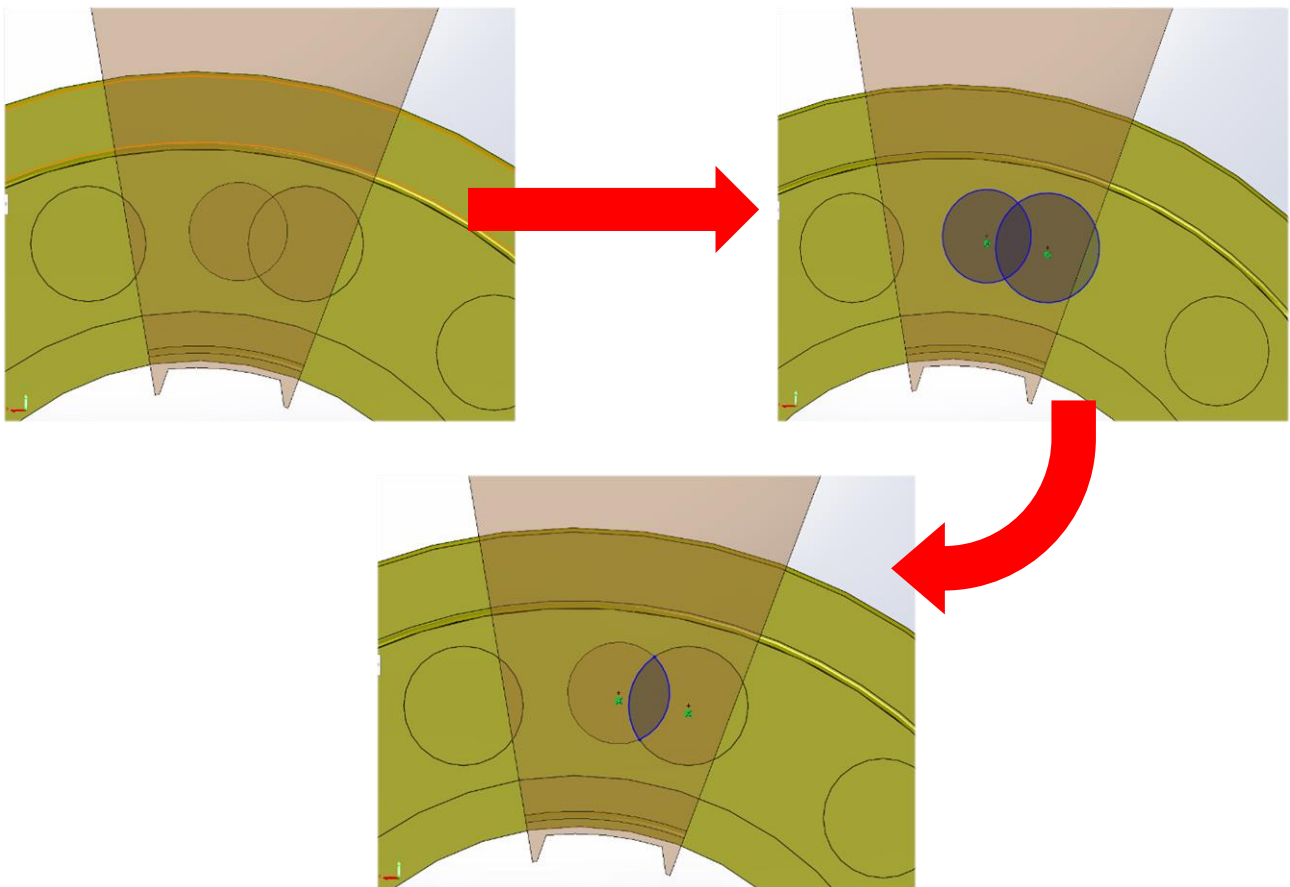
Figure 4.2 - Flow area definition for a generic relative angular position

The point where the flow area starts to increase from zero and the one where it goes back again to zero have been specifically searched by imposing a tangency condition to the circumferences of the rotor and the distribution. They appear two times each in every entire working cycle at relative angular displacement equal to 0.34° aBDC and 29.66°aBDC for the inlet phase and 0.34°aTDC and 29.66° aTDC for the outlet phase.

Here is reported the plot generated by the points of the flow areas collected in *Excel®*:
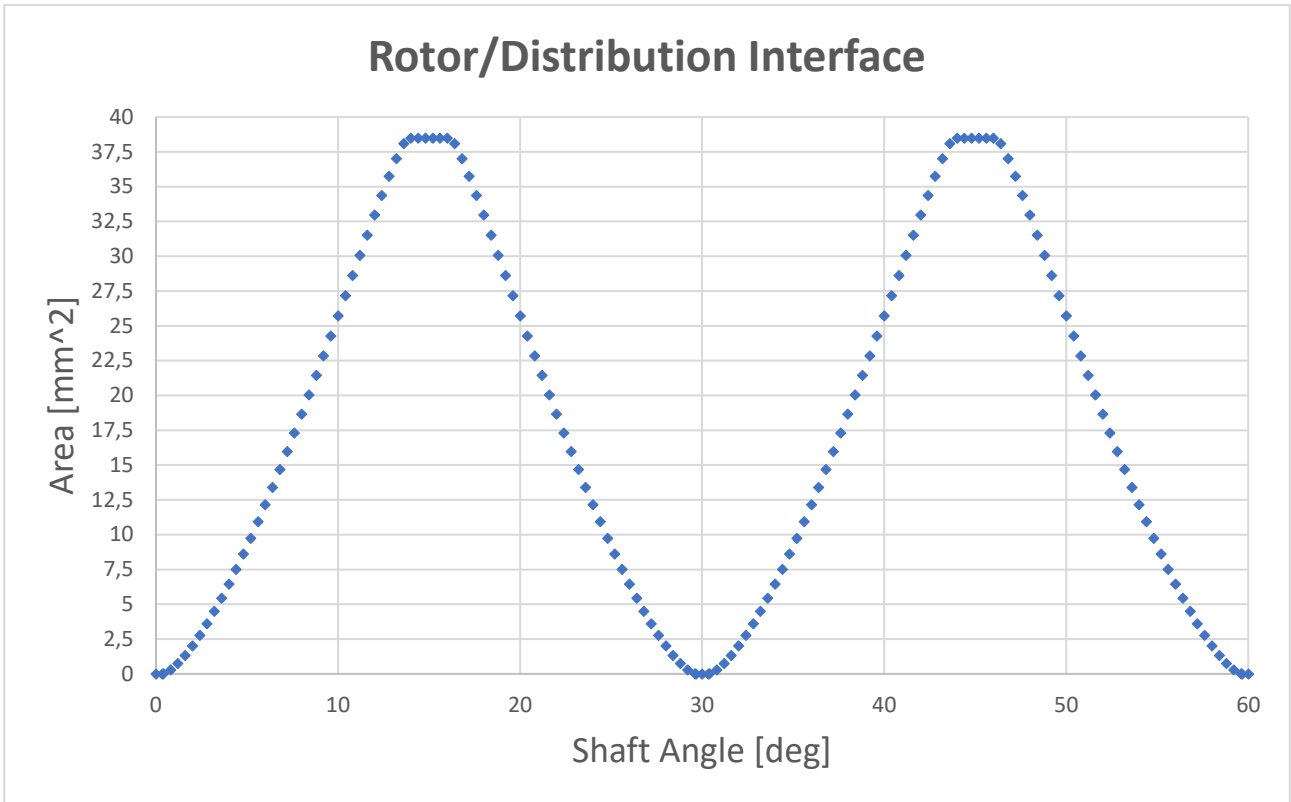
Figure 4.3 - Flow area vs shaft angle in the rotor/distribution interface

The next important step has been the division of the trend into inlet and outlet flow areas and the interpolation of these results in order to get a higher number of points to use as an input for the simulation. Since the distribution ducts are alternatively connected to the two constant volume chambers, it is reasonable to think that in order to make the subdivision of the two phases it is sufficient to take just half cycle for each one and to impose zero flow area to the other half.

4.2) Inlet Flow Area

The interpolation of the *Excel®* data has been done on *Matlab®*, just as for the volume ones. The *"spline"* typology has been chosen again, but this time particular attention has been paid for some particular intervals of the shaft angle. There are indeed some windows in which the flow area value is constant and equal to the minimum or to the maximum. In the case of the inlet flow area, the minimum (which is equal to $0\ mm^2$, situation in which the piston chamber is completely isolated from this flow area) is present inside the working cycle for the angular position values $0° \leq \vartheta \leq 0.34°$ and for $29.66° \leq \vartheta \leq 60°$. The maximum flow area, which is equal to $38.48\ mm^2$, is found for $14° \leq \vartheta \leq 16°$. The interpolation has been made on 60000 points, the same number with which the volume values have been extracted from the second cycle (as previously explained in chapter 3.2). In the next page it is reported the script for the evaluation of the inlet flow area in one working cycle.

```
%% Inlet Flow Area

clear all
clc

SA=xlsread('Aree_di_Passaggio.xlsx', 'D5:D159');          %Shaft Angle reading
Surf_in=xlsread('Aree_di_Passaggio.xlsx', 'F5:F159');     %Inlet Flow Area reading

X=0:0.001:60;

int_in_spline=interp1(SA,Surf_in,X,'spline');
int_in=int_in_spline;

int_in(1:341)=0;                          %Imposed Min Flow Area
int_in(14001:16001)=max(Surf_in);         %Imposed Max Flow Area
int_in(29661:60001)=0;                    %Imposed Min Flow Area
```

Here is finally reported the plot that represent the inlet flow area with respect to the shaft angular position.
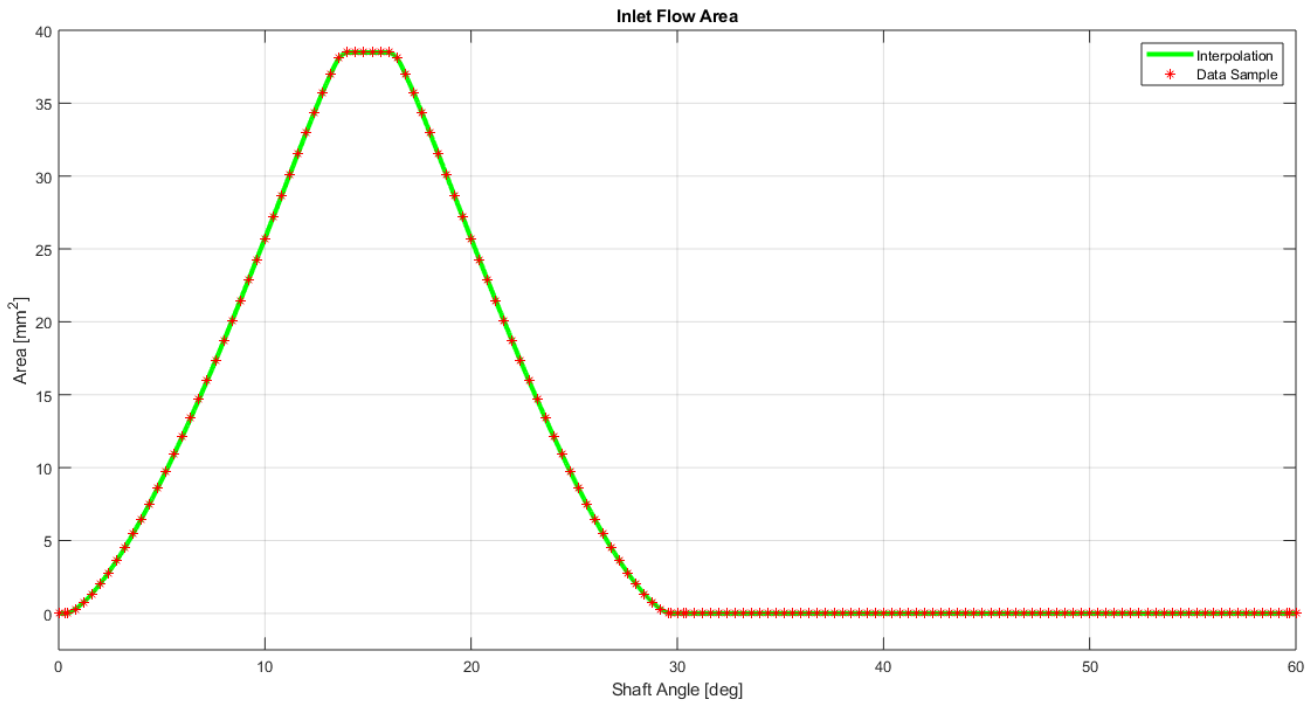
Figure 4.4 - Inlet flow area with respect to shaft angular position

4.3) Outlet Flow Area

Also for what concerns the outlet flow area the trend with respect to the angular position has been defined by means of a spline interpolation, later piecewise adjusted according to the presence of the maximum and minimum surface values. This time the minimum flow area is found for $0° \leq \vartheta \leq 30.34°$ and for $59.66 \leq \vartheta \leq 60°$, while the maximum one for $44° \leq \vartheta \leq 46°$. The numerical values are obviously the same than the ones of the inlet phase. In the next page it is reported the developed script.

```
%% Outlet Flow Area

clear all
clc

SA=xlsread('Aree_di_Passaggio.xlsx','D5:D159');          %Shaft Angle reading
Surf_out=xlsread('Aree_di_Passaggio.xlsx','G5:G159');  %Outlet Flow Area reading
X=0:0.001:60;

int_out_spline=interp1(SA,Surf_out,X,'spline');
int_out=int_out_spline;

int_out(1:30341)=0;                      %Imposed Min Flow Area
int_out(44001:46001)=max(Surf_out);      %Imposed Max Flow Area
int_out(59661:60001)=0;                  %Imposed Min Flow Area
```

Here is also shown the plot of the outlet flow area with respect to the shaft angular position.
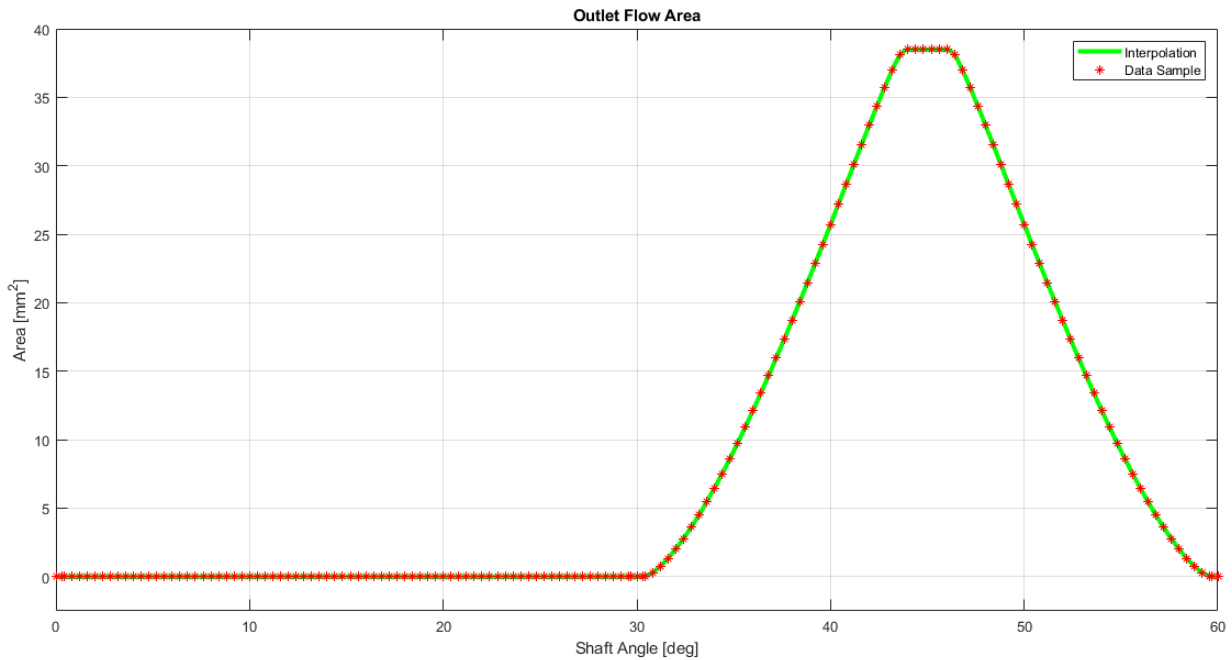
Figure 4.5 - Outlet flow area with respect to shaft angular position

The plateau corresponding to the maximum surface area is due to the fact that the diameter of the distribution duct is greater than the one of the rotor (they measure respectively 8.2 mm and 7 mm). For this reason, the circular surface of the hole of the latter lies on the one of the distribution for a certain angle window in which the flow area is constant, maximum and equal to:

$$\frac{\pi * d_{rotor\_hole}^2}{4} = \frac{\pi * 7^2}{4} = 38.48 \ mm^2 \ (eq. \ 4.3.1).$$

5) Radial Piston Hydraulic Motor Simulation

After that the volume, the volume derivative and the flow areas trend with respect to the shaft angle have been calculated and saved as matrices in dedicated *.txt* files, they have been converted into the *.data* format compatible with *Amesim®*. This has been done through the function *"Data Import"* present in the *"Tools"* section.
Along with the previous four variable parameters, other boundary conditions have been imposed:

- constant inlet flow rate equal to $Q_{in} = 50\ L/min$;
- constant shaft torque request equal to $T_{input} = 1000\ Nm$;
- motor inertia equal to $J_{mot} = 0.01\ kgm^2$, as indicated in the technical catalogue.

The chosen fluid properties are the following ones:

- advanced typology;
- operating temperature equal to 40°C;
- density equal to $\rho = 850\ kg/m^3$;
- bulk modulus equal to 17000 bar;
- absolute viscosity equal to 51 cP;
- absolute viscosity of air/gas equal to 0.02 cP;
- saturation pressure equal to 1000 bar;
- air/gas content equal to 0.1%;
- polytropic index for air/gas/vapor content equal to 1.4;
- high saturated vapor pressure equal to -0.5 bar;
- low saturated vapor pressure equal to -0.6 bar;
- absolute viscosity of vapor equal to 0.02 cP;
- effective molecular mass of vapor equal to 200;
- air/gas density at atmospheric pressure and zero Celsius degrees equal to $\rho_{gas} = 1.2\ kg/m^3$;

The boundary working conditions and the main fluid parameters have been chosen accordingly to the information that can be found in the technical catalogues released by the constructor itself.
The examined hydraulic motor belongs to the MS family models: more specifically, it has been identified as a MSE02 with fixed displacement. The declared main maximum operating conditions are:

- maximum average operating pressure equal to 400 bar;
- maximum torque equal to 2500 Nm;
- maximum shaft speed equal to 265 rpm;
- maximum delivered power equal to 22 kW.

The oil properties have been chosen considering the adoption of an ISO 11158 mineral fluid.
The simulation of the motor has been conducted with two different strategies. First, a layout with eight chambers linked in parallel has been studied. Then, in order to get a simpler and more compact design, a layout with vectorial blocks has been developed. Both of them follow a closed loop approach, in which the torque is used as the feedback parameter.

5.1) Simulation with Chambers in Parallel

The blocks used for the simulation belong to four of the main categories of the whole *Amesim®* library. Here they are reported following this subdivision.

- 1D Mechanical blocks:

  - [MECRL0], rotary load with two ports. Friction has not been considered.
  - [TORQC], torque converter: it sends to the rotary load both the input constant torque value and the closed loop feedback torque obtained by the calculations.
  - [MECADS0A], angle sensor: it enables an output port containing the shaft instantaneous angular position signal.
  - [MECRSS0A], rotary speed sensor: it enables an output port containing the shaft instantaneous rotational speed signal. It is important to put a gain for signal output equal to 360/60 min/rev, so that the speed is correctly converted into degrees per second. This is important because the volume and volume derivative evaluations have been made with angles in degrees.
  - [VELXC0], conversion of two incoming signals into linear velocity in m/s and displacement in m. The two input signals actually come from the volume derivative and from the volume.
  - [F000], zero force source: connected to the piston base.

- Signal and Control blocks:

  - [CONS00], constant signal. It has been used for input parameters such as torque value and angle phasing between chambers (since there are eight chambers, the phasing between them is of 360/8=45°).
  - [SPLT0], two-ways splitter junction; it has been used for taking the same signal to two different blocks.
  - [DYNDUP2], dynamic duplicator: it receives one signal and sends it to the eight chambers. It has been used for shaft angle and shaft speed of rotation.
  - [GA00], gain. Used for conversions of unit of measurements.
  - [MEAN0], mean value of input. Used to visualize the mean values of the most important parameters, such as velocity and flow rate.
  - [JUN3P], comparison junction summing both inputs. Used for the eight chambers phasing summing 45° to the inlet shaft angle signal.
  - [MUL00], multiplying junction. It has been utilized for calculations derived from the theory.
  - [SSINK], plug for signal port.
  - [SIGFXA01], dynamic x table. Through this block the volume and volume derivative have been imported into the simulation environment. The x value is the shaft angle.
  - [MOD00], modulo function. The minimum value has been set as zero and the maximum one as 60 degrees (which is equal to the piston working cycle).
  - [GENSUM1], general summing junction. It has been used for the total feedback torque calculation from each single piston contribution.
  - [SIGTRANS0] and [SIGRECEI0], signal transmitter and signal receiver.

- Hydraulic blocks:

  - [FP04], indexed hydraulic fluid properties.
  - [QS00], piecewise linear hydraulic flow source. Set as constant, single stage and equal to 50 L/min.
  - [HC00], simple hydraulic chamber. Two of these blocks have been used to simulate the two constant volume chambers formed by the distribution and distribution housing coupling. Their values are 22 and 14 cubic centimetres.
  - [H3NODE3], hydraulic junction with three ports.
  - [HYDVORF0], variable hydraulic orifice. Two blocks have been defined; they respectively read the imported data of the inlet and of the outlet flow area. The maximum signal value has been set to 60, in order to respect the periodicity of the system.
  - [QT000], hydraulic flow rate sensor.
  - [PT002], hydraulic pressure sensor. It has been used to calculate the feedback torque by multiplying pressure and volume derivative. The signal gain has to be correctly defined taking into account the various unit of measurements conversions (the volume derivative is in millimetres per degrees and the pressure is in bar). It has been set to $\frac{-360*10^{-4}}{2*pi}$.
  - [HYDORG10], hydraulic orifice – laminar, rectangular flat. It has been used for the flow rate leakages definition. This aspect will be further explored.
  - [HYDORF0], hydraulic orifice – fixed. It simulates the restriction that the oil has to pass across to get to the return line. The geometry has been set circular with a diameter of 11.5 mm.
  - [TK000], tank modelled as a constant pressure source.
  - [DIRECT], hydraulic lines set as direct connections.

- Hydraulic Components Design blocks:

  - [BAP11], piston. Since the rod is not present, its value has been set to zero. For what concerns its diameter, it has been set equal to the square root of 4/pi. In this way it has been defined an imaginary equivalent piston with a surface of unitary value. This has been made because by doing so it has been possible to send as linear velocity and displacement inputs the flow rate and the volume respectively. This can be easily seen by writing two simple equations.

$$Q \ [\frac{cm^3}{s}] = W[\frac{m}{s}] * A[mm^2] \ \textit{(eq. 5.1.1)}$$
$$V[cm^3] = x[m] * A[mm^2] \ \textit{(eq. 5.1.2)}$$

  Q is the flow rate, *W* the piston speed, *A* the piston surface area, *V* the oil volume and *x* the piston linear displacement. Naturally, if the surface is equal to $1 \ mm^2$, the flow rate and the volume numerically coincide with the velocity and the linear displacement.
  - [BHC11], hydraulic volume with pressure dynamics. It simulates the piston chamber volume.
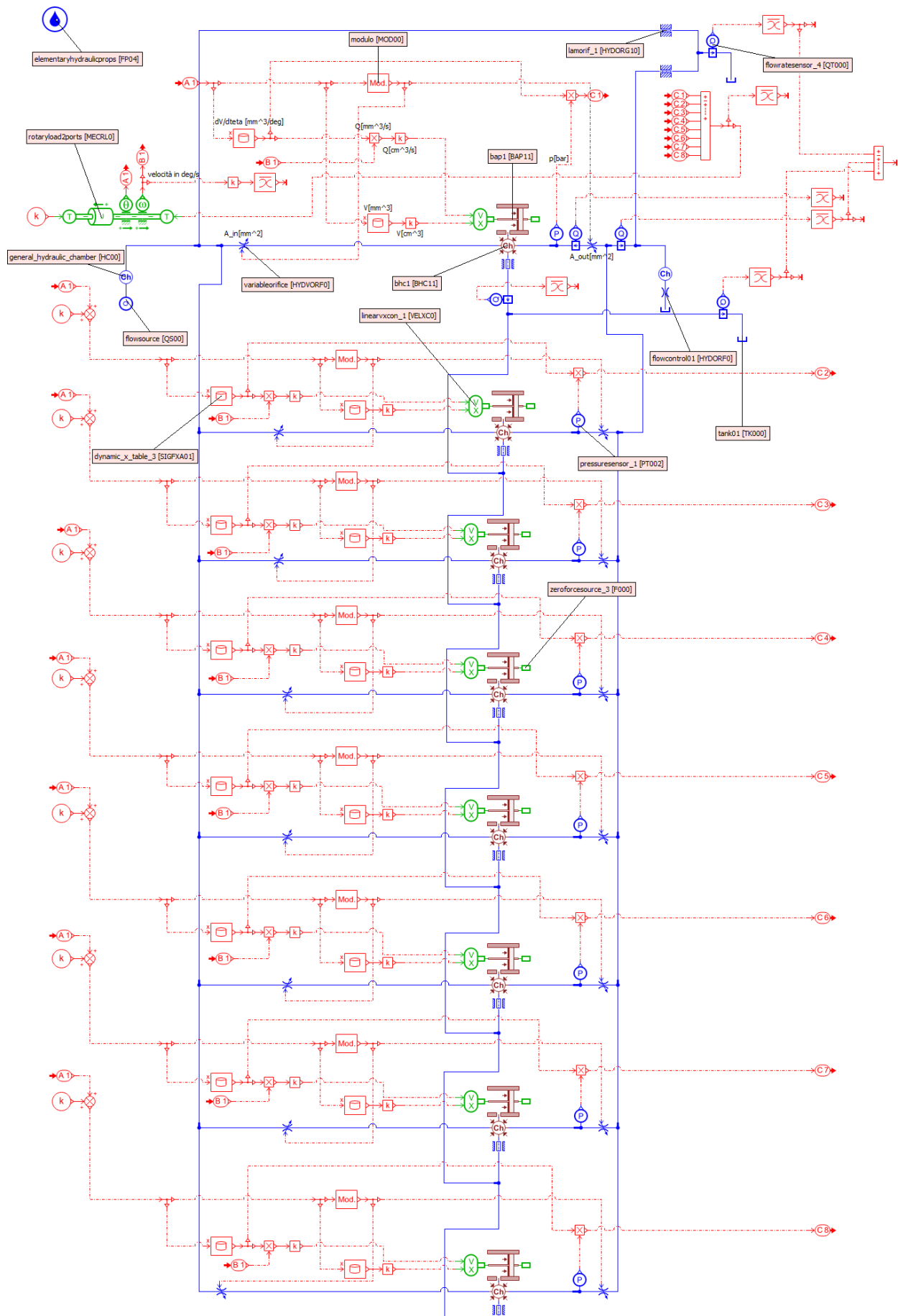
Figure 5.1 – Sketch of the simulation done with eight chambers in parallel

Starting from the shaft, an equilibrium equation is defined:

$$T_{feedback} - T_{input} = J_{mot} * \alpha \text{ (eq. 5.1.3)}$$

Naturally, if the two torques are different a rotary acceleration (α) is induced. The shaft angular position and the rotational speed are measured through the devoted sensors and separately sent to the various chambers. About the shaft angle it has to be pointed out that, for each *i-th* piston, its value is summed by *[45·(i-1)]°* in order to respect the angular phasing. Looking at one single chamber, the blocks that import the volume and volume derivative trends depend from the shaft angle signal line. The second one is multiplied with the signal of the speed of rotation: in this way the flow rate across one single chamber is obtained, as it can be seen in equation 5.1.4.

$$Q_i = \frac{\partial V_i}{\partial \vartheta} * \omega \text{ (eq. 5.1.4)}$$

Since its preferable unit of measurement for interpreting it as linear piston speed should be in cubic centimetres per seconds, a signal gain of 1/1000 is needed due to the fact that the volume derivative has been imported in cubic millimetres over degrees. The same correction has to be done for the volume, so to consider it as the fictional piston linear displacement. In this way the piston motion is completely simulated.

Also the inlet and outlet flow area signals are coming from the shaft angle one, after the filtering of the modulus block. So, the total inlet constant flow rate of the hydraulic line, once subdivided into the different parallel chambers, is regulated in dependence of the flow areas angular evolution. After the hydraulic volume that simulates the one of the piston chamber, the pressure sensor measures the in-chamber pressure level and extracts it for the multiplication with the volume derivative. In this way a torque is calculated:

$$T_i = \frac{\partial V_i}{\partial \vartheta} * p_i \text{ (eq. 5.1.5)}$$

This is the *i-th* torque produced by the *i-th* piston. The sum of all the eight singular contributions gives as a result the feedback torque, which is then sent back to the shaft. The shaft speed is again calculated taking into account the angular acceleration α already seen in equation 5.1.3 and another iteration starts.

At the piston chambers outlet, after the passage through the outlet flow area, the hydraulic lines join together and are ultimately directed to the tank. Here the total average discharged flow rate is lower than the inlet one. This is due to the leakages present in the machine. Two main typologies have been identified: leakages through piston and chamber walls and leakages through rotor and distribution. While the first ones are physically linked to the piston chamber, the others are located just next to the constant volume chambers before (inlet) and after (outlet) the flow areas.

The *Run Parameters* that have been adopted are:

- start time equal to 0 s;
- final time equal to 0.3 s;
- print interval equal to 0.00001 s.

5.2) Simulation with Vectorial Blocks

The simulation developed with vectorial blocks follows the same logic of the previous procedure. Obviously, the results of both the strategies should be the same. The main advantage in this method is the better compactness and simplicity, since less components are requested: if some parameters are desired to be changed (for example to study different working conditions of the motor), a much faster manipulation is needed. Here are reported all the blocks used for the model implementation.

- 1D Mechanical blocks:

  o [MECRL0], rotary load with two ports. Friction has not been considered.
  o [TORQC], torque converter: it sends to the rotary load both the input defined torque value and the closed loop feedback torque obtained by the calculations.
  o [MECADS0A], angle sensor: it enables an output port for the shaft instantaneous angular position signal.
  o [MECRSS0A], rotary speed sensor: it enables an output port for the shaft instantaneous rotational speed signal. Even this time the gain for signal output has been put equal to 360/60 min/rev.
  o [MECTS0A], torque sensor. It sends as an output signal the measured torque.
  o [TWTSG1], conversion between rotary mechanical and signal variables. It has been used to receive the shaft rotational speed and the shaft angle and to transmit the feedback torque from the pistons back to the shaft.

- Signal and Control blocks:

  o [CONS00], constant signal. It has been used for input parameters such as torque value.
  o [SPLT0], two-ways splitter junction; it has been used for taking the same signal to two different blocks.
  o [MEAN0], mean value of input. Used to visualize the mean values of the most important parameters, such as velocity and flow rate.
  o [SSINK], plug for signal port.
  o [GA00], gain. Just used for better visualization of some results.
  o [MOD00], modulo function. The minimum value has been set as zero and the maximum one as 60 degrees (which is equal to the piston working cycle).
  o [DIV00], division junction. Used for some considerations about leakages and volumetric efficiency.
  o [GENSUM1], general summing junction. It has been used for verifying the equivalence of the input flow rate with the sum of the output average flow rate and the average total leakages.

- Hydraulic blocks:

  o [FP04], indexed hydraulic fluid properties.
  o [QS00], piecewise linear hydraulic flow source. Set as constant, single stage and equal to 50 L/min.

o [HC00], simple hydraulic chamber. Two of these blocks have been used to simulate the two constant volume chambers formed by the distribution and distribution housing coupling. Their values are 22 and 14 cubic centimetres.
o [H3NODE3], hydraulic junction with three ports.
o [QT000], hydraulic flow rate sensor.
o [PT002], hydraulic pressure sensor. This time it has just been used for pressure trend visualization.
o [HYDORG10], hydraulic orifice – laminar, rectangular flat. It has been used for the flow rate leakages definition in the interface between distribution and rotor.
o [HYDORF0], hydraulic orifice – fixed. It simulates the restriction that the oil has to pass across to get to the return line. The set geometry is obviously the same that the one adopted in the previous simulation.
o [TK000], tank modelled as a constant pressure source.
o [DIRECT], hydraulic lines set as direct connections.

- Hydraulic Components Design blocks:

o [HCDVECRPT0], hydraulic vectorial rotary piston. This block has been used to simulate the pistons of the motor. This time just the volume (along with shaft angular position and speed) is needed as an input, since the volume derivative is calculated as an internal variable.
o [HCDVECC0], vectorial hydraulic component design volume with pressure dynamics. It has been used to simulate the piston chamber volume.
o [HCDVECVORF0], hydraulic vectorial variable orifice. It imports the flow areas data and receives as an input the shaft angle. It has been used for the inlet and the outlet flow areas.
o [HCDVECFLOWSUM0], hydraulic vectorial flow rate sum. It is needed to go from the vectorial blocks to the one-dimensional ones and vice versa, summing or subdividing the flow rate.
o [H3VECNODE2], hydraulic vectorial junction 3 ports.
o [HCDVECVORG0], hydraulic vectorial orifice – laminar, rectangular flat, variable gap. It has been used for the modelling of the leakages between piston and chamber walls.

All the components taken from the Hydraulic Components Design library are of the vectorial type. In these blocks it is necessary to indicate the vector size, the volume spacing and the periodicity. Obviously, all the blocks communicating together must have these three parameters equal, or the simulation can't work. The selected values are the following ones:

- vector size has been chosen equal to eight, since the rotor has eight pistons;
- volume spacing has been selected as *regular*;
- the periodicity has been put equal to a full shaft rotation, so equal to 360°.

In figure 5.2, reported in the following page, it is shown the final sketch obtained with the vectorial blocks strategy.
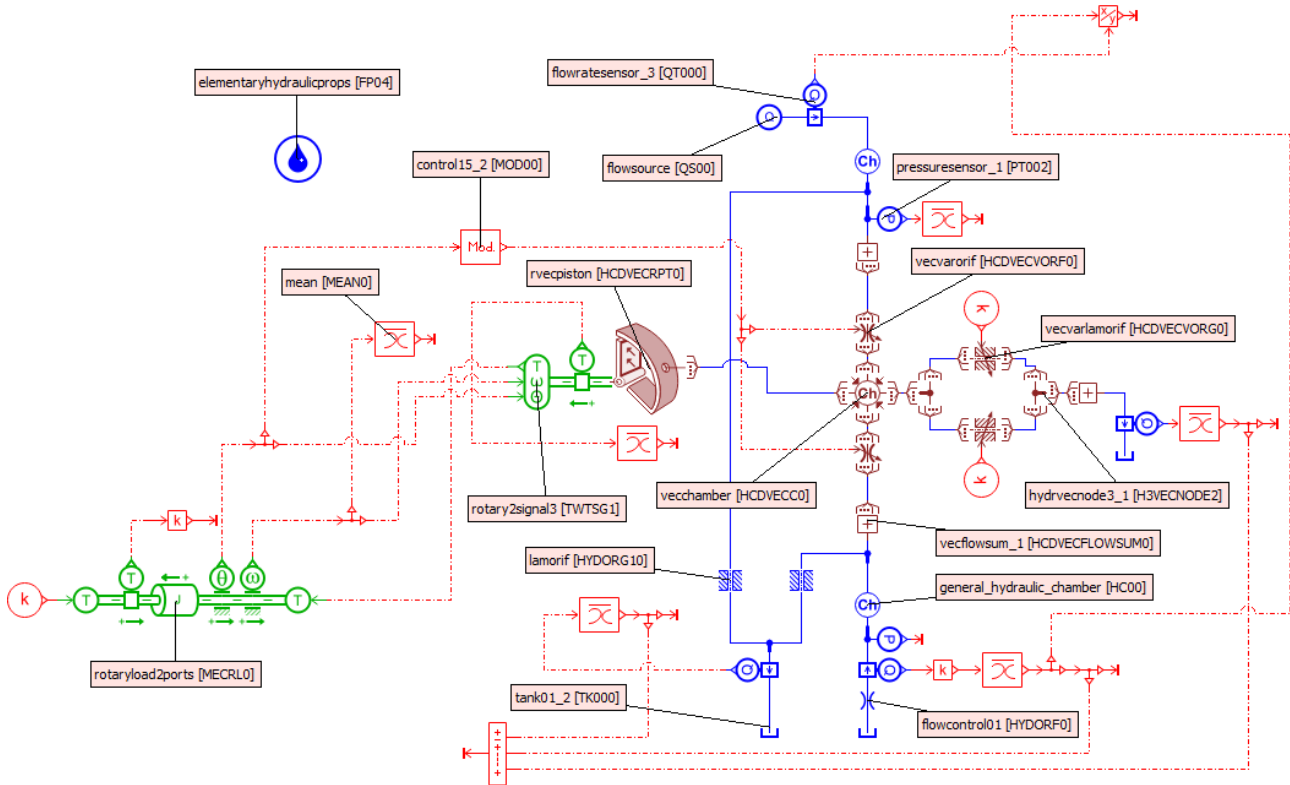
Figure 5.2 – Sketch of the simulation done with the vectorial components

The shaft representation is the same of the simulation with eight parallel chambers. Two torques are confronted by an equilibrium equation, in which an angular acceleration is calculated and consequently also the shaft speed of rotation. This time the feedback torque is directly evaluated by the rotary piston block, so less control components can be used. The angle and speed signals are read as an input by this element. The pressure needed for the torque calculation is taken as an input from the vectorial chamber, which simulates the piston chamber oil volume. This component is able to compute the pressure dynamics receiving as inputs volume and flow rates into its four ports.

The flow areas need again as an input the shaft angle filtered by the modulo function, with a maximum signal value equal to 60. Also the flow leakages through piston and chamber walls need an input: a constant parameter equal to zero has been chosen, since their flow area is considered constant in time. Flow losses between the distribution and rotor interface has been modelled with simple hydraulic components as it has been done in the previous simulation.

The simple single hydraulic line is constituted, as in the parallel simulation, by the input constant flow rate, the high-pressure line constant volume chamber formed with the distribution/distribution housing coupling, the inlet flow area, the piston chamber, the outlet flow area, the low-pressure line constant volume chamber and the restriction that leads to the tank environment with zero pressure.

The same *Run Parameters* used in the parallel simulation has been set.

5.3) Simulations Results

In this chapter the results of the mainly significative parameters are shown. In the most of the following plots the two simulations are directly confronted: as it will be seen, the two methods correctly lead to the same outcomes. A natural transient period is present at the beginning of every plot since the simulations need time to settle down on the right results.

5.3.1 Shaft Speed
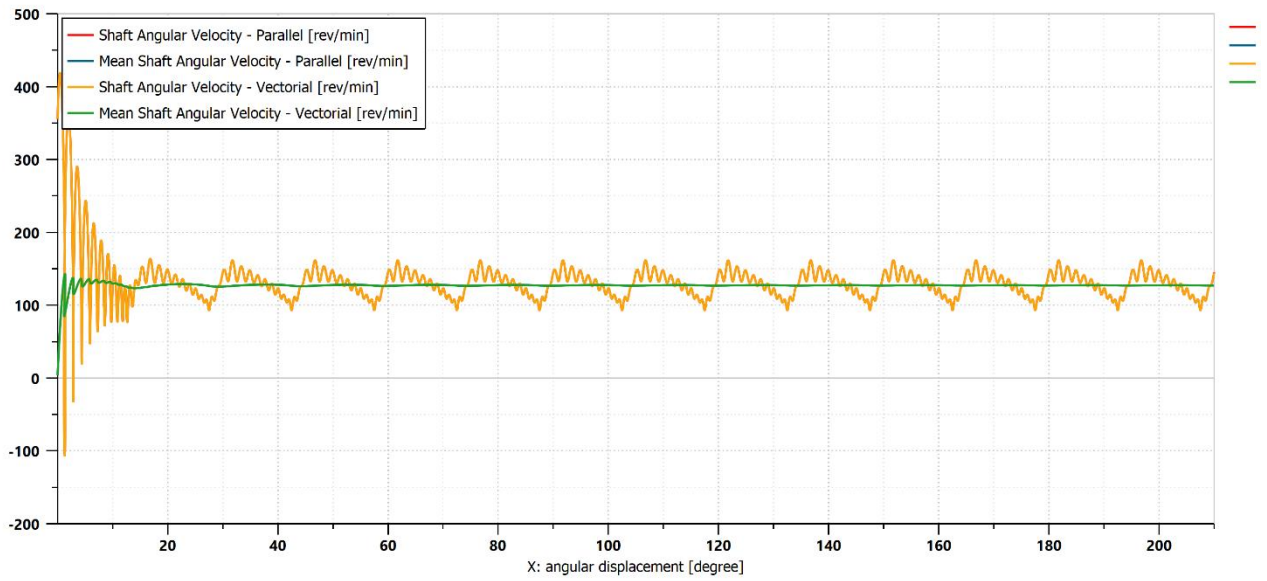
Figure 5.3 - Shaft speed of rotation with respect to shaft angle

The shaft rotational speed has an oscillatory behaviour with a quite high ripple. The noise that can be seen is due to the defined inertia, that has been chosen accordingly to the declared value found in technical catalogues. It represents just the motor not in mounted condition, so the vehicle is not taken into consideration. It is reasonable to think that, once the mounting has been done the considerable mass of the vehicle amplifies the inertia and so the various oscillations are strongly reduced (both noise and ripple). The results of the two simulations are practically coincident. The speed oscillates between the values of 161.54 rpm and 93.01 rpm. This anyway does not precisely represent the actual ripple due to the higher frequency noise that alter the trend shape. The mean value is equal to 127.24 rpm. Considering the input shaft torque the requested average power is equal to:

$$P_{avg,mot} = T_{input} * \omega_{avg} = 1000 * 127.24 * \frac{2*pi}{60} = 13.32 \ kW \ (eq. \ 5.3.1).$$

5.3.2 Piston Chamber Inlet Flow Rate
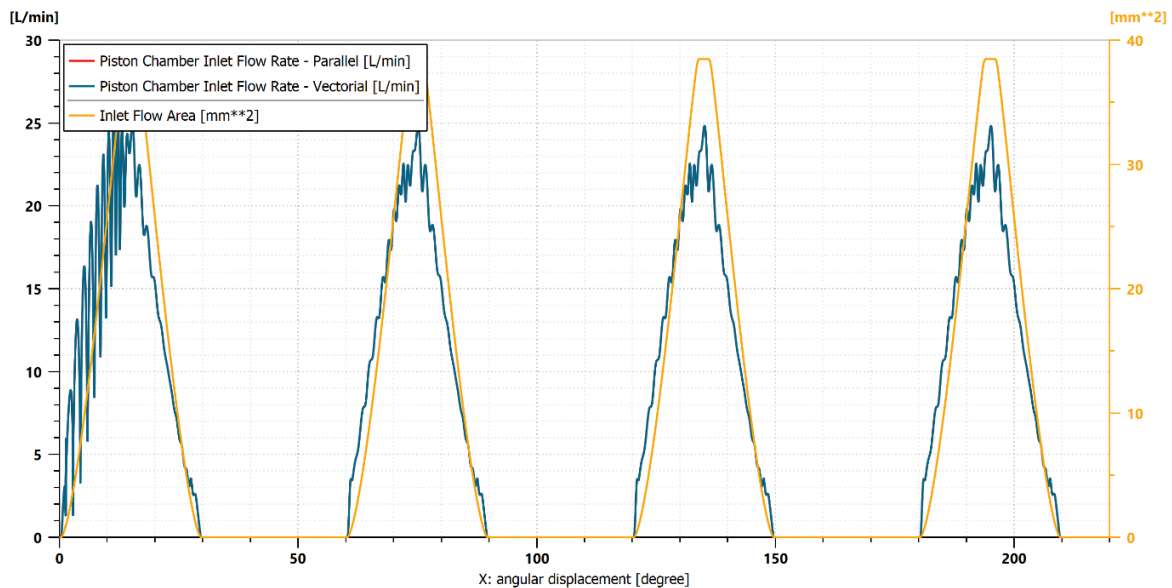
Figure 5.4 - Piston chamber inlet flow rate with respect to shaft angle

In figure 5.4 it can be seen the flow rate that enters into one single piston chamber. In yellow, on a secondary axis, it is reported the inlet flow area as a reference. It can be correctly seen that when its value is zero there is no oil flow rate. Its trend has a *triangular-like* shape with respect to the shaft angle, and this recalls the volume derivative one. The peak instantaneous flow rate value is circa 24.83 L/min.

5.3.3 Piston Chamber Outlet Flow Rate
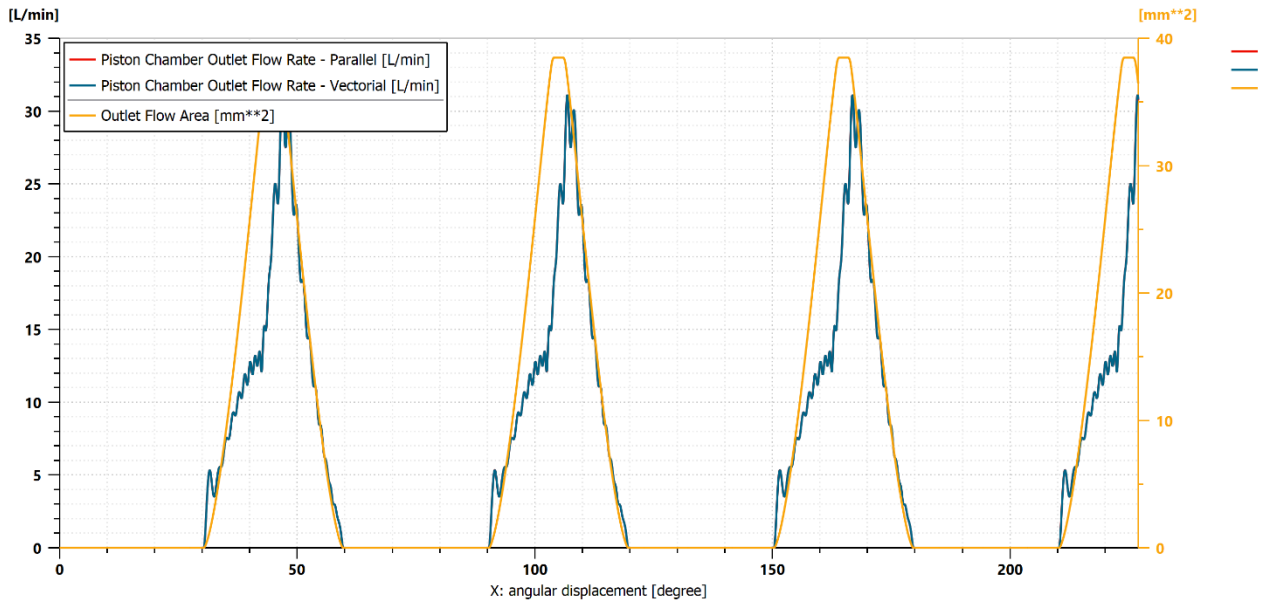
Figure 5.5 - Piston chamber outlet flow rate with respect to shaft angle

Here is reported the outlet flow rate, so the rate of oil volume exiting from the piston chamber. Again, the outlet flow area is plotted for reference: when it is equal to zero, no oil passage is possible. Even this time it can be seen a triangular-like shape that recalls the one of the volume derivative, but a little bit more corrugated than what seen in figure 5.4. The peak flow rate value is equal to 31.10 L/min.

5.3.4 Piston Chamber Pressure
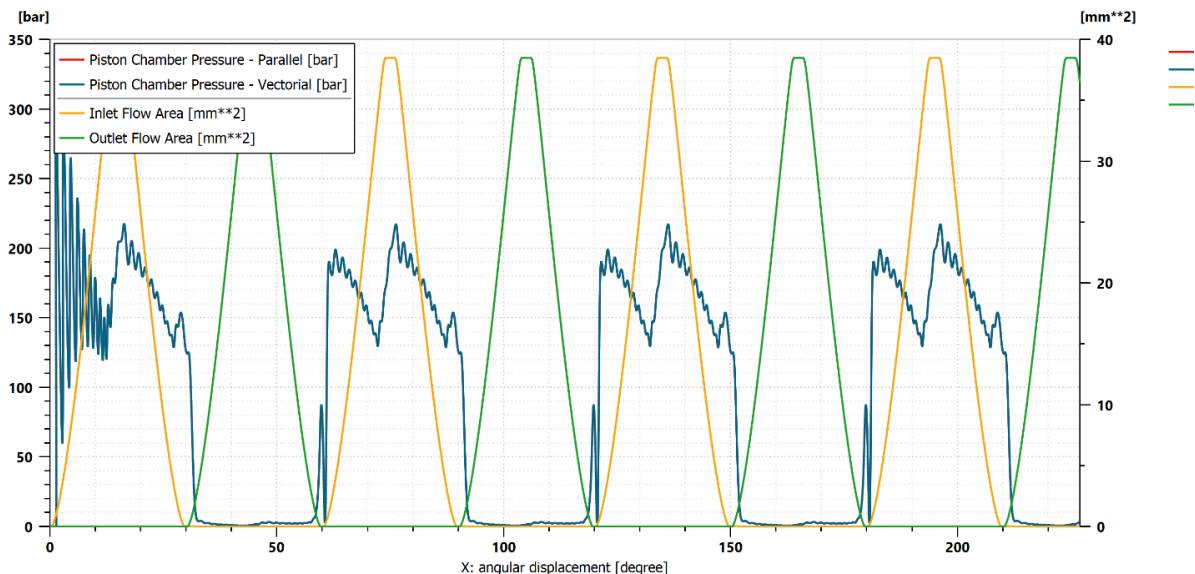
Figure 5.6 - Piston chamber pressure with respect to shaft angle

In figure 5.6 the piston chamber pressure dynamics are reported, alongside the evolution of the inlet and outlet flow areas. It can be seen that when the piston chamber communicates with the high-pressure line (inlet flow area open), the pressure oscillates between high pressure values (p_{max} = 217 bar and p_{min} = 129 bar circa). When it instead communicates with the low-pressure line, the chamber pressure reaches very low values of some unities of bar. It is interesting to note that, in the little angle window in which the chamber is isolated, the oil pressure undergoes a steep local peak when the piston is in the Bottom Dead Centre position (at $i \cdot 60°$, with i = 0,1,2…). There is again some noise in the calculations, due to the defined inertia value.

5.3.5 Motor Outlet Flow Rate
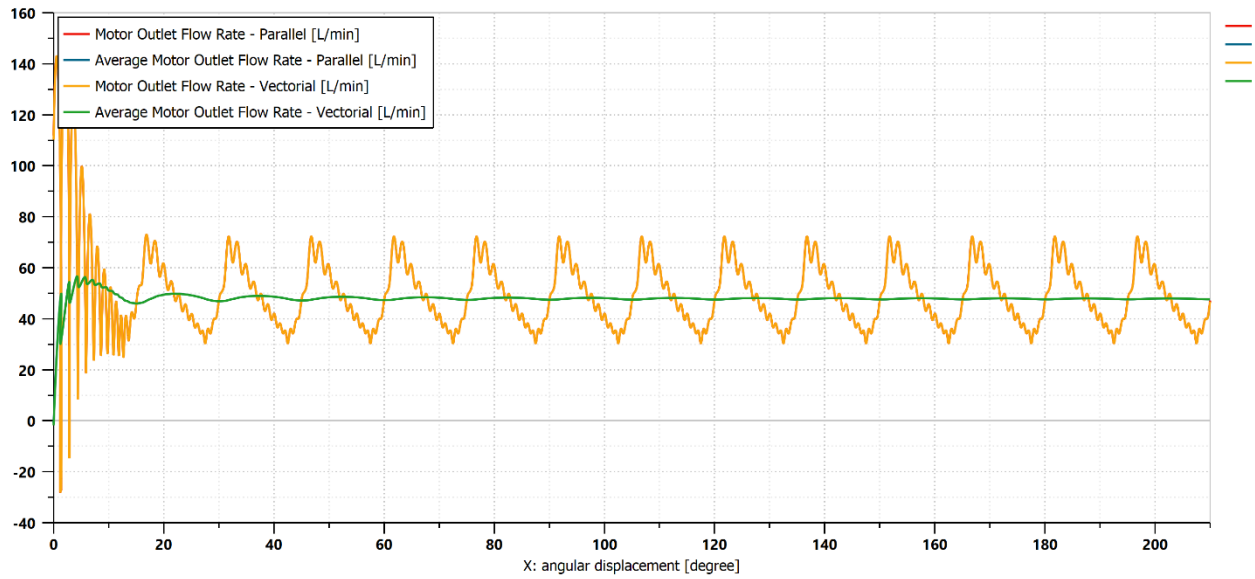
Figure 5.7 - Motor outlet flow rate with respect to shaft angle

This picture depicts the trend of the total discharged flow rate by the motor with respect to the shaft angle. Its maximum and minimum values are respectively 72.25 L/min and 30.33 L/min circa. The mean flow rate is equal to 47.84 L/min: it is lower with respect to the input one because of the leakages. This value has been obtained with a higher simulation time than the one that can be seen in the picture to get a better stabilization of the result. As shown in chapter 3.4, the flow rate oscillation period is equal to 15°, which is one fourth of the working cycle.

5.3.6 Delta Pressure Across the Motor

In figure 5.8, present in the next page, it is reported the evolution of the delta pressure across the hydraulic motor. Its maximum and minimum values are respectively 218 bar and 130 bar circa, and they are slightly higher than what can be found inside the piston chamber. This is due to a light pressure drop that is induced to the oil crossing the flow area. Making a direct comparison between the two plots (figure 5.6 and 5.8), it can be seen that the piston chamber pressure follows almost perfectly the one of the total delta pressure when the inlet flow area is open. The average Δp_{mot} is equal to 173.83 bar.
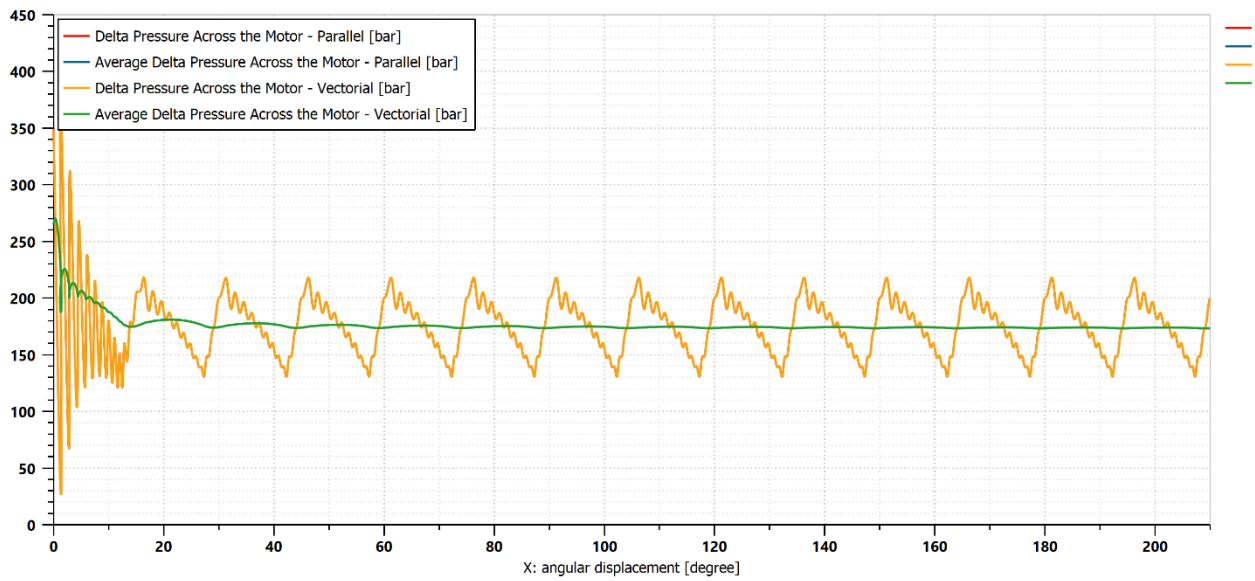
Figure 5.8 Delta pressure across the motor with respect to shaft angle

5.3.7 Feedback Shaft Torque
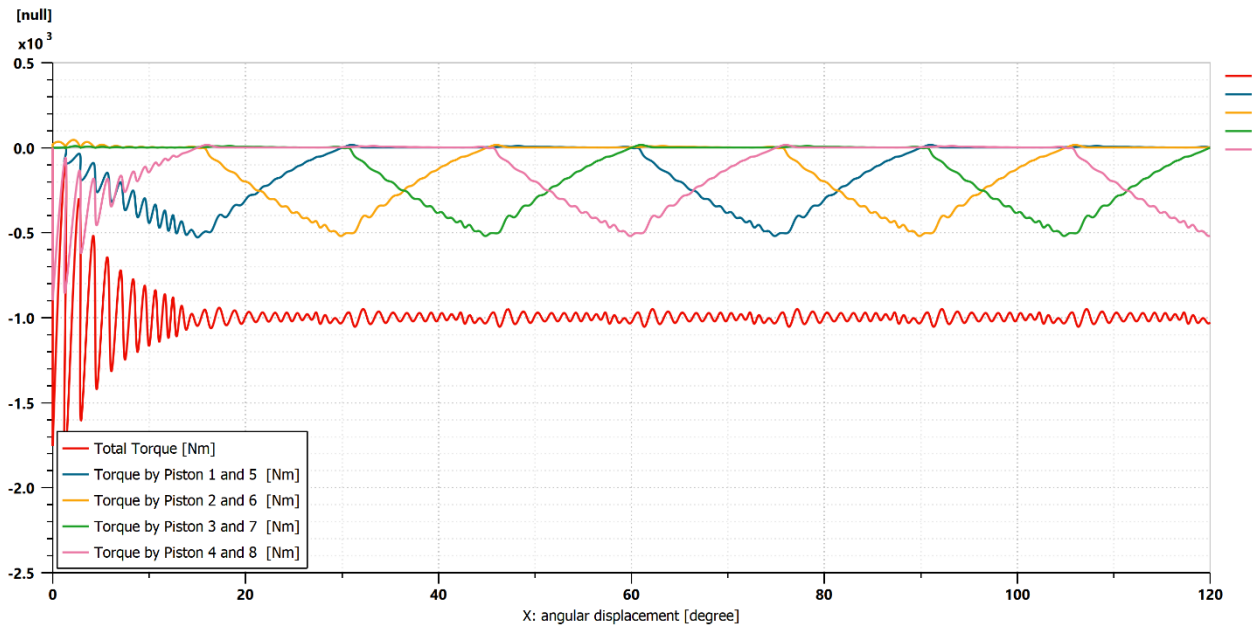
Figure 5.9 – Feedback torque calculation with respect to shaft angle

In this final plot it can be seen the development of the calculated shaft torque, which is used as the closed loop system feedback. Since the eight pistons simultaneously work in couples at four different cycle instants, the torques of pistons *i* and *i+4* are the same. The total torque is simply the sum of the contributions coming from all the pistons, and its average value is equal to the one which has been set as the constant input: 1000 Nm.

5.4) Flow Rate Leakages Modelling

Flow leakages are a very important parameter to identify, since they are one of the factors that define the difference between an ideal hydraulic machine and a real one. First of all, it has to be remembered that in this case there can be two different leakage sources:

1) flow losses through piston and chamber walls;
2) flow losses through the distribution and rotor interface.

For each simulation the leakages have been modelled according to the best possible simplified hypothesis.

5.4.1 Flow Losses Through Piston and Chamber Walls

The area through which the leakages of the piston chamber flow is a circular crown that generates a volume taking into account the variable axial length, defined by the piston geometry and by the piston reciprocal motion. It has been simplified with two different equivalent annular orifices whose dimensions have been set imposing an average value each one. Circumferentially in fact, the piston can be divided into two different sections. The thickest one has a variable axial length before that the inclined surface starts, while the thinner one is affected by the presence of the bushing and of the roller. They have been respectively approximated as constant average axial dimensions equal to 12.5 mm and 3 mm. These two parts have been considered equal in perimetral dimension: in other words, each one is developing for half the perimeter. In figure 5.10 it is reported a comparison with the actual piston and the approximated one used for the simulation of the leakages.
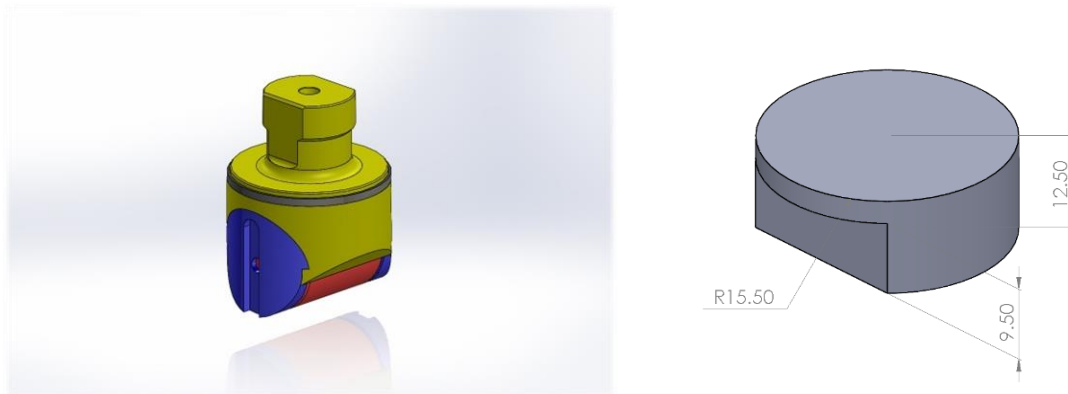
Figure 5.10 – Piston CAD and piston geometry simplification for flow losses calculation

In *Amesim®* environment the two piston parts have been modelled by means of two laminar rectangular orifice blocks put in parallel, since they can anyway simulate an annular cross section by setting the right parameters. In this case it was imposed:

- *width* equal to half the perimeter of the piston:

$$w = \frac{p}{2} = \pi * \frac{d}{2} \ (eq. \ 5.4.1),$$

where *d* is the piston diameter;
- *length* equal to 12.5 mm and 3 mm for the two different blocks respectively;
- *clearance* equal to 0.025 mm.

From the results obtained with this procedure it has been possible to find a single equivalent annular orifice with constant axial length. After some simulation trials taking as a reference always the same clearance between piston and chamber walls, this value has been found to be equal to 4.835 mm. This procedure has been done both for the simulation in parallel and with vectorial blocks.
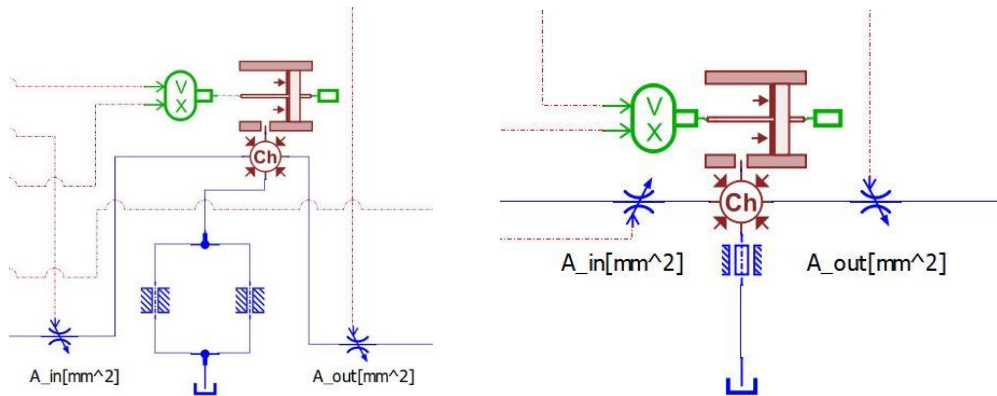
Figure 5.11 – Piston/chamber walls leakages with piston modelling and equivalent annular orifice in the simulation in parallel

Here in the following picture, it is reported the trend of the flow leakages in a single piston chamber. Obviously, the total leakage is the sum of the contributions given by the two laminar orifice blocks, which represent the different piston sections.
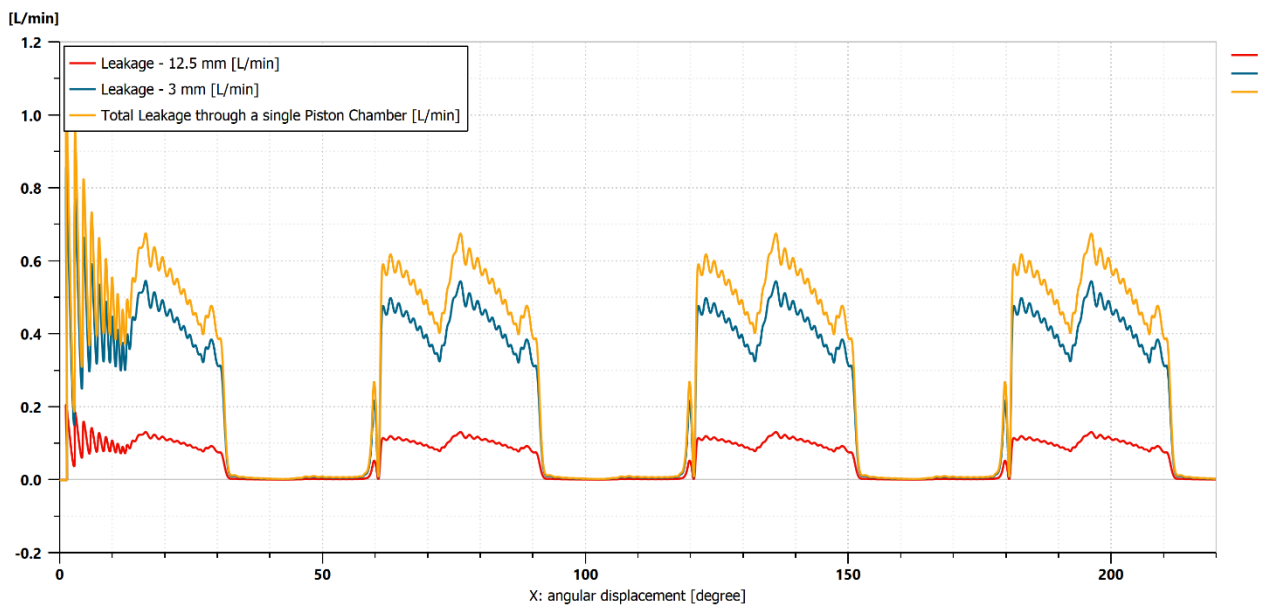
Figure 5.12 – Flow losses through piston and chamber walls considering one single chamber

A final comparison is made between all the simulations (parallel, vectorial, with two laminar orifices and with one equivalent annular orifice). The total flow losses through the piston and chamber walls are examined; they consider the contribution of all the eight pistons. As it can be seen all the four runs lead to the same results.
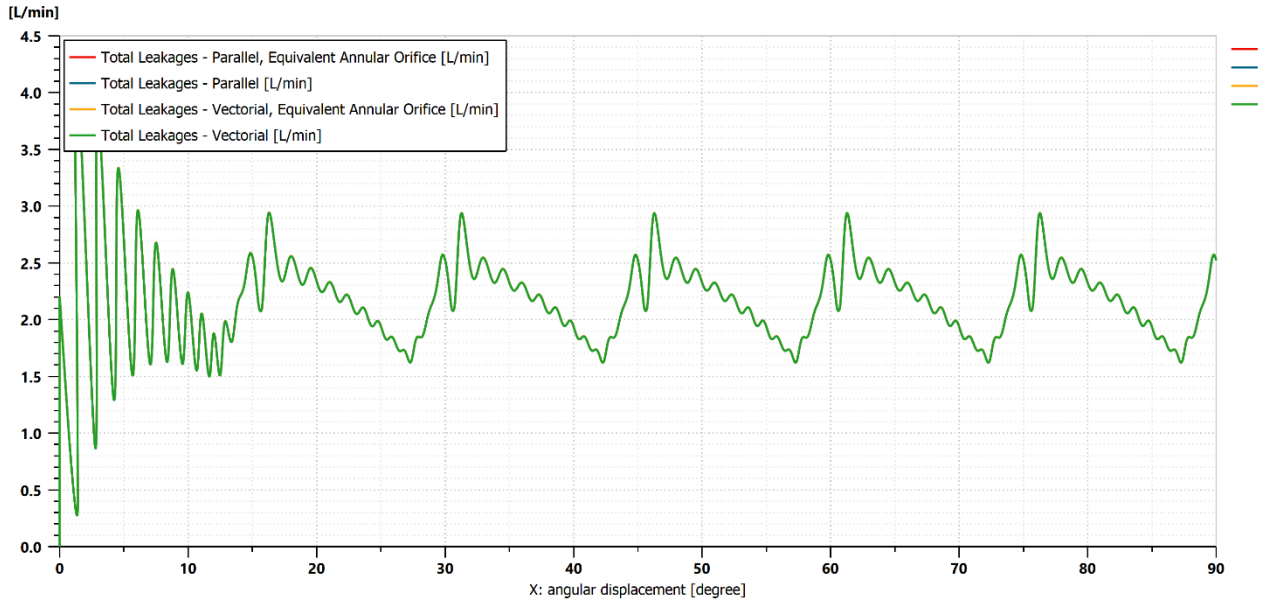
Figure 5.13 – Total leakages for each different simulation

5.4.2 Flow Losses Through Distribution and Rotor Interface

For what concerns the flow losses between the rotor and the distribution, due to the design characteristics of the latter a very low clearance can be considered. This thanks to the springs that exert a certain preload on the component, *pushing* it towards the rotor. The leakages also in this case can be divided into two contributions: the first one regards the flow losses in the inlet phase, so when the oil enters in the piston chamber. The second one regards the outlet phase, so when the oil exits from the piston chamber. The blocks adopted for their simulation are again the ones of the laminar rectangular orifice, capable to simulate the annular one simply by defining the proper parameters. The surface where the oil leaks happen is here represented.
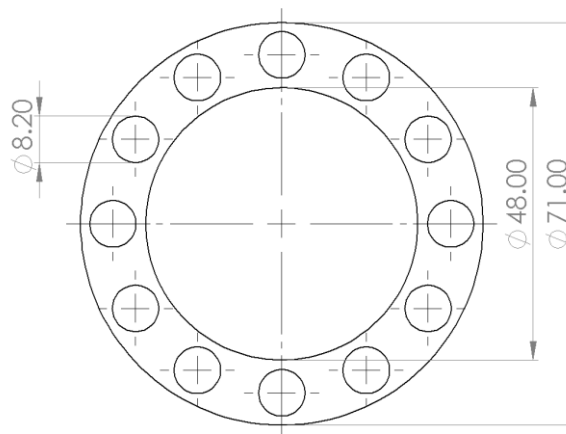
Figure 5.14 – Area of the interface of the distribution with the rotor

The actual flow area has been calculated taking into account the surface of the circular crown seen in figure 5.14, subtracting from it the twelve holes area. The input parameters for the two laminar orifices have been chosen as:

- clearance equal to 0.01 mm;
- width equal to the external perimeter, so:

$$w = p_{ext} = 71 * \pi = 223.05 \ mm \ (eq. \ 5.4.2);$$

- length equal to half of an equivalent parameter, obtained by imposing the actual interface area equal to an area without the presence of the twelve holes. Here is reported the procedure that has been made to obtain this parameter.

$$S_{total} = \frac{\pi}{4} * (d_{ext}^2 - d_{int}^2) = 2149.63 \ mm^2;$$
$$S_{hole} = \frac{\pi}{4} * d_{hole}^2 = 52.81 \ mm^2;$$
$$S_{actual} = S_{total} - 12 * S_{hole} = 1515.91 \ mm^2;$$
$$V_{actual} = S_{actual} * g = 15.1591 \ mm^3;$$
$$V_{eq} = g * p_{ext} * x_{eq}.$$

Where p_{ext} is the external perimeter, g is the distribution/rotor clearance and x_{eq} is the equivalent length used in the laminar orifice block. Considering $V_{actual} = V_{eq}$, x_{eq} can be finally calculated as:

$$x_{eq} = \frac{V_{actual}}{g*p_{ext}} = \frac{S_{actual}}{p_{ext}} = 6.796 \ mm \ (eq. \ 5.4.3).$$

This parameter has to be divided by two because of the two different contributions indicated at the beginning of the paragraph. All these considerations can be perfectly adapted for both the parallel and vectorial simulations. The blocks have to be put in communication with the hydraulic line after the high pressure, constant volume chamber for what concerns the inlet phase and before the low pressure, constant volume chamber for what concerns the outlet phase, as it can be seen in figures 5.1 and 5.2. In the following picture the leakages of the inlet and outlet phases are reported.
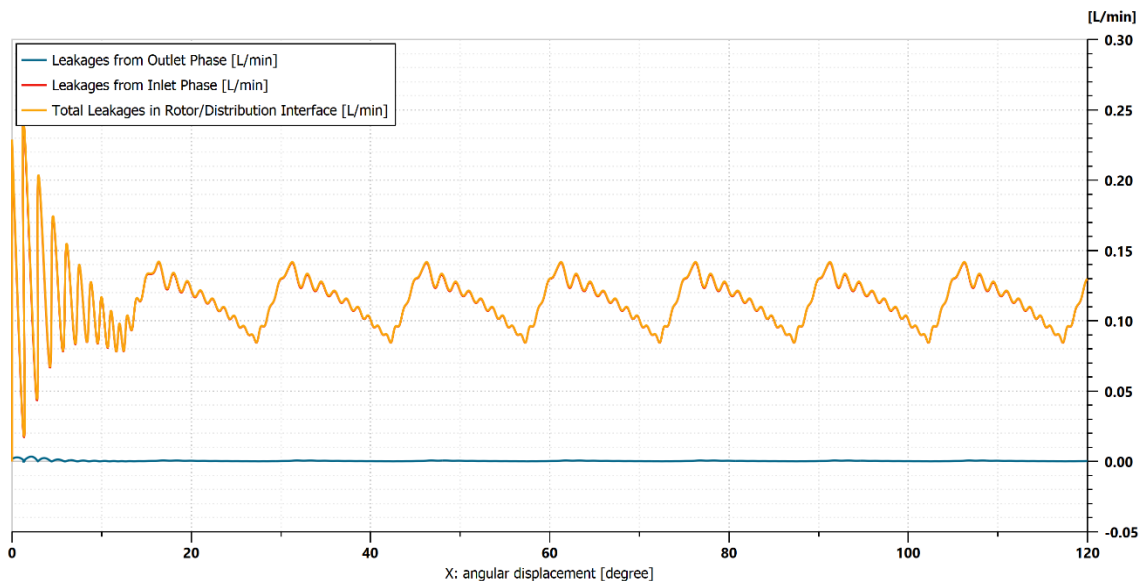
Figure 5.15 – Leakages present in the rotor/distribution interface

In figure 5.15 it can be seen that the losses due to the outlet phase are very much lower with respect to the ones of the inlet phase, to the point that they can also be considered negligible. This because in the outlet phase a much lower pressure is present than in its counterpart.

In figure 5.16 a final plot is presented: all the motor flow leakages can be seen, as long as the average total flow loss.
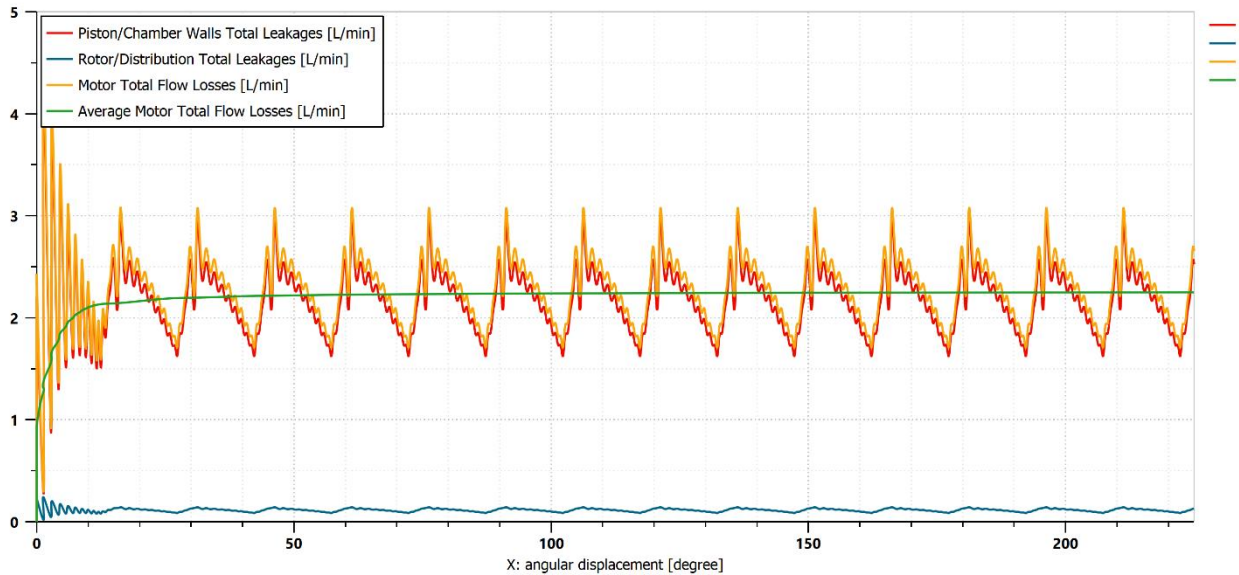
Figure 5.16 – Total motor flow losses and their contributions

It can be seen that the total motor losses main contribution (according to the assumptions made in this chapter) is the piston/chamber walls one. At the defined working conditions, which has been imposed as input torque equal to 1000 Nm and input flow rate equal to 50 L/min, the average total leakages are equal to 2.26 L/min.

5.4.3 Shaft Speed of Rotation Dependency with respect to Clearances

A final study has been conducted on the evaluation of the average shaft speed changing the values of the clearances of the two leakage sources. A full factorial plan has been developed, with the following characteristics:

- two key factors (piston/chamber wall clearance, rotor/distribution interface clearance);
- five levels.

The values of the five levels are reported in the following table:

Lvl	Piston/Chamber Walls Clearance [mm]	Rotor/Distribution Interface Clearance [mm]
1	0 *(no leaks)*	0 *(no leaks)*
2	0.005	0.005
3	0.01	0.01 *(main simulation adopted value)*
4	0.025 *(main simulation adopted value)*	0.02
5	0.05	0.05

25 simulations have been run in *Amesim®* environment, so that every possible combination between the two different parameters have been considered. The mean shaft speed and the average leakage flow rate have been extracted for each one and saved into a dedicated *Excel®* file. The results, obtained with operating conditions equal to Q_{inlet} = 50 L/min and T = 1000 Nm, are here reported.

Test	Piston/Chamber Walls Clearance [mm]	Rotor/Distribution Interface Clearance [mm]	Average Leakages [L/min]	Average Shaft Speed [rpm]
1	0	0	0	136.84
2	0	0.005	0.009	132.77
3	0	0.01	0.109	132.51
4	0	0.02	0.896	130.42
5	0	0.05	13.979	95.67
6	0.005	0	0.009	132.77
7	0.005	0.005	0.023	132.73
8	0.005	0.01	0.122	132.47
9	0.005	0.02	0.912	130.35
10	0.005	0.05	13.998	95.63
11	0.01	0	0.137	132.47
12	0.01	0.005	0.151	132.43
13	0.01	0.01	0.249	132.17
14	0.01	0.02	1.037	130.07
15	0.01	0.05	14.119	95.32
16	0.025	0	2.142	127.52
17	0.025	0.005	2.156	127.48
18	0.025	0.01	2.255	127.22
19	0.025	0.02	3.041	125.13
20	0.025	0.05	16.103	90.36
21	0.05	0	16.048	91.32
22	0.05	0.005	16.062	91.28
23	0.05	0.01	16.160	91.02
24	0.05	0.02	16.944	88.91
25	0.05	0.05	30.232	53.13

From these data a three-dimensional plot has been generated in *Matlab®*, in which the two clearance values have been put onto the *x* and *y* axis and the average shaft speed on the *z* one. In order to better visualize the result a surface has been interpolated starting from these 25 points. In figure 5.17 this plot is reported.

Mean Shaft Speed of Rotation with respect to Clearances
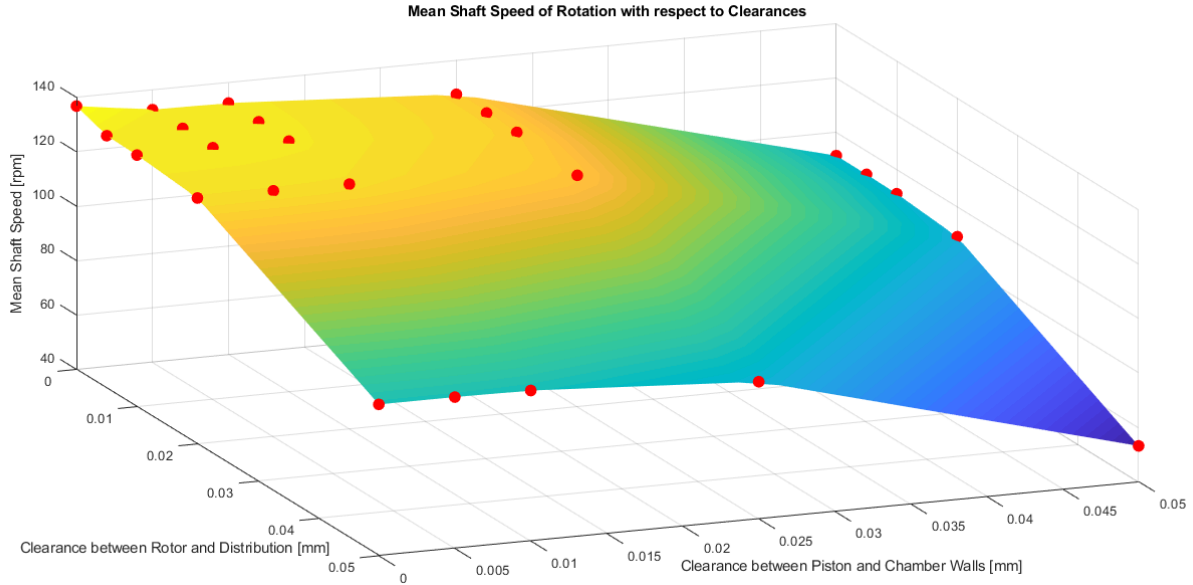
Figure 5.17 – Shaft speed of rotation with respect to clearance between rotor and distribution and piston and chamber walls

It can be seen that naturally the two parameters have similar effects on the average shaft speed. Increasing the clearance, also the leaks increase and the shaft rotary speed decreases. It is interesting to note that the clearance between the piston and the chamber walls is slightly more impacting on the shaft speed with respect to the one between the rotor and the distribution. This can't be clearly seen by the plot, but looking at the numerical values present in the table. Keeping the first ones equal to zero and the second ones ranging from the minimum to the maximum value, the shaft speed decreases from 136.84 rpm to 95.67 rpm. With the opposite logic, the velocity decreases from 136.84 rpm to 91.32 rpm. More in general, the curves with constant piston/walls clearance are a little less steep with respect to the ones at fixed rotor/distribution clearance.

5.5) Volumetric Efficiency Calculation

Considering the modelled leakages, it has been possible to calculate the hydraulic volumetric efficiency of the motor. Since the simulation has been conducted with the simplification of no friction at shaft level, mechanical efficiency can't be instead evaluated (and consequently the overall one). In order to understand the dependency of η_{vol} with respect to the different working conditions, different simulations have been run. For each trial the flow rates have been examined and their mean values written in an *Excel®* file. As a reminder, it is recalled that:

$$\eta_{vol} = \frac{1}{1+\frac{Q_L}{V*\omega}} \ (eq.\ 5.5.1).$$

The study has been done with two approaches:

a) variable shaft torque and constant input flow rate equal to 50 L/min;
b) constant shaft torque equal to 1000 Nm and variable shaft rotary speed (obtained by varying the motor input flow rate).

It is important to point out that the variability indicates that the referred parameter is just regulated among the multiple simulations and still maintained constant in each one.

5.5.1 Volumetric Efficiency with Variable Shaft Torque

Here is reported the table with the results. The mean velocity has been obtained looking at the *mean* block related to the rotary velocity sensor. Steps of 100 Nm between 0 and 2500 Nm have been done, so a total of 26 points have been found.

Torque [Nm]	Mean Velocity [rpm]	Q_th [L/min]	Q_Leak [L/min]	Volumetric Efficiency [/]
0	134.37	50.088	0.085	99.831%
100	133.51	49.767	0.290	99.421%
200	132.81	49.506	0.505	98.990%
300	132.10	49.241	0.725	98.549%
400	131.40	48.980	0.940	98.117%
500	130.71	48.723	1.160	97.675%
600	130.01	48.462	1.380	97.231%
700	129.31	48.201	1.600	96.787%
800	128.62	47.944	1.820	96.343%
900	127.93	47.687	2.040	95.898%
1000	127.24	47.430	2.260	95.452%
1100	126.54	47.169	2.480	95.005%
1200	125.86	46.915	2.700	94.558%
1300	125.17	46.658	2.920	94.110%
1400	124.48	46.401	3.145	93.652%
1500	123.80	46.147	3.365	93.204%
1600	123.11	45.890	3.585	92.754%
1700	122.43	45.637	3.810	92.295%
1800	121.75	45.383	4.030	91.844%
1900	121.07	45.130	4.250	91.393%
2000	120.39	44.876	4.475	90.932%
2100	119.71	44.623	4.695	90.480%
2200	119.03	44.369	4.920	90.018%
2300	118.35	44.116	5.140	89.565%
2400	117.68	43.866	5.375	89.102%
2500	117.00	43.613	5.590	88.639%

The torque, the mean velocity and the mean leakage flow rate are data directly taken from the simulations. The theoretical flow rate has been calculated with the classic formulation:

$$Q_{th} = V * \omega \text{ (eq. 5.5.2)}$$

The volumetric efficiency itself has been calculated with the eq. 5.5.1. In figure 5.18 it is reported the plot derived from these results.
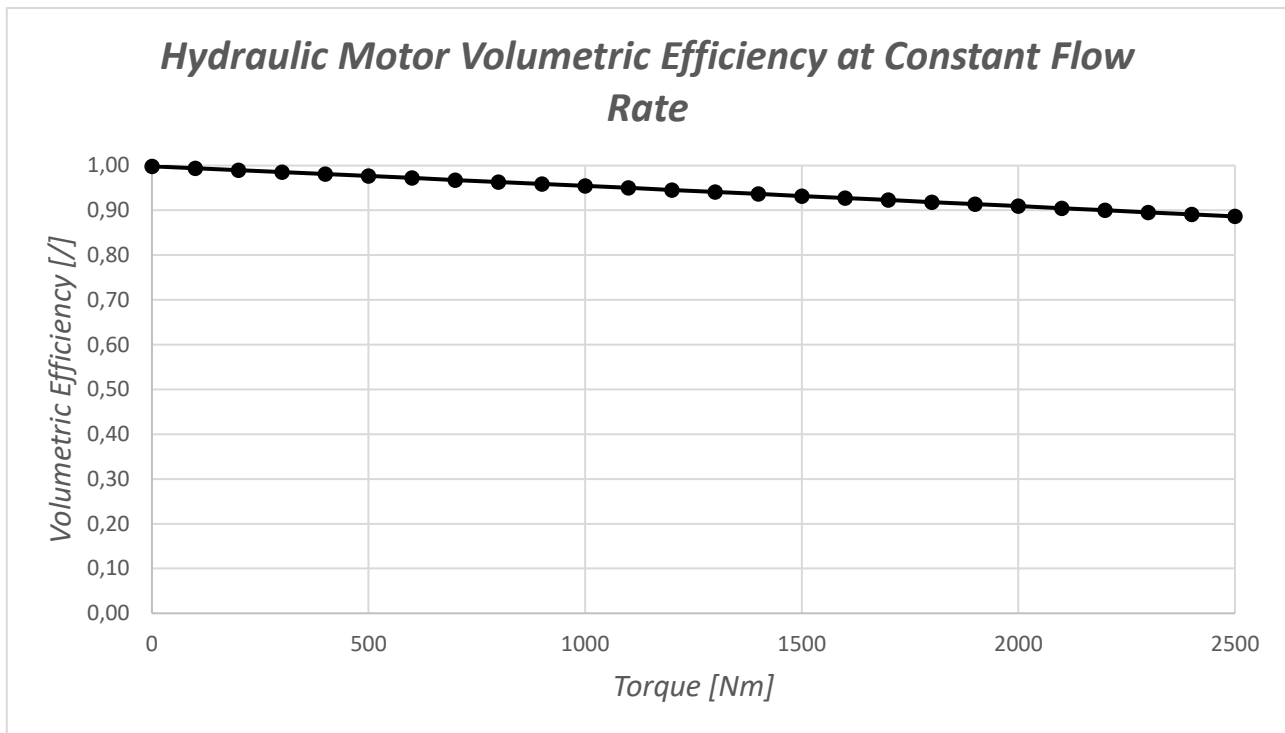
Figure 5.18 – Hydraulic volumetric efficiency as a function of shaft torque

As it can be seen in the picture, the trend resembles the linear dependency indicated by the theoretical formulation. The lower the load, the lower the volumetric efficiency: at torque equal to 2500 Nm the hydraulic volumetric efficiency reaches its minimum value, corresponding to 88.64%.

5.5.2 Volumetric Efficiency with Variable Shaft Velocity of Rotation

Here the torque has been maintained constant in all the runs. In the following table it can be seen the results obtained at different input flow rates and, consequently, at different shaft speed.

Q_in [L/min]	Mean Velocity [rpm]	Q_th [L/min]	Q_Leak [L/min]	η_{vol} [/]
0	0.00	0.000	0.000	0.000%
5	7.55	2.814	2.178	56.373%
10	20.89	7.787	2.176	78.159%
20	47.48	17.699	2.192	88.980%
30	74.06	27.606	2.211	92.585%
40	100.65	37.518	2.232	94.385%
50	127.24	47.430	2.260	95.452%
60	153.84	57.345	2.286	96.166%
70	180.46	67.268	2.317	96.670%
80	207.07	77.187	2.352	97.043%
90	233.67	87.102	2.394	97.325%
100	260.28	97.022	2.440	97.547%

The calculations made to obtain the efficiency are obviously the same of the ones seen in chapter 5.5.1. In figure 5.19 it is reported the plot with the results shown in the table.

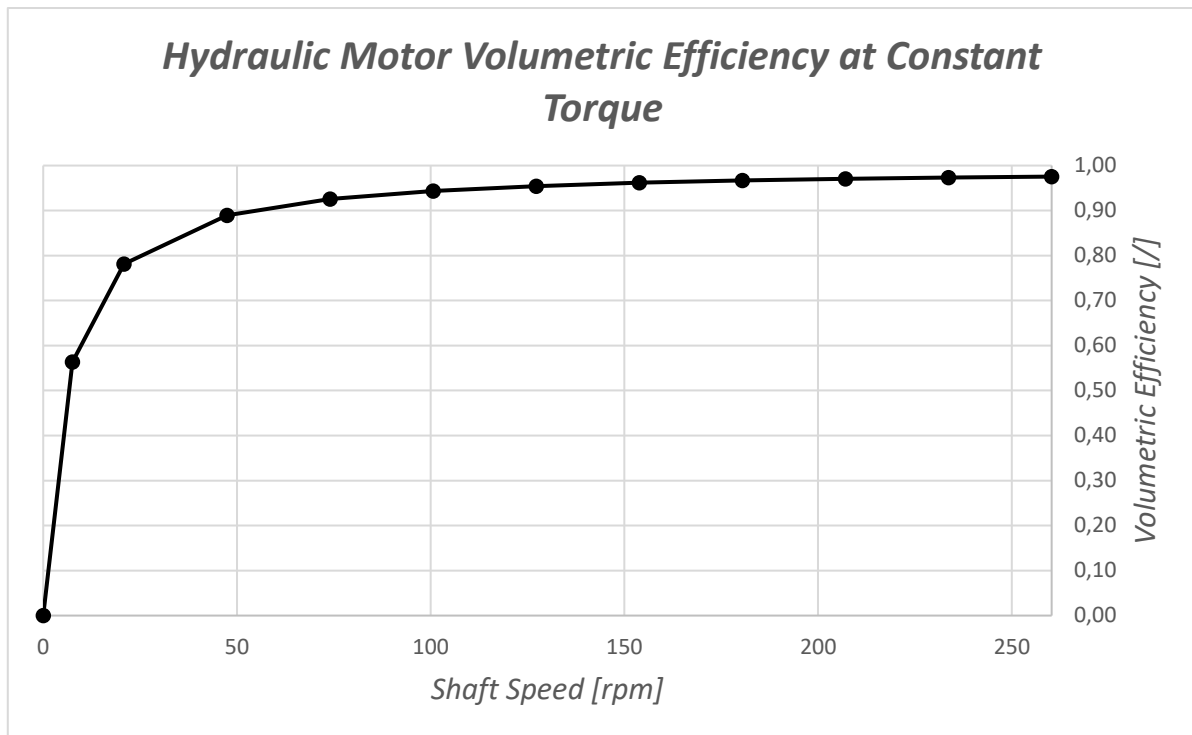*Figure 5.19 – Hydraulic volumetric efficiency as a function of shaft speed of rotation*

The theoretical considerations are confirmed again by the results of the simulations. The hydraulic volumetric efficiency starts equal to zero at shaft standing still and increases with the shaft speed. It has to be remembered that the increase in speed is obtained by an increase in the motor input flow rate.

6) Analysis of the Impact of the Number of Pistons

Among the parameters that affect the motor performances, the pistons number is one of the most important. In this chapter the motor is studied under the assumption that this variable can be changed maintaining the same cycles per shaft revolution n_{cycles} and the same motor displacement V. If these two parameters are maintained constant it's obvious that increasing the number of pistons $n_{pistons}$ the unit displacement V_0 has to be reduced.

In order to calculate the chamber volume and the unit displacement for each case, simple equivalent cylindrical chambers have been considered. Starting from the real configuration with eight pistons, an equivalent piston lift L_{eq} has been calculated by imposing the actual volume evolution over shaft angle (the one that can be seen in figure 3.3) and a constant diameter equal to 31 mm.

$$L_{eq}(\vartheta) = \frac{4*Vol(\vartheta)}{\pi*D^2} \ (eq. \ 6.1)$$

For the cases in which the number of pistons is different than eight, the equivalent lift has been maintained the same, while the diameter has been changed according to the following considerations: Keeping the same motor displacement,

$$V = V_0 * n_{cycles} * n_{pistons} = V_{8pistons} = V_{xpistons}$$

$$V_{0,8pistons} * n_{cycles} * n_{8pistons} = V_{0,xpistons} * n_{cycles} * n_{xpistons}$$

$$V_{0,xpistons} = V_{0,8pistons} * \frac{n_{8pistons}}{n_{xpistons}}$$

Knowing that $V_0 = Vol_{max} - Vol_{min} = \frac{\pi}{4} * D^2 * (L_{max} - L_{min})$, having the same lift implies:

$$\frac{\pi}{4} * D^2_{xpistons} * (L_{max} - L_{min}) = \frac{\pi}{4} * D^2_{8pistons} * (L_{max} - L_{min}) * \frac{n_8}{n_x}$$

In conclusion:

$$D_{xpistons} = \sqrt{\frac{n_{8pistons}}{n_{xpistons}}} * D_{8pistons} \ (eq. \ 6.2)$$

Using this last formula, it has been possible to calculate the volume trend with respect to the shaft angle for every desired *"x pistons"* condition keeping the same motor displacement. All these calculations have been done on an *Excel®* file. In figure 6.1 it can be seen the trend of the volume with respect to the shaft angle in the cases of seven, eight, nine, ten and eleven pistons. Even if they have less and less practical use, higher pistons numbers have been further studied just for the sake of understanding how this factor really affects the hydraulic motor behaviour.
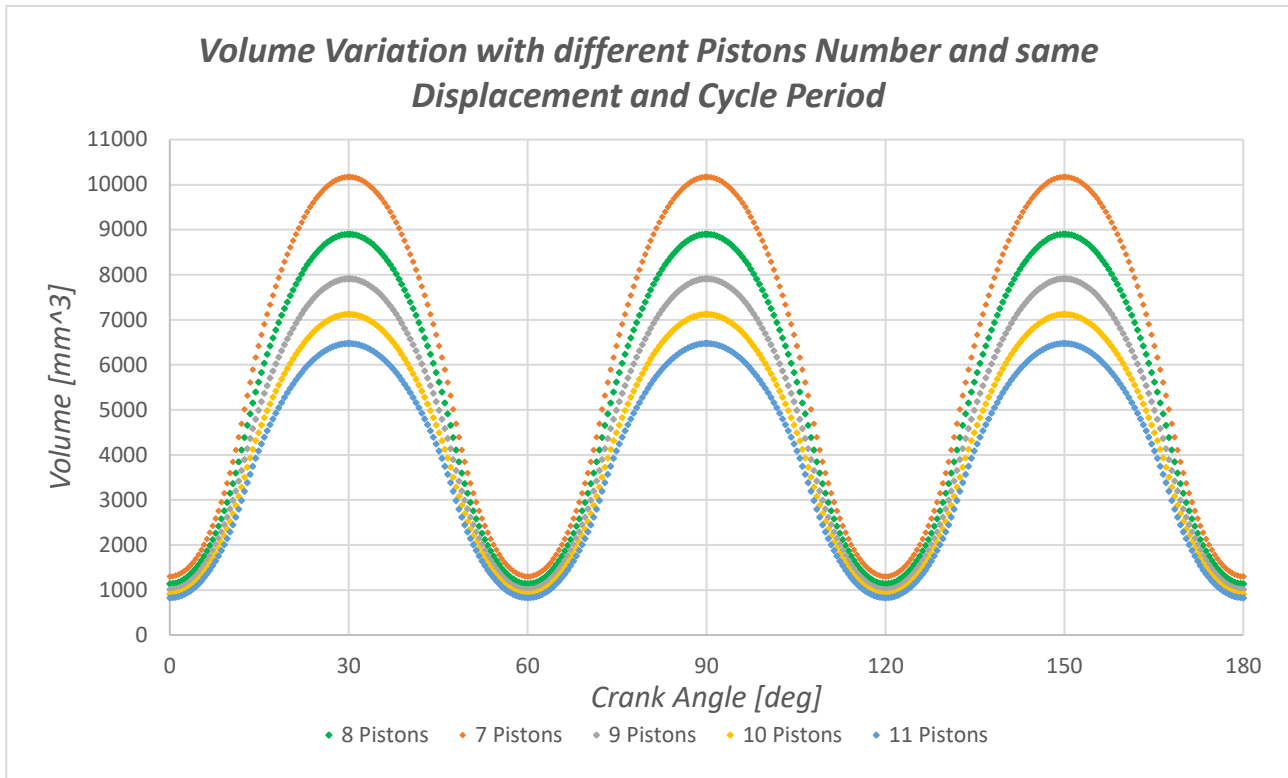
Figure 6.1 - Volume with respect to shaft angle having different numbers of pistons and same displacement and cycle duration

Since the study has been conducted again by means of simulations in *Amesim®* environment, it has been necessary to export the data on *Matlab®* for an interpolation and to save them into a *.data* file. This is the same procedure used for the main simulation that has been explained in chapters 3 and 5. Also the same simulation layout has been used, this time with the simplification of the total absence of leakages from the motor. In this way the desired volume and volume derivative trends with respect to the shaft angle have been calculated and imported into the *Amesim®* environment. In the following picture there is the plot of the shaft speed with pistons numbers that range from seven to eleven.

Figure 6.2 – Shaft speed with respect to shaft angle and with different pistons numbers [@ Q = 50 L/min and T = 1000 Nm]

It can be seen how the oscillation period is strongly affected by the number of pistons. Looking at it from the lowest to the largest one, the different cases are ordered in this way:

1. Eleven pistons;
2. Seven pistons;
3. Ten pistons;
4. Eight pistons;
5. Nine pistons.

It can be seen that if the oscillation period increases also the ripple does it. The average shaft speed remains equal for all the cases since also the motor displacement is the same.
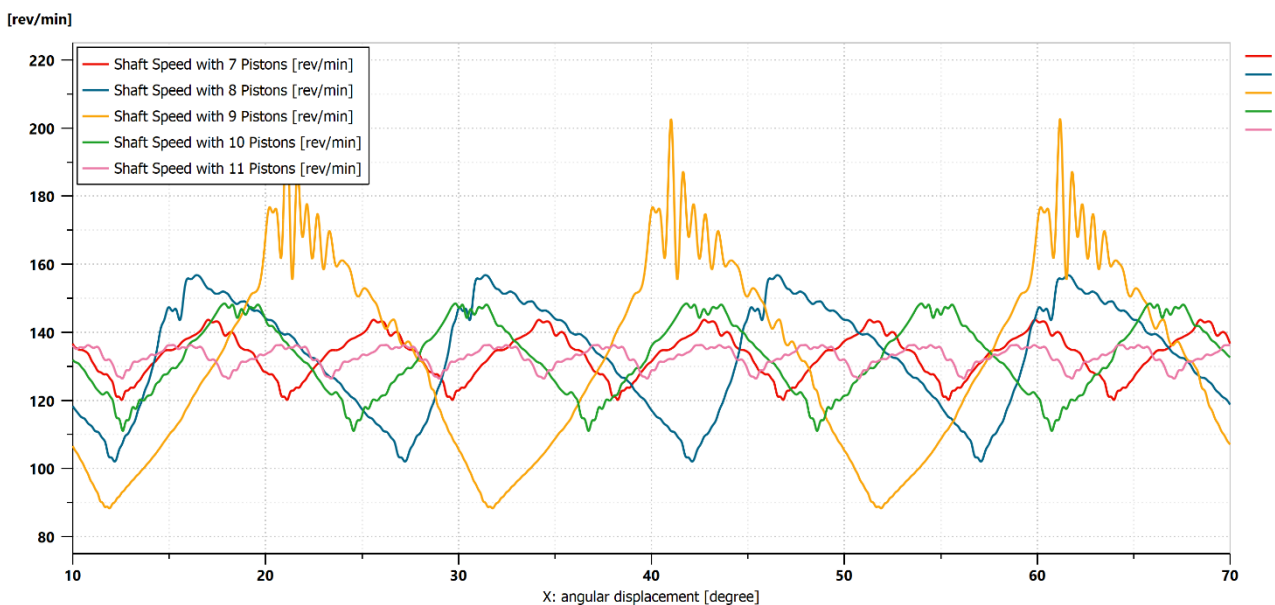Looking at the number of pistons and at its relationship with the working cycle duration, four different *families* have been found (just considering $n_{pistons} \geq n_{lobes} = 6$).

1. Prime numbers (or multiples of just prime numbers): there are N pistons that work in different points of the working cycle.
2. Numbers that are multiple of 2: there are N/2 piston couples that work in different points of the working cycle.
3. Numbers that are multiple of 3: there are N/3 piston groups that work in different points of the working cycle.
4. Numbers that are multiple of 6: there are N/6 piston groups that work in different points of the working cycle.

These relations are strictly determined by the piston angular phasing. In the following paragraphs these four families are going to be separately analysed.

6.1) Prime Number of Pistons

If there are N pistons and N is a prime number, as indicated before all the pistons are working at different working cycle points. Here some examples are reported.

	7 pistons		11 pistons		13 pistons	
	ϑ [deg]	ϑ_{cycle} [deg]	ϑ [deg]	ϑ_{cycle} [deg]	ϑ [deg]	ϑ_{cycle} [deg]
p1	0.00	0.00	0.00	0.00	0.00	0.00
p2	51.43	51.43	32.73	32.73	27.69	27.69
p3	102.86	42.86	65.45	5.45	55.38	55.38
p4	154.29	34.29	98.18	38.18	83.08	23.08
p5	205.71	25.71	130.91	10.91	110.77	50.77
p6	257.14	17.14	163.64	43.64	138.46	18.46
p7	308.57	8.57	196.36	16.36	166.15	46.15
p8			229.09	49.09	193.85	13.85
p9			261.82	21.82	221.54	41.54
p10			294.55	54.55	249.23	9.23
p11			327.27	27.27	276.92	36.92
p12					304.62	4.62
p13					332.31	32.31
Δteta_p [deg]	51.43		32.73		27.69	
	7 groups of 1 piston		11 groups of 1 piston		13 groups of 1 piston	

The *Δteta_p* parameter indicates the angular phasing of the pistons, and can be easily calculated with the formula:

$$\Delta teta_p = \frac{360}{n_{pistons}}$$

The *θ* parameter indicates the absolute angular position of the piston starting from a reference point equal to 0°. The ϑ_{cycle} parameter simply indicates the angular position of the piston rescaled inside the working cycle, which is recalled to be equal to 60°. It can be easily seen on the table that each piston is working at a different angle inside it. Here are reported some pictures that help to better visualize what has just been explained.
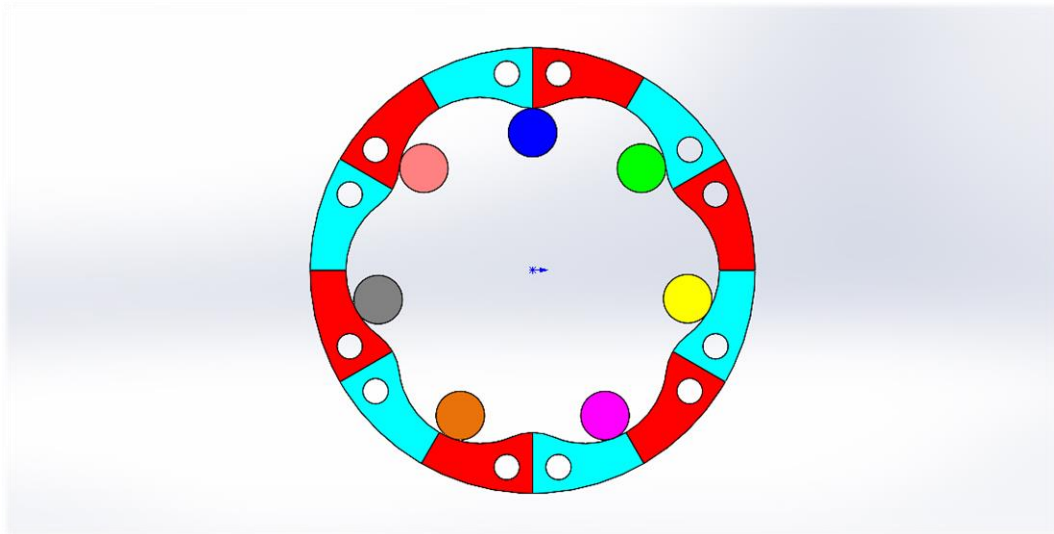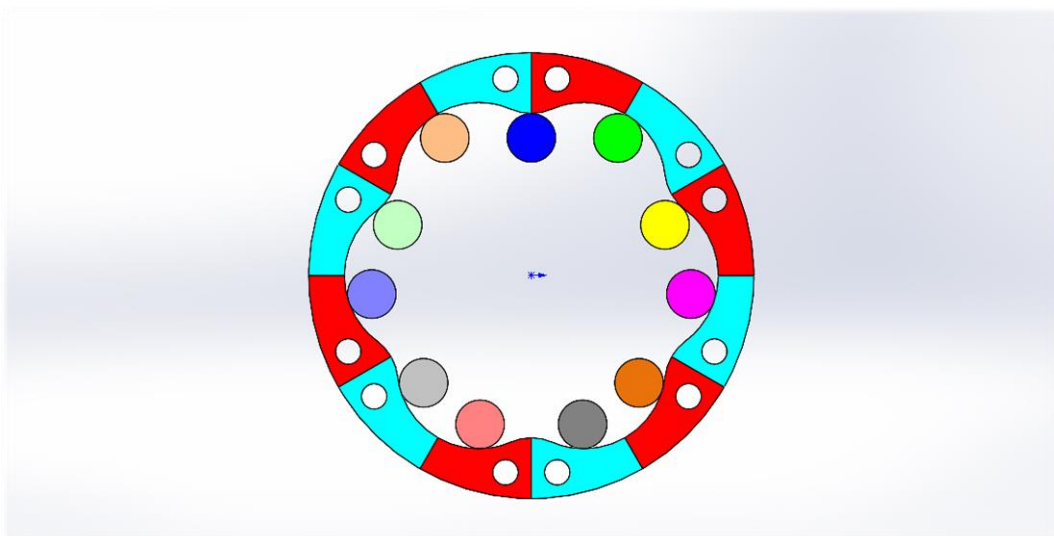

Figure 6.3 - 7 pistons configuration

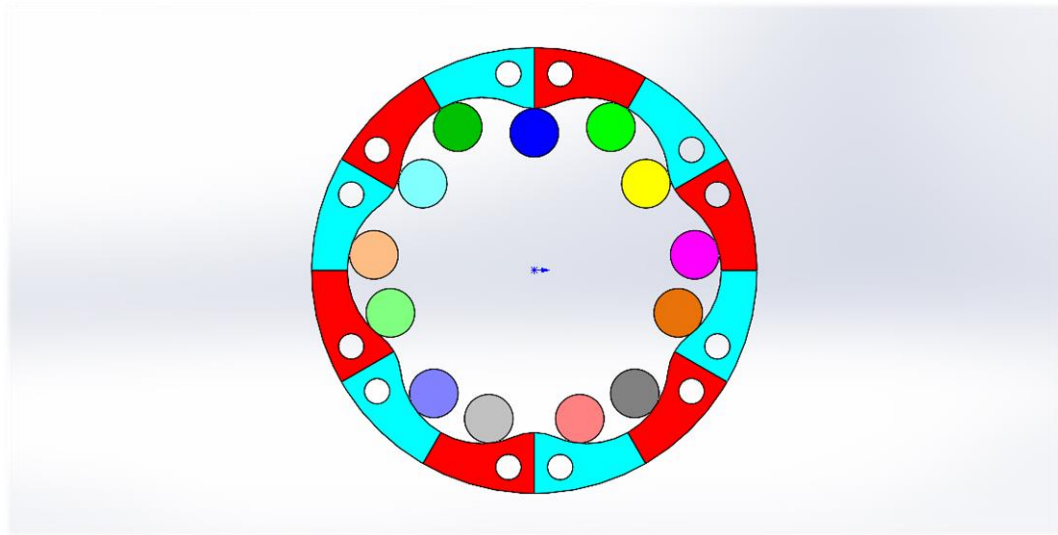*Figure 6.4 - 11 pistons configuration*

Figure 6.5 - 13 pistons configuration

The piston angular position is represented by the contact point of the rollers with the cam profile. Their dimension is purely indicative and does not represent the possibly applicable real value. The red sections are the ones of the oil inlet and the light blue the ones of the oil outlet. For each roller colour a different working point in the cycle is present.

6.2) Number of Pistons Multiple of Two

If there are N pistons and N is a multiple of two, the pistons are working in couples at different working cycle points. Here some examples are reported.

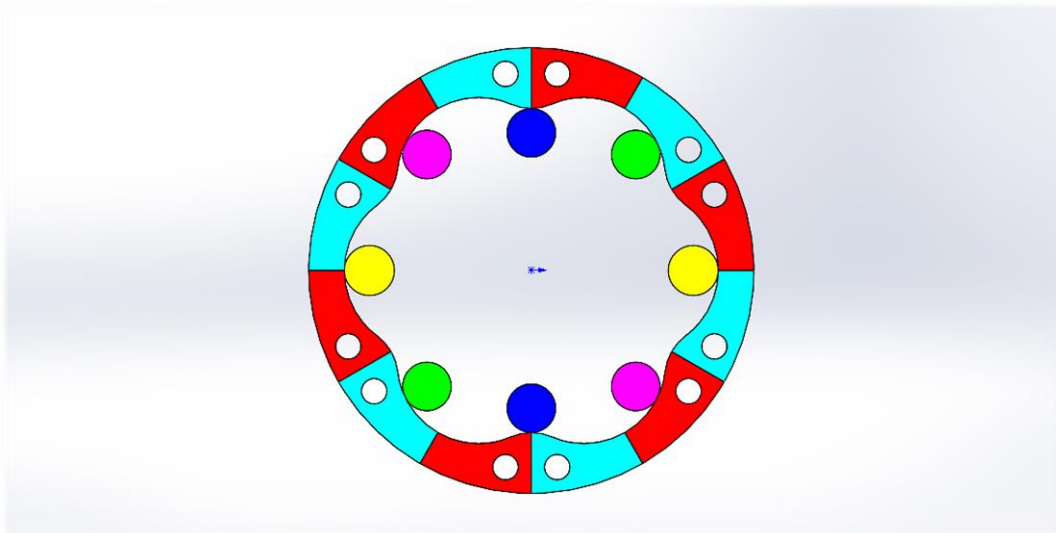|	8 pistons		10 pistons		14 pistons	
	θ [deg]	ϑ_{cycle} [deg]	θ [deg]	ϑ_{cycle} [deg]	θ [deg]	ϑ_{cycle} [deg]
p1	0.00	0.00	0.00	0.00	0.00	0.00
p2	45.00	45.00	36.00	36.00	25.71	25.71
p3	90.00	30.00	72.00	12.00	51.43	51.43
p4	135.00	15.00	108.00	48.00	77.14	17.14
p5	180.00	0.00	144.00	24.00	102.86	42.86
p6	225.00	45.00	180.00	0.00	128.57	8.57
p7	270.00	30.00	216.00	36.00	154.29	34.29
p8	315.00	15.00	252.00	12.00	180.00	0.00
p9			288.00	48.00	205.71	25.71
p10			324.00	24.00	231.43	51.43
p11					257.14	17.14
p12					282.86	42.86
p13					308.57	8.57
p14					334.29	34.29
Δteta_p [deg]	45		36		25.71	
	4 groups of 2 pistons		5 groups of 2 pistons		7 groups of 2 pistons	

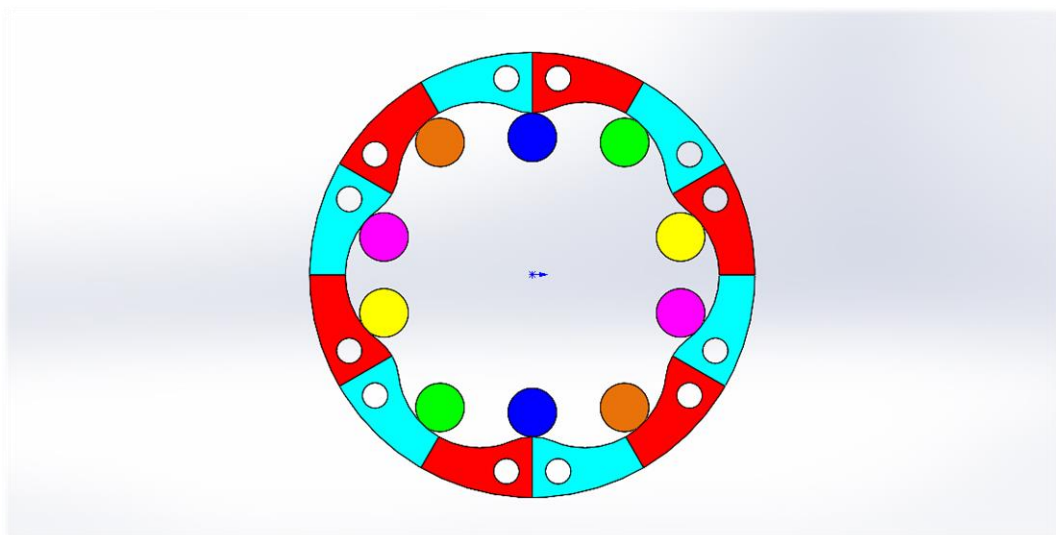*Figure 6.6 - 8 pistons (actual configuration)*

Figure 6.7 - 10 pistons configuration

Figure 6.8 - 14 pistons configuration

6.3) Number of Pistons Multiple of Three

If there are N pistons and N is a multiple of three, the pistons are working in groups of three at different working cycle points. Here some examples are reported.

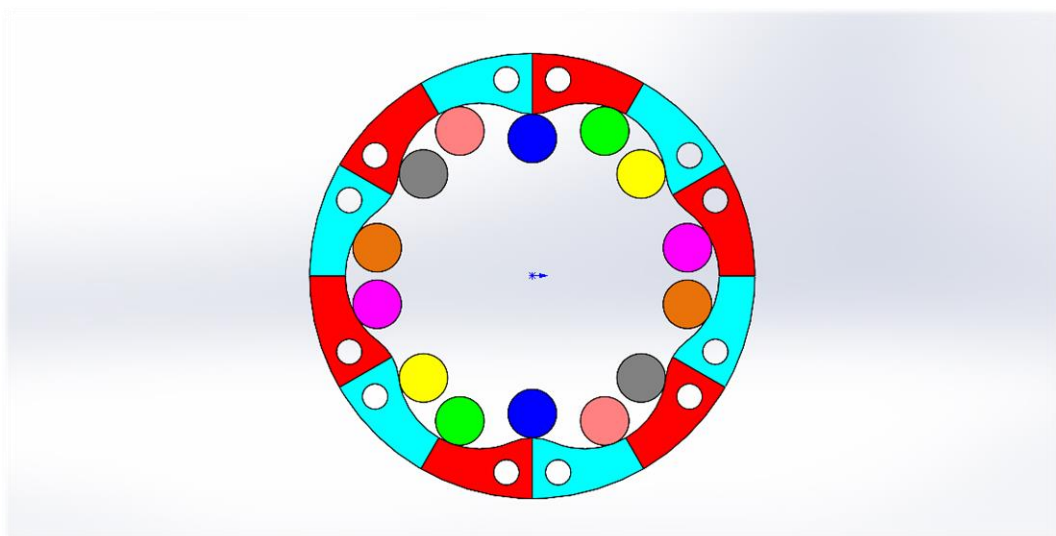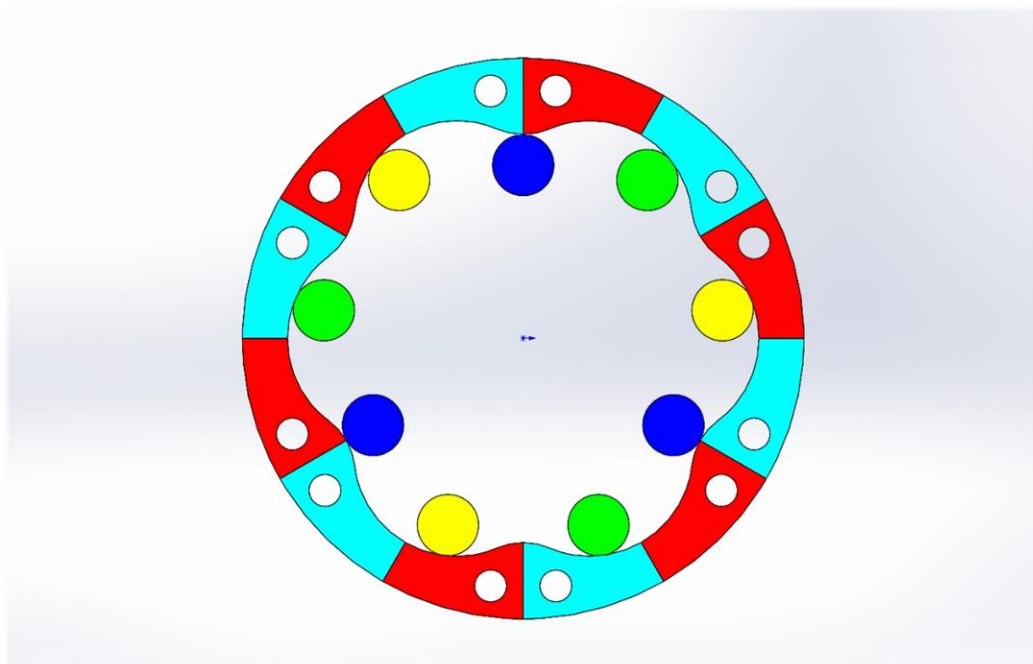|	9 pistons		15 pistons	
	ϑ [deg]	ϑ_{cycle} [deg]	ϑ [deg]	ϑ_{cycle} [deg]
p1	0.00	0.00	0.00	0.00
p2	40.00	40.00	24.00	24.00
p3	80.00	20.00	48.00	48.00
p4	120.00	0.00	72.00	12.00
p5	160.00	40.00	96.00	36.00
p6	200.00	20.00	120.00	0.00
p7	240.00	0.00	144.00	24.00
p8	280.00	40.00	168.00	48.00
p9	320.00	20.00	192.00	12.00
p10			216.00	36.00
p11			240.00	0.00
p12			264.00	24.00
p13			288.00	48.00
p14			312.00	12.00
p15			336.00	36.00
Δteta_p [deg]	40		24	
	3 groups of 3 pistons		5 groups of 3 pistons	

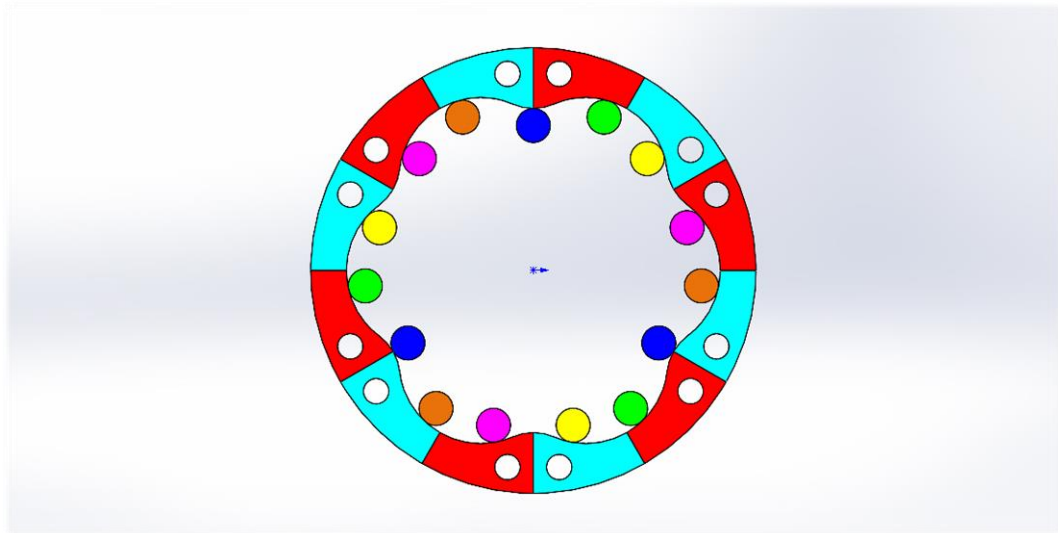*Figure 6.9 - 9 pistons configuration*

Figure 6.10 - 15 pistons configuration

6.4) Number of Pistons Multiple of Six

If there are N pistons and N is a multiple of six (in other words multiple both of two and three), the pistons are working in groups of six at different working cycle points. In this case a consideration has to be done: configurations with six and twelve pistons have to be avoided because they lead to stall conditions, in which all the pistons are in Bottom Dead Centre or/and Top Dead Centre positions. Here some examples are reported.

	12 pistons		18 pistons	
	ϑ [deg]	ϑ_{cycle} [deg]	ϑ [deg]	ϑ_{cycle} [deg]
p1	0.00	0.00	0.00	0.00
p2	30.00	30.00	20.00	20.00
p3	60.00	0.00	40.00	40.00
p4	90.00	30.00	60.00	0.00
p5	120.00	0.00	80.00	20.00
p6	150.00	30.00	100.00	40.00
p7	180.00	0.00	120.00	0.00
p8	210.00	30.00	140.00	20.00
p9	240.00	0.00	160.00	40.00
p10	270.00	30.00	180.00	0.00
p11	300.00	0.00	200.00	20.00
p12	330.00	30.00	220.00	40.00
p13			240.00	0.00
p14			260.00	20.00
p15			280.00	40.00
p16			300.00	0.00
p17			320.00	20.00
p18			340.00	40.00
Δteta_p [deg]	30		20	
	2 groups of 6 pistons		3 groups of 6 pistons	
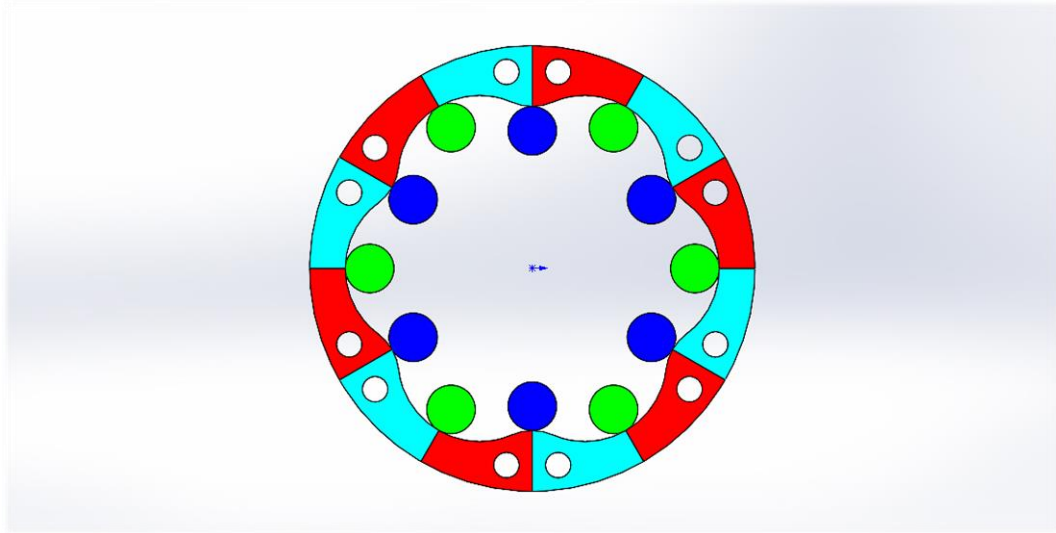
Figure 6.11 - 12 pistons configuration (in stall condition)
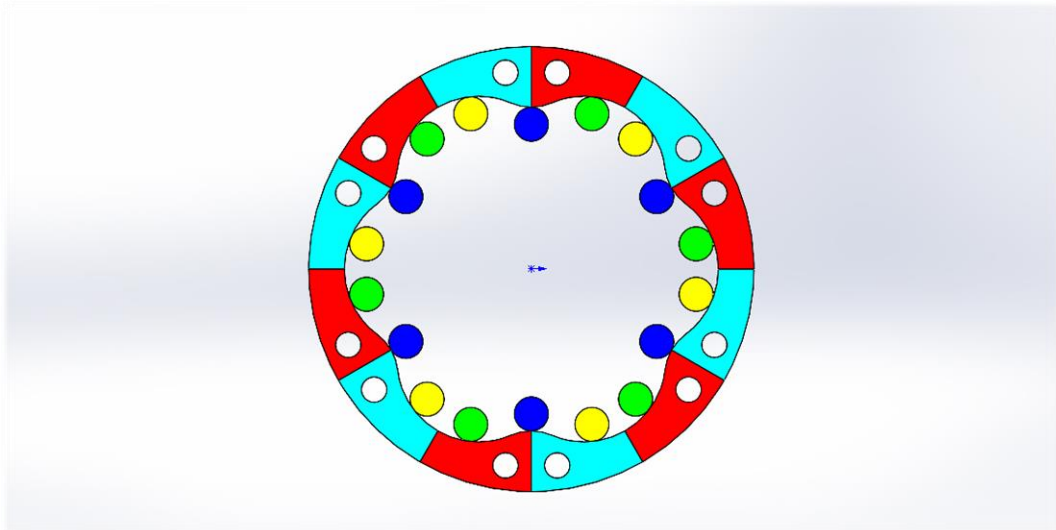
Figure 6.12 - 18 pistons configuration

6.5) *Oscillations and Ripples Evaluation*

After the study of the subdivision in the previous four groups and their understanding, the next and final step has been the quantification of these considerations in terms of motor performance: for this reason, the shaft velocity trend with respect to shaft angle has been calculated in order to evaluate the oscillation period and the ripple. Dedicated simulations in *Amesim®* environment have been conducted for each piston number configuration. After their results have been obtained, a table has been written on *Excel®* and two plots reported in figure 6.13 and 6.14 have been derived from it.

Pistons Number	Velocity Oscillation Period [deg]	Velocity Ripple [rpm]
7	8.57	23.55
8	15.00	54.72
9	20.00	91.57
10	12.00	37.40
11	5.45	9.90
13	4.61	8.23
14	8.58	23.52
15	12.00	39.48
16	7.50	22.70
17	3.53	5.03
18	20.00	91.53
21	8.57	22.05
24	15.20	51.55
27	6.67	15.83
30	12.00	40.14
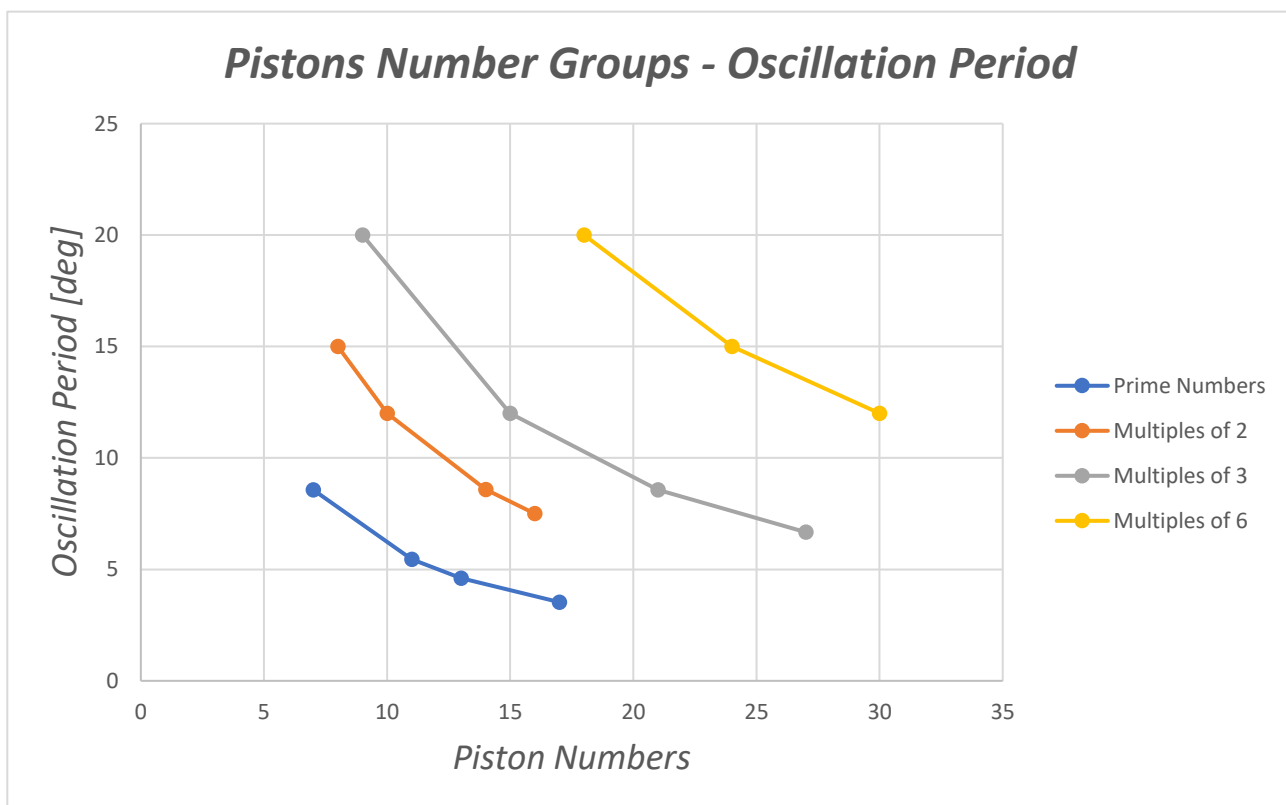
Figure 6.13 – Shaft angular speed oscillation period with respect to the number of pistons

From this plot it can be seen the general trend, common to all the four groups, according to which increasing the number of pistons the oscillation period decreases. This is not valid in general, but just singularly inside each one of the four different categories: the shaft speed with 30 pistons still has higher oscillations with respect to the 7 pistons configuration. This trend can be understood by the

grouping of the pistons. If the pistons number is prime, all the pistons (as already said) work at different cycle points. The oscillations are for this reason strongly reduced.

The higher oscillations present in the other *"families"* are due to the fact that the pistons are divided in groups that work in parallel (in other words, at the same cycle points). For example:

- in a configuration with 16 pistons, the motor works with 16/2 = 8 groups of 2 pistons, so with eight pistons in different working cycle conditions.
- in a configuration with 21 pistons, the motor works with 21/3 = 7 groups of 3 pistons, so with seven pistons in different working conditions.
- in a configuration with 24 pistons, the motor works with 24/6 = 4 groups of 6 pistons, so with just four pistons in different working conditions.

More generally, for each one of the four categories it can be said that the more the groups in which the pistons can be subdivided, the lower the oscillation period.
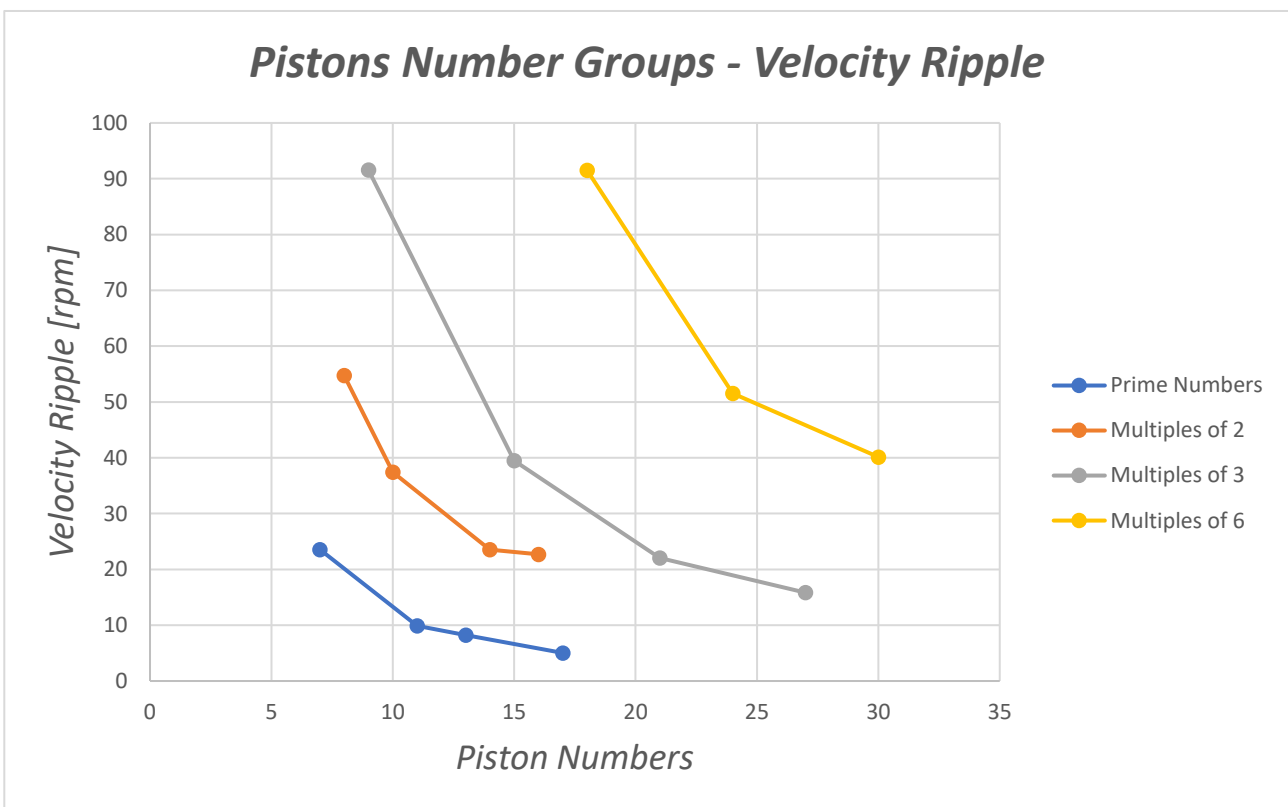

Figure 6.14 - Shaft angular speed ripple with respect to the number of pistons

The same considerations done for the velocity oscillations period can be done also for the velocity ripple. In this case quite steeper curves are generated, so a stronger dependence between the two depicted parameters is present.

It is important anyway to remember that better behaviour in terms of velocity ripple does not implies that an optimal solution has been found. For example, the eight pistons configuration has a great advantage with respect to the seven one: the continuous balancing of the radial loads thanks to the symmetry of the system. For this reason, this architecture is preferred and has been put in production.

7) Variable Displacement

The hydraulic motor studied in this work has a fixed displacement, due to the two constant volume chambers that communicate with the ones of the pistons. Despite its simplicity, this configuration can be considered quite *"rigid"*, possibly resulting in a low operational flexibility. Nevertheless, it is also possible to overcome this limit by means of dedicated components.
Looking at the classic formulation:

$$Q = V * \omega \text{ (eq. 7.1)},$$

It can be easily seen that if the motor is fed with the same inlet flow rate Q, a decrease in the displacement V inevitably leads to a rotational speed ω increase. This concept can be applied as previously suggested on the studied motor by means of a dedicated distribution, designed in such a way that thanks to the coupling with its dedicated housing it forms three (or even more) constant volume chambers. In this chapter the solution with three chambers is analysed, maintaining the same cam profile and the same number of pistons.
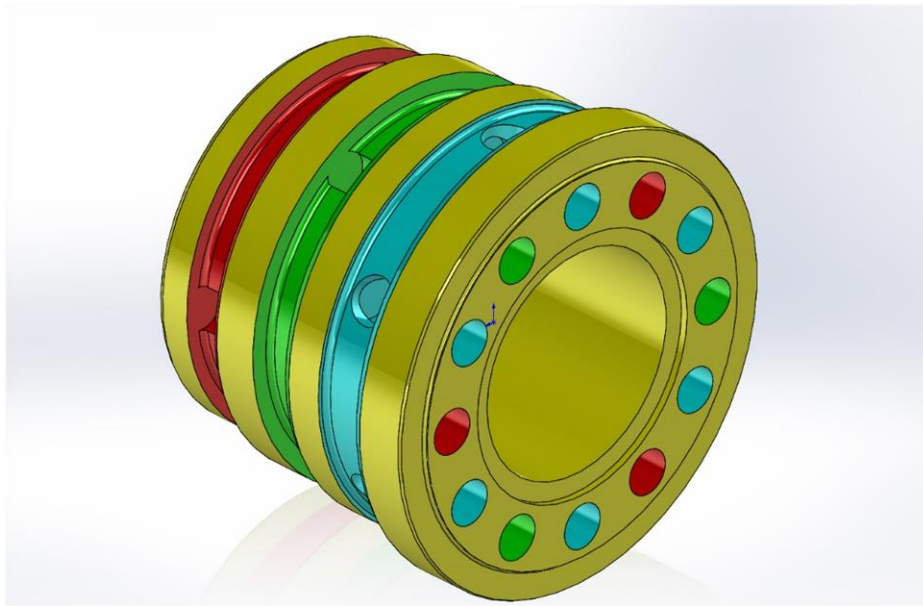

Figure 7.1 - Three chambers distribution

Among these three constant volume chambers, two communicate with the high and low pressure lines (red and light blue respectively) and their status can only be commutated acting on the hydraulic circuit linked with the motor. The third one (coloured in green), located in between, is not directly linked to the hydraulic circuit. It communicates with one of the other two by means of a spool controlled by a pilot line, that determines according to its position if this environment is at high or low pressure. With this strategy, the displacement can be discretely interchanged between two values. In normal operating conditions the middle chamber communicates with the high pressure one. Considering the data evaluated in chapter 3, in this configuration the displacement is equal to:

$$V_{max} = n_{pistons} * n_{cycles} * V_0 = 372.7584 \, \frac{cm^3}{rev} \text{ (eq. 7.2)}$$

So, the motor in this configuration is perfectly equivalent to the one with fixed displacement. When the spool is actuated, the middle chamber communicates with the low pressure one. Now there are less flow areas that send pressurized oil to the pistons (it can be said that in this way some parts of the cam profile that contribute to the torque production are *deactivated*). In this case the displacement is equal to:

$$V_{min} = n_{pistons} * \frac{n_{cycles}}{2} * V_0 = 186.3792 \frac{cm^3}{rev} = \frac{V_{max}}{2} \text{ (eq. 7.3)}$$

In figure 7.2, 7.3, 7.4 and 7.5 there are reported some views that help to better visualize the two different working conditions just explained. It has also been done a simplified 3D model containing the distribution (in yellow), the seat (in light brown) and the spool (in purple).
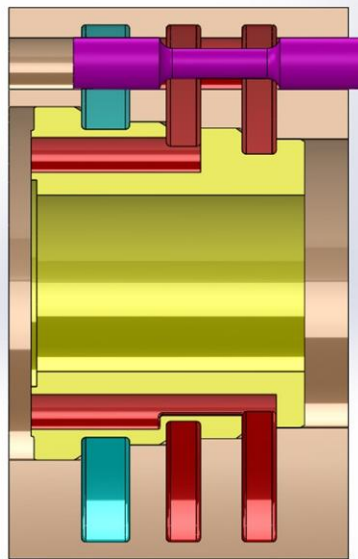

Figure 7.2 - Maximum displacement working condition (two high pressure chambers in red, one low pressure chamber in light blue)
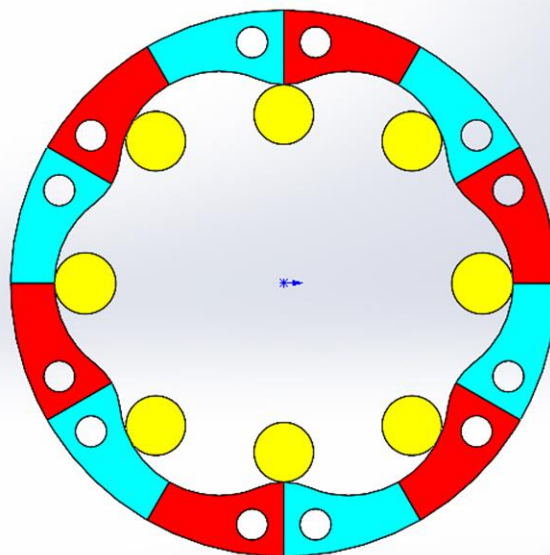

Figure 7.3 - Maximum displacement working condition (six cycles per shaft revolution)
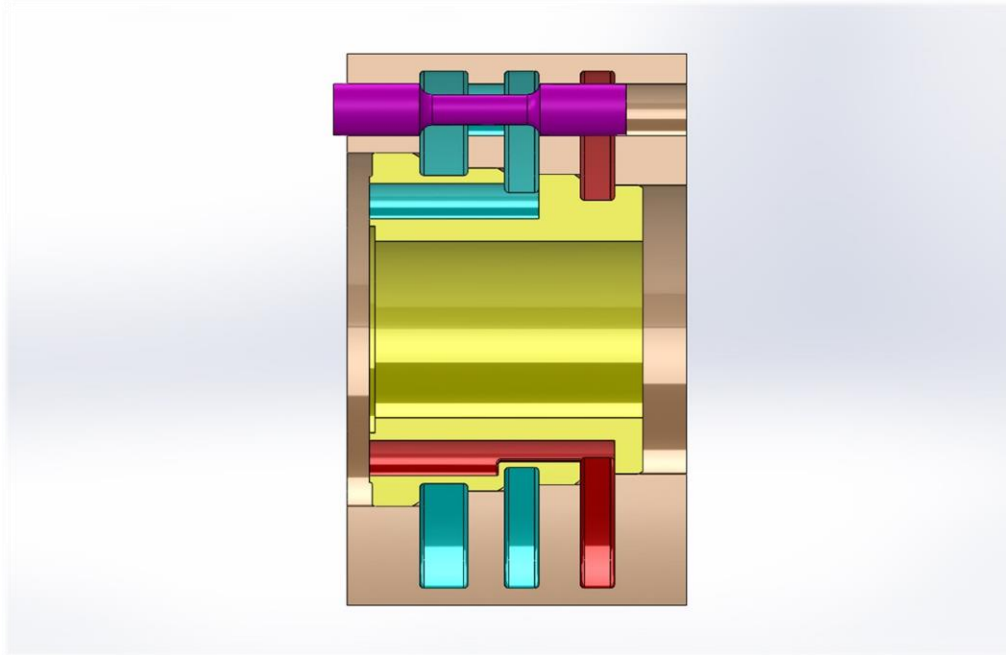
Figure 7.4 - Minimum displacement working condition (one high pressure chamber in red, two low pressure chambers in light blue)
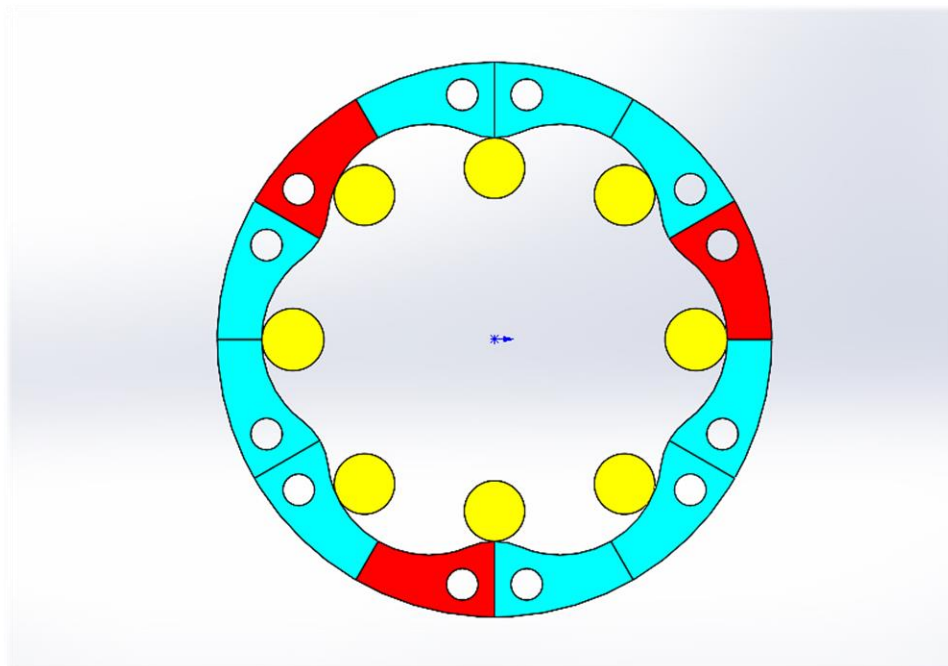
Figure 7.5 - Minimum displacement working condition (three cycles per shaft revolution)

From the previous pictures it can be seen how the middle chamber is the one that, according to the spool position, imposes the displacement value by defining the number of work cycles per shaft revolution, rendering *active* or *non-active* some strokes of the cam. In the case of the six lobes stator, in which every lobe is originally contributing to the torque for half of its development, three of them are deactivated when the displacement is reduced. Obviously with different configurations different results can be obtained.

Referring to equations 7.2 and 7.3, being the minimum displacement the half of the maximum one it is logical to think that maintaining the same inlet flow rate the speed has to be the double.

7.1) Motor Simulation at Minimum Displacement

A simulation has been developed in *Amesim®* environment in order to check the outcomes of this layout modification. The sketch has been directly derived by the main vectorial one seen in chapter 5, and the simplification of no flow losses has been adopted; the only modification needed has been the one of the flow areas development with respect to the shaft angle, since the piston motion remains the same in both situations.

More precisely:

- The maximum displacement working condition perfectly coincides with the one of the main simulations seen in chapter 5.
- The minimum displacement working condition has the only particularity that each piston sees in sequence one inlet flow area (high pressure line communication) and three outlet flow areas (low pressure line communication).

For this reason, a dedicated *.data* file has been generated with the new flow areas versus shaft angle points. Here is reported the *Matlab®* script written to obtain the desired data. The *.xlsx* file that can be seen in the script is the one already mentioned in chapter 4.1.

```matlab
clear all
clc
CA=xlsread('Aree_di_Passaggio.xlsx', 'D5:D159');          %Shaft Angle

%% 1) Inlet
Surf_in=xlsread('Aree_di_Passaggio.xlsx', 'F5:F159');     %Inlet Flow Area, T=60°
X=0:0.001:60;

int_in_spline=interp1(CA,Surf_in,X,'spline');
int_in=int_in_spline;

int_in(1:341)=0;
int_in(14001:16001)=max(Surf_in);
int_in(29661:60001)=0;

Xint_Vmin=0:0.001:120;
Aint_Vmin(1:60001)=int_in;
Aint_Vmin(60002:120001)=0;
%Aint_Vmin = Inlet Flow Area, T=120°, minimum displacement

%% 2) Outlet
Surf_out=xlsread('Aree_di_Passaggio.xlsx', 'G5:G159');    %Outlet Flow Area, T=60°

int_out_spline=interp1(CA,Surf_out,X,'spline');
int_out=int_out_spline;

int_out(1:30341)=0;
int_out(44001:46001)=max(Surf_out);
int_out(59661:60001)=0;

Xout_Vmin=0:0.001:120;
Aout_Vmin(1:60001)=int_out;
Aout_Vmin(60001:90001)=int_out(30001:60001);
Aout_Vmin(90001:120001)=int_out(30001:60001);
%Aout_Vmin = Outlet Flow Area, T=120°, minimum displacement
```

Here is reported the plot of the flow areas obtained from the script previously shown:
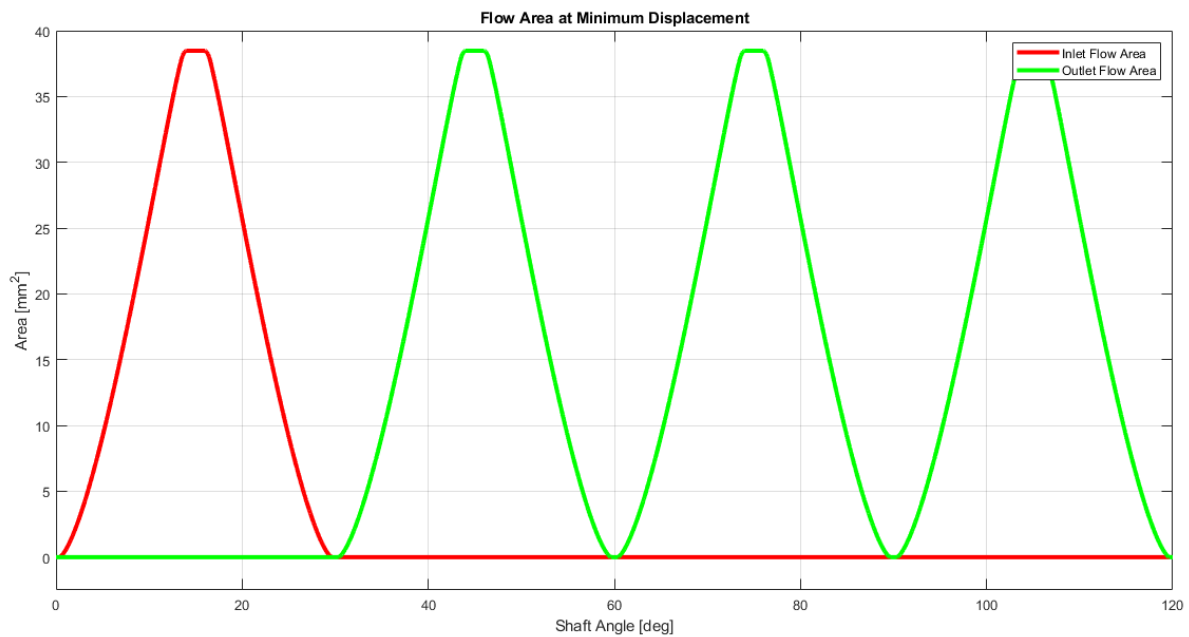

Figure 7.6 - Flow areas trend with respect to shaft angle at minimum displacement

Obviously, since the period over which the flow areas evaluation has been brought from 60° to 120°, one last modification has to be made into the simulation: the modulo function block has to be updated with the new parameter *"maximum output value"* equal to 120.

Here are now reported some of the most significative parameters with respect to the shaft angle, obtained with a constant input flow rate equal to 50 L/min and a constant shaft torque equal to 1000 Nm.
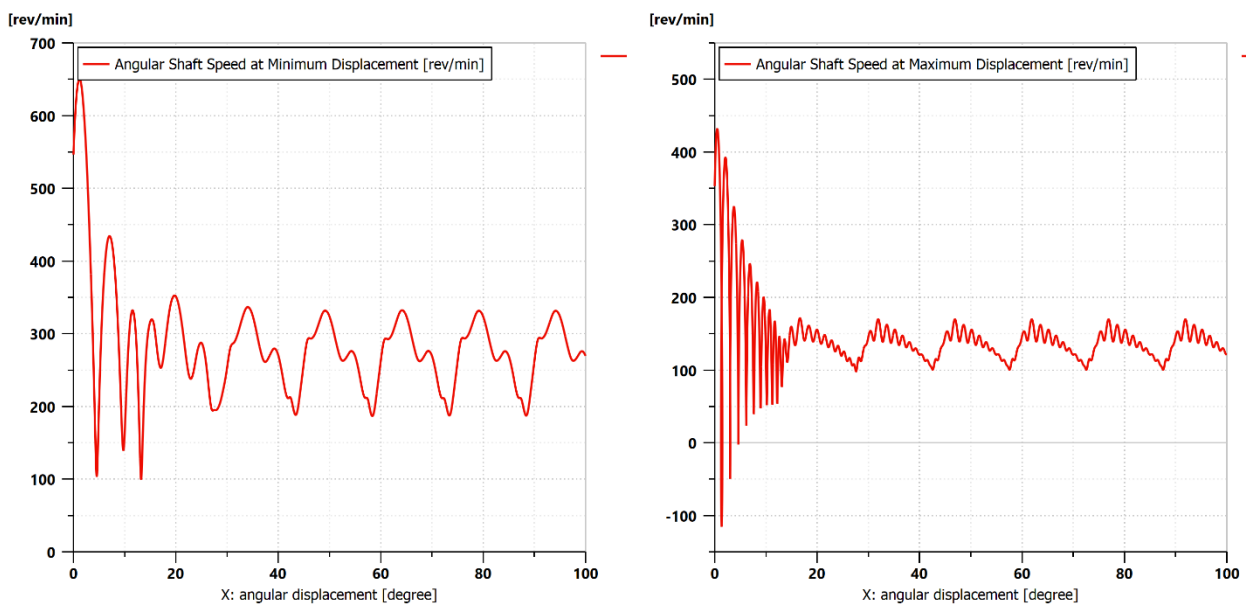
7.1.1 Motor Shaft Speed

Figure 7.7 - Shaft angular speed with respect to shaft angle

In figure 7.7 it can be seen the trend of the shaft speed of rotation with respect to the shaft angle. As previously indicated, with the minimum displacement the shaft rotates at higher revolutions per minute. The mean shaft speeds respectively measure 262.97 rpm and 132.84 rpm: the result obtained with the halved displacement is almost perfectly doubled, confirming the theoretical considerations. The little discrepancy is possibly due to the fact that the fluid properties have been chosen as *advanced*, so fluid compressibility, aeration and cavitation phenomena are all taken into account. It can also be seen how in the case of reduced displacement there is a higher ripple, while the inertia effect is less pronounced (so less noise in the calculations is produced).
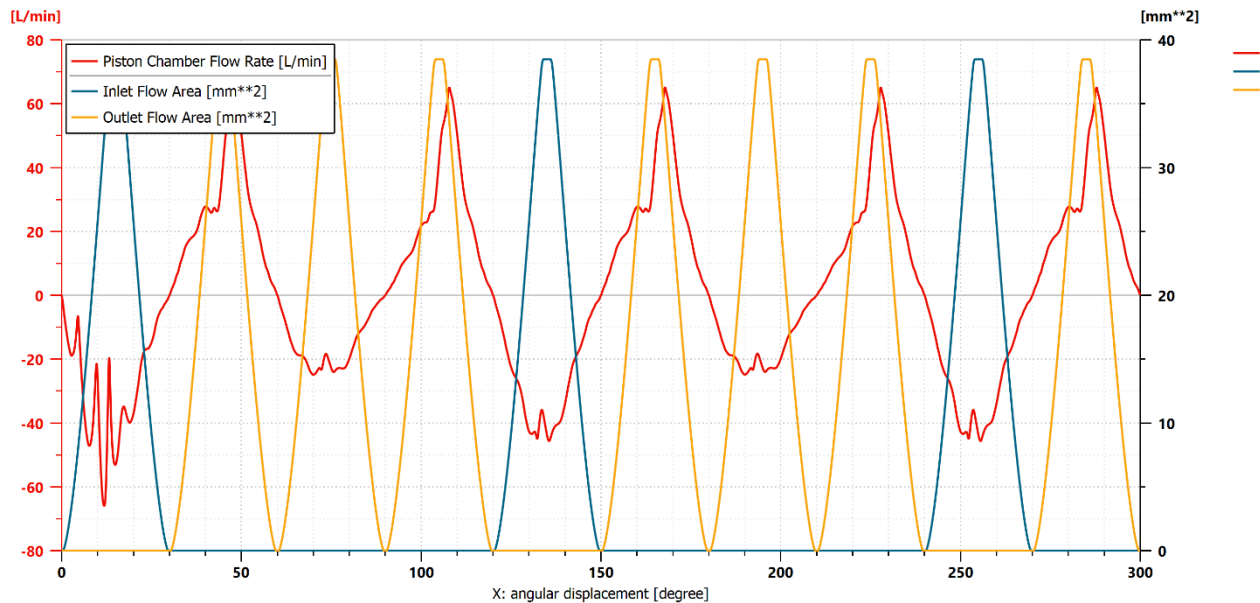
7.1.2 Piston Chamber Flow Rate

Figure 7.8 – Piston chamber flow rate at minimum displacement configuration

In this picture it is reported the flow rate trend relative to the shaft angle that flows into and out from the piston chamber. For the comparison with the maximum displacement, figures 5.4 and 5.5 can be taken as a reference. The peak flow rate value in delivery phase is obviously higher than its counterpart, and is equal to 65 L/min circa. It can be seen that there is a quite high asymmetry inside each working cycle between inlet and outlet flow rate.

7.1.3 Piston Chamber Pressure

In figure 7.9, located in the next page, it is reported the plot of the piston chamber pressure with respect to the shaft angular position at minimum displacement configuration. For the comparison with its counterpart, figure 5.6 can be taken as a reference. Also in this case the observed parameter peak is higher: it reaches about 450 bar. Despite the relative peaks located at the BDC position ($\vartheta = n * 60°$, with n=0,1,2,3…), the pressure value remains close to zero during all the three repetitions in which the outlet flow area is seen. Since a reduced displacement leads to an increase in pressure, particular attention has to be paid about the working conditions in which the displacement reduction is effectively possible. At reduced displacement in fact, higher pressure levels can be found and so a

lower maximum torque can be sustained (with respect to the one present in normal operating condition) in order to avoid problems of mechanical nature.
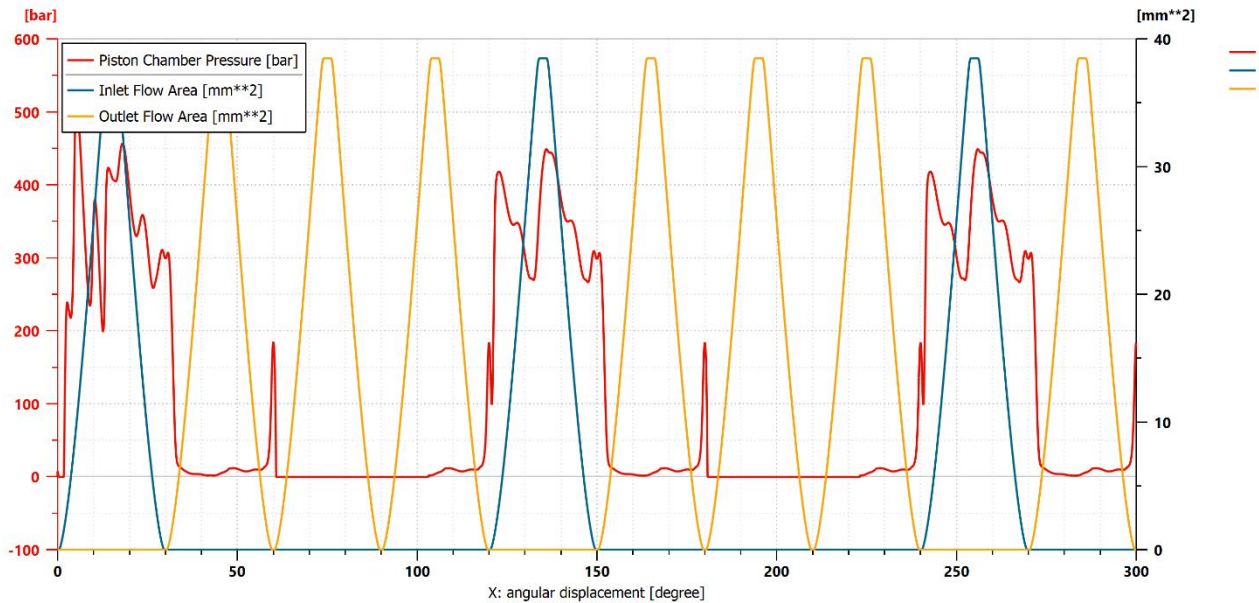

Figure 7.9 – Piston chamber pressure at minimum displacement configuration

When the piston crosses the second outlet flow area, the pressure reaches some units of bars under the zero value. For this reason, the flow rate seen in figure 7.8 is entering into the chamber also in this part of the working cycle.

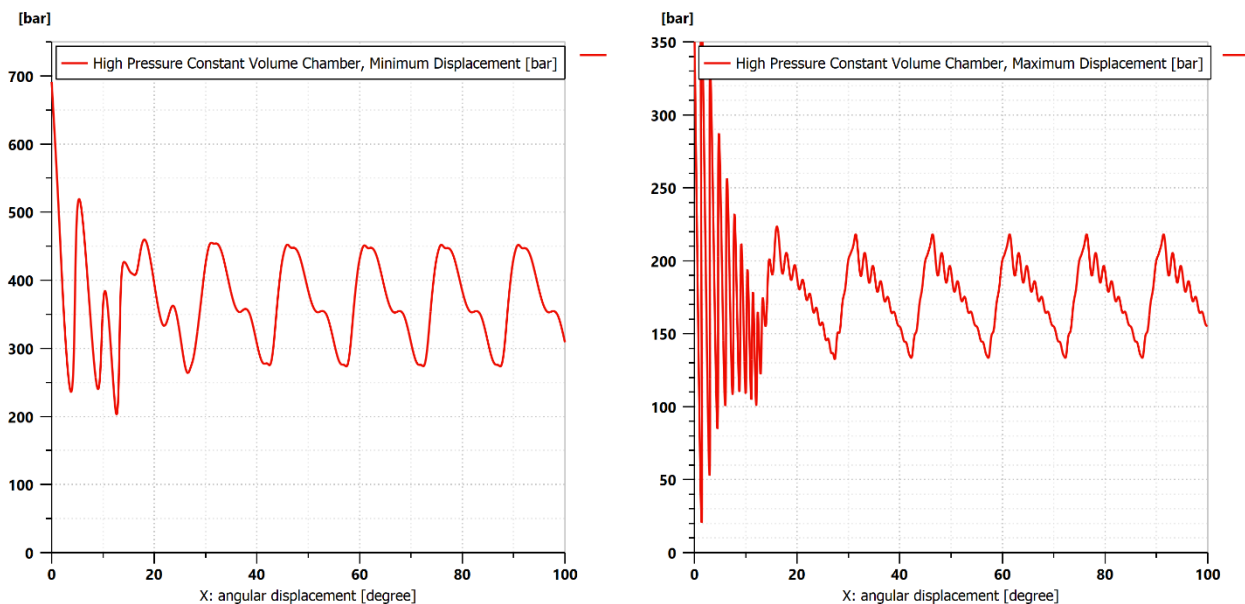### *7.1.4 High Pressure Constant Volume Chamber*

Figure 7.10 – Pressure with respect to shaft angle in the high-pressure constant volume chamber

Here it is reported the plot of the pressure with respect to the shaft angle present in the high-pressure constant volume chamber. It can be seen that at minimum displacement the noise effect of the inertia

is less incisive and that the pressure values are higher with respect to the maximum configuration. Their average values are respectively equal to 360.33 bar and 173.33 bar. A much higher ripple is also present in the first situation.

In general, the higher ripple seen in the minimum displacement working condition can be explained by the fact that the number of cycles per shaft revolutions has been reduced from 6 to 3 (and consequently the working cycle period has been increased from $T_{\Delta\vartheta} = 60°$ $T_{\Delta\vartheta} = 120°$): for this reason, the pistons need to cover a longer path between two consecutive active regions, and so the ripple is enhanced.

7.1.5 Pistons Phasing

When the displacement is maximum there are 4 groups of two pistons: in a generic angular position in which the BDC and TDC conditions are not present, two of them (so four pistons in total) actively participate to the torque production (their in-cycle angular position is between $\vartheta = 0°$ and $\vartheta = 30°$). When the displacement is minimum, all the pistons are working at different working cycle points and just two pistons are contributing to the torque (since now six of them are in the inactive lobe part, which lays in the in-cycle range between $\vartheta = 30°$ and $\vartheta = 120°$).

	θ [deg]	ϑ_{cycle} (@$n_{cycles} = 6$) [deg]	ϑ_{cycle} (@$n_{cycles} = 3$) [deg]
p1	5.00	5.00	5.00
p2	50.00	50.00	50.00
p3	95.00	35.00	95.00
p4	140.00	20.00	20.00
p5	185.00	5.00	65.00
p6	230.00	50.00	110.00
p7	275.00	35.00	95.00
p8	320.00	20.00	80.00

Looking at the table (in which a generic angular position is represented), the pistons that actively contributes to the torque production are highlighted in grey: at minimum displacement just two of them gives a contribution.

In figures 7.11 and 7.12 it is reported the plot with each single piston chamber pressure, so that the different phasing between the two systems can be better appreciated.
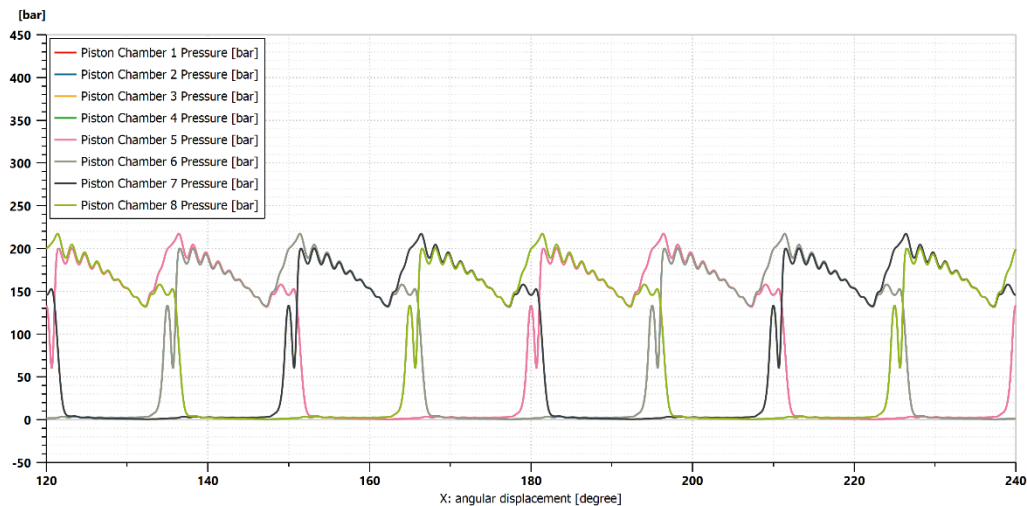

Figure 7.11 – Piston chambers pressure contribution at maximum displacement
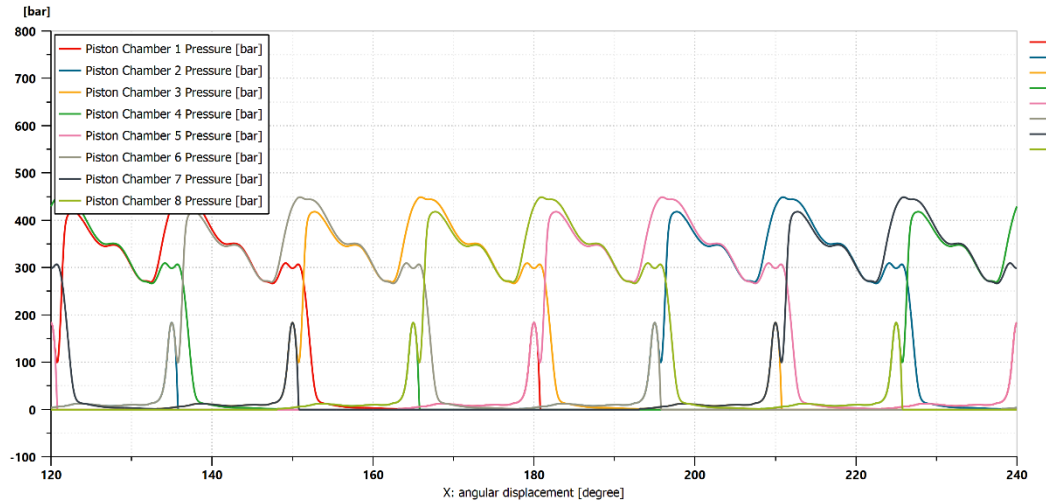
Figure 7.12 – Piston chambers pressure contribution at minimum displacement

In these two plots, where a range of 120° is defined on the *x axis*, it can be seen that at maximum displacement the pistons work in couples inside each cycle. At minimum displacement instead, all the eight pistons work at different points. Looking at a precise shaft angle, for example 160°, it can be also seen that in the case of maximum displacement four pistons (2, 3, 6 and 7) are contributing to the torque (the pressure in the chamber is higher than zero), while in the case of reduced displacement just pistons 3 and 6 are producing work.

Appendix A) Clarification on Shaft Speed Calculation

In chapter 3, in order to check the piston chamber volume and volume derivative evaluations, it has been done a comparison between calculations with two different formulations. For the first one, it has been used the classic formula correlating speed and flow rate that can be seen in *eq. 3.4.1*. The second one is derived from theoretical considerations and calculates the average desired parameter taking into account the instantaneous values considering the *F(ϑ)* function (*eq. 1.1.3*). While in the pump working conditions the two approaches have led to the same result in terms of delivered flow rate, the same can't be written about the speed in the motor working condition. In fact:

$$\begin{cases} \omega_{approach\ 1} = 134.14\ rpm \\ \omega_{approach\ 2} = 136.02\ rpm \end{cases}$$

This discrepancy between the two results can be due to a problem relative to the *F(ϑ)* function formulation. In the case of the pump working condition, the average F value exactly coincides with the displacement, as it can be further seen:

$$\begin{cases} Q = V * \omega \\ Q_{avg} = \overline{F(\vartheta) * \omega} = \overline{F(\vartheta)} * \omega \end{cases}$$

So, $V = \overline{F(\vartheta)}$.

In the case of a hydraulic motor, for which the speed has to be calculated, the situation is different. Looking again at the equations:

$$\begin{cases} \omega = \dfrac{Q}{V} \\ \omega_{avg} = \overline{\left(\dfrac{Q}{F(\vartheta)}\right)} = Q * \overline{\left(\dfrac{1}{F(\vartheta)}\right)} \neq \dfrac{Q}{\overline{F(\vartheta)}}\ ! \end{cases}$$

In the case of the motor operating conditions, the results obtained with the two approaches do not coincide since the inverse of the displacement is equal to $\overline{\dfrac{1}{F(\vartheta)}}$ (and different than $\dfrac{1}{\overline{F(\vartheta)}}$).
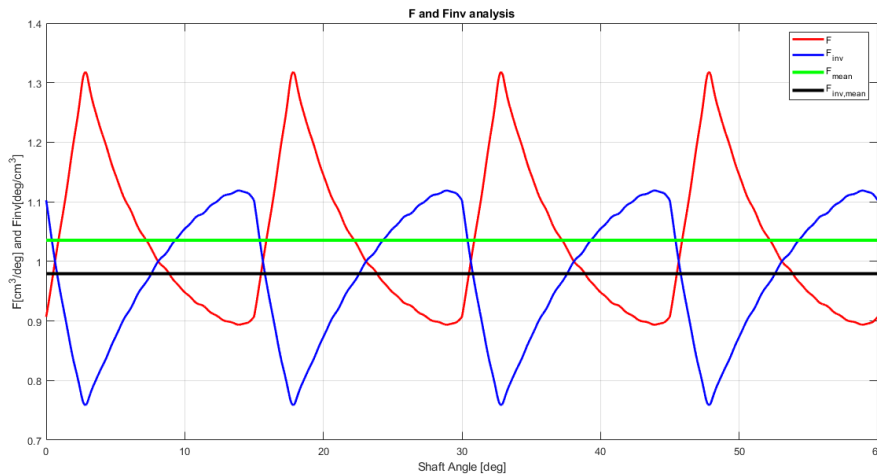

Figure A.1 - F and 1/F functions with their average values

If, absurdly, the average shaft speed is calculated taking into account just the average of $F(\vartheta)$

$$\omega_{avg} = \overline{\left(\frac{Q}{F(\vartheta)}\right)} = \frac{Q}{\overline{F(\vartheta)}}$$

Then the result is perfectly coincident with the one obtained by the classic flow rate/displacement/speed formulation. So, even if with small intensity, there is a problem with this procedure in the case of the hydraulic motors. Further investigations have to be conducted in order to overcome this incongruence.

Conclusions

The work of this thesis can be seen as a sort of *reverse engineering* task: starting from the actual machine, it has been tried to quantitatively study its behaviour with the aim to obtain a global model valid for radial piston hydraulic motors in general. The one obtained from this analysis is satisfactory in terms of the reliability of the results. The computation could be anyway optimized by making a more profound investigation (even experimentally supported) on the areas through which the leakages flow and considering also the shaft friction. Moreover, the newly developed vectorial approach has been found to be perfectly coincident with the classic one constituted by parallel chambers.

A further step could be the implementation on *Amesim®* environment of a more complete simulation, in which an entire hydrostatic transmission is designed and simulated: in order to obtain this, it should be sufficient to substitute the constant flow source and the tank blocks across the motor with a pump model and a hydraulic circuit.

Bibliography

1. NERVEGNA N., RUNDO M., Passi nell'Oleodinamica, *Epics Edizioni, Collana Politeko*, 2020

2. VACCA A., FRANZONI G., Hydraulic Fluid Power: Fundamentals, Applications and Circuit Design, *John Wiley and Sons*, 2021

3. AA.VV., L'Oleodinamica nell'Ambito Industriale e Mobile, *ASSOFLUID*, 2008

4. RUNDO M., Automotive Fluid Power Systems, *Lecture Slides*, 2021

5. RAVELLO V., Electric and Hybrid Propulsion Systems, *Lecture Slides*, 2020

6. CORVAGLIA A., Simulazione di una Pompa di Lubrificazione a Lunetta, *Master Degree Thesis*, 2016

7. Poclain Hydraulics, *Website*, https://www.poclain-hydraulics.com/it/

8. Poclain Hydraulics, *Technical Catalogue*, MS02-MSE02 Hydraulic Motors, https://www.poclain-hydraulics.com/it/prodotti/motori/ms/ms-mse02

9. Poclain Hydraulics, *Technical Catalogue*, MS Range Hydraulic Motors, https://www.poclain-hydraulics.com/it/cataloghi

10. Poclain Hydraulics, *Technical Catalogue*, Installation Guide, https://www.poclain-hydraulics.com/_upload/ressources/media/pdf/B59689D.pdf